EVALUATION OF THE RELATIONSHIP BETWEEN FRACTURE CONDUCTIVITY, FRACTURE FLUID PRODUCTION, AND EFFECTIVE FRACTURE LENGTH

A Dissertation

by

ELYEZER P. LOLON

Submitted to the Office of Graduate Studies of
Texas A&M University
in partial fulfillment of the requirements for the degree of

DOCTOR OF PHILOSOPHY

December 2004

Major Subject: Petroleum Engineering

EVALUATION OF THE RELATIONSHIP BETWEEN FRACTURE CONDUCTIVITY, FRACTURE FLUID PRODUCTION, AND EFFECTIVE FRACTURE LENGTH

A Dissertation

by

ELYEZER P. LOLON

Submitted to Texas A&M University
in partial fulfillment of the requirements
for the degree of

DOCTOR OF PHILOSOPHY

Approved as to style and content by:

Duane A. McVay (Chair of Committee)	Akhil Datta-Gupta (Member)
Stephen A. Holditch (Member)	Robert R. Berg (Member)
Stephen A. Holditch (Head of Department)	

December 2004

Major Subject: Petroleum Engineering

ABSTRACT

Evaluation of the Relationship Between Fracture Conductivity, Fracture Fluid Production, and Effective Fracture Length. (December 2004)
Elyezer P. Lolon, B.S., Bandung Institute of Technology, Indonesia
M.S., Texas A&M University
Chair of Advisory Committee: Dr. Duane A. McVay

Low-permeability gas wells often produce less than predicted after a fracture treatment. One of the reasons for this is that fracture lengths calculated after stimulation are often less than designed lengths. While actual fracture lengths may be shorter due to fracture growth out of zone, improper proppant settling, or proppant flowback, short calculated fracture lengths can also result from incorrect analysis techniques. It is known that fracturing fluid that remains in the fracture and formation after a hydraulic fracture treatment can decrease the productivity of a gas well by reducing the relative permeability to gas in the region invaded by this fluid. However, the relationships between fracture fluid cleanup, effective fracture length, and well productivity are not fully understood.

In this work I used reservoir simulation to determine the relationship between fracture conductivity, fracture fluid production, effective fracture length, and well productivity. I simulated water saturation and pressure profiles around a propped fracture, tracked gas production along the length of the propped fracture, and quantified the effective fracture length (i.e., the fracture length under single-phase flow conditions that gives similar performance as for multiphase flow conditions), the "cleanup" fracture length (i.e., the fracture length corresponding to 90% cumulative gas flow rate into the fracture), and the "apparent" fracture length (i.e., the fracture length where the ratio of multiphase to single-phase gas entry rate profiles is unity).

This study shows that the proppant pack is generally cleaned up and the cleanup lengths are close to designed lengths in relatively short times. Although gas is entering along entire fracture, fracturing fluid remains in the formation near the fracture. The water saturation distribution affects the gas entry rate profile, which determines the effective fracture length. Subtle changes in the gas rate entry profile can result in significant changes in effective fracture length. The results I derived from this work are consistent with prior work, namely that greater fracture conductivity results in more effective well cleanup and longer effective fracture lengths versus time. This study provides better explanation of mechanisms that affect fracturing fluid cleanup, effective fracture length, and well productivity than previous work.

To my wonderful sisters, Olivia and Eunike, and brothers, Daniel and Samuel

The fear of the LORD is the beginning of knowledge [Proverbs 1:7]

ACKNOWLEDGEMENTS

I would like to express my sincere gratitude to:

- Dr. Duane A. McVay, chair of my advisory committee, for his guidance, support, and patience throughout the course of this research. Without his help, this dissertation would not exist.
- Drs. Stephen A. Holditch, Akhil Datta-Gupta, and Robert Berg for serving as members of my advisory committee, and for their strong support of my research topic. I especially thank Dr. Holditch for his critical suggestions regarding the content of this dissertation.
- Mr. Stephen K. Schubarth for providing field data and input particularly with the modeling technique.
- Dr. Tom Blasingame for his assistance with the model validation using pressure transient and production analyses during the early phase of this research.
- Dr. W. John Lee for his participation in the final defense of this work.
- The management of Norton Proppants Inc. for their support of this research.
- The faculty and staff of the Harold Vance Department of Petroleum Engineering, Texas A&M University for the computing and printing facilities used in this work.

TABLE OF CONTENTS

LIST OF FIGURES

FIGURE Page

FIGURE Page

FIGURE Page

FIGURE Page

FIGURE Page

FIGURE Page

LIST OF TABLES

CHAPTER I
INTRODUCTION

To develop low permeability gas reservoirs, wells normally require hydraulic fracturing. This method usually involves pumping a large volume of fracturing fluid mixed with propping agents or proppants to create a long and highly conductive fracture. Following this treatment, the well productivity typically increases as reflected by increased gas flow rates and ultimate well recovery. In some cases, low-permeability gas wells produce less than predicted after a fracture treatment. One of the reasons for less-than-expected performance is that fracture lengths achieved are less than designed lengths. These short apparent fracture lengths can result from excessive height growth, tip screen out, poor proppant transport, proppant flowback, or a combination of these factors. However, they can also be attributable to insufficient polymer degradation where the fracturing fluid cleans up very slowly. Unfortunately, the calculated fracture lengths from pressure buildup tests or production data analysis may not represent the actual propped lengths, as both techniques often use inappropriate reservoir/well models. That is to say, the calculated fracture lengths from the these methods are often less than designed lengths, even after a large amount of proppant has been injected or fracture treatment models indicate a longer propped fracture. Thus, it is necessary to find the reasons and the factors responsible for short calculated propped lengths.

The use of water-based fluid pumped with proppant is widely accepted as an effective and economical procedure in hydraulic fracture treatments, especially in tight gas reservoirs. This fracturing fluid leaks off into the formation during the fracture treatment. After the treatment, some of this fluid is produced, and some remains in the formation reducing the relative permeability to gas in the invaded zone. Field data often show that the fracturing fluid cannot readily be removed from the proppant pack and the invaded zone around the fracture within days or weeks. In severe cases, the fluid can cause damage to the formation resulting in a significant reduction in formation permeability at the face of the fracture. In any event, the presence of fracturing fluid in the proppant pack and formation can prevent propped fractures from achieving optimal stimulation.

A review of over 150 fracture treatments in Moxa Arch Frontier formation wells in the Green River Basin, southwestern Wyoming, was conducted in this work. Hydraulic fracture treatments in this formation started in the late 1970's.[1] The initial stimulations in the late 1970's consisted of water-based fluids and 20/40 mesh sand with sporadic use of other fluids (emulsions and oil based) and sintered bauxite.

This thesis follows the style and format of the *Journal of Petroleum Technology*.

While some wells were successful, the production history of other wells did not show the type of production decline associated with stimulated tight gas sands. This unexpected production response was later incorrectly attributed to formation clay swelling and damage caused by the water-based fracturing fluids. This conclusion led to the use of CO_2 foam and Intermediate Strength Proppants (ISP) in the fracture treatments in the late 1980's.[2,3] Due to the poor performance of the CO_2 foam treatments, the fracture treatments returned to water-based fluids and sand proppants in early 1992. The poor performance of the CO_2 foam treatments was attributed to ineffective proppant placement, which resulted in wide and short fractures.[1] In late 1992, the fracture treatments in the Frontier formation were re-evaluated. At this time, the operator used cross-linked gels and ISP proppants. It was believed that even though the ISP treatments (with CO_2 foam) had been tried prior to 1992, they were tried in such a way that significant conductivity increases over sand was not achieved. As a result, the operator was more aggressive with gel breakers and proppant concentration in an attempt to increase the in-situ fracture conductivity above the historically achieved values. The cross-linked gel and ISP treatments after 1992 were considered successful, resulting in significant increases in gas production from the Moxa Arch Frontier formation.

Fig. 1.1 shows the performance of the ISP versus sand treatments in the Moxa Arch Frontier formation based on the fracture treatments conducted after 1992.[2,3] The reservoir permeability was obtained from production data analysis. The effective fracture length was calculated using the following equation: $(L_f)_{\text{eff}} = wk_f/31.4k$ where wk_f is the estimated proppant conductivity achieved. In Fig. 1.1, the portion of the fracture that cleans up was assumed to have a dimensionless fracture conductivity (C_r) of 10. The data in Fig. 1.1 indicate that, for a given formation permeability, the effective fracture length for the ISP treatments is longer than that for the sand treatments. Greater effective stimulation and improved well productivity for the ISP treatments were attributed to the fact that the ISP treatments resulted in greater fracture conductivities and, thus longer effective fracture lengths.

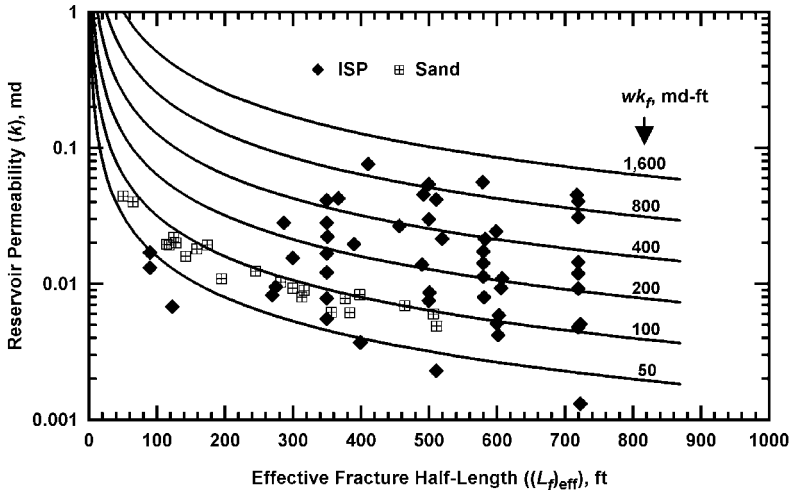

Fig. 1.1—A comparison of estimated effective fracture lengths for ISP versus sand treatments.

In this work I used reservoir simulation to study the effect of fracture conductivity on fracture fluid cleanup and effective fracture length. I simulated the water saturation and pressure distribution around a propped fracture, tracked the gas production along the length of the propped fracture, and quantified the effective fracture lengths. There are various ways that the effective fracture length can be described. In this work, the effective fracture length is described as (1) cleanup length, (2) effective length, and (3) apparent length. For this study the "cleanup" fracture length is the fracture length corresponding to 90% cumulative gas flow rate into the fracture. The "cleanup" length is what I determine by direct observation of our simulation results. The "effective" fracture length is the fracture length under single-phase flow conditions that gives similar performance as for multiphase flow conditions. The "effective" fracture length is what engineers get from single-phase flow methods (e.g., pressure buildup tests, production data analysis, etc.). And finally, I define the "apparent" length as the fracture length in which the ratio of the multiphase gas rate profile to the single-phase gas rate profile becomes unity. The use of each terminology will be given under the simulation results chapter.

In the remainder of this dissertation I summarize the previous studies pertinent to our work (Chapter II) and then describe the methodology used (Chapter III). The results of this work are presented in Chapter IV. Chapter V summarizes the accomplishments achieved in this work and presents explanations concerning the results derived from this work. Finally, based on the results of this work, in Chapter VI, I present the conclusions and recommendations which allow operators to better design optimal fracture treatments for typical gas reservoirs.

CHAPTER II
LITERATURE REVIEW

In this chapter I present the prior literature upon which I have based my present work. This literature review was necessary to summarize what has been done and, more importantly, what has not been done to address the problem concerning fracture fluid cleanup and effective fracture length. At the end of this chapter I discuss the need for this research and, present the objectives of this work. My literature review focused on the following major topics:

- Fracture fluid cleanup
- Fracture fluid degradation
- Post-fracture treatment evaluation

2.1 Fracture Fluid Cleanup

The productivity of hydraulically fractured gas wells is often less than optimal because of the presence of fracturing fluid in the fracture and formation around the fracture. This fluid reduces the relative permeability to gas in the invaded zone around the fracture and, in some cases, may damage the formation resulting in a significant reduction in formation permeability at the face of the fracture. The effect of fracturing fluid on the productivity of a gas well was first studied by Tannich.[4] He suggested that gas enters the fracture near the wellbore if the fracture conductivity is low and concluded that the effective fracture length and well productivity will be decreased. **Fig. 2.1** shows a schematic of cleanup model presented by Tannich. The figure illustrates that flow is initiated near the wellbore first and, then the fracturing fluid cleans up gradually out along the fracture as the production continues.[4] Tannich concluded that the productivity of a fractured well will increase with time as the fracturing fluid is removed because the effective fracture length is increasing. His study showed that one-half of the fracturing fluid injected is generally recovered within 2 to 6 days. As such, he concluded that if the relative conductivity of the fracture is high, as in most tight gas reservoirs, damage from residual fracture fluid in the formation is not critical and does not limit stimulation, primarily because the surface area of the fracture is large. He also concluded that cleanup proceeded slower if the fracture fluid viscosity is high. His cleanup model, however, does not take into account capillary forces in the reservoir, closure stress effects, and/or area of possible damage around the fracture (i.e., due to clay swelling, fine migration, etc.).

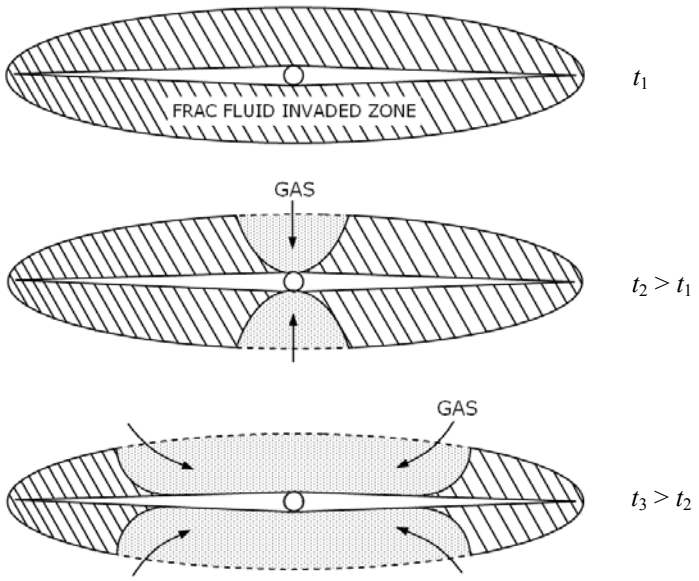

Fig. 2.1—Schematic of cleanup model after Tannich.[4]

Soliman and Hunt[5] used numerical simulation to investigate the effects of fracture conductivity (wk_f), fracture half-length (L_f), and capillary pressure (P_c) on fracture fluid cleanup. Their study showed that the gas breakthrough into the fracture occurs near the wellbore if the fracture conductivity is low and it occurs at the tip of the fracture if the fracture conductivity is high. They concluded that fracture fluid cleanup is directly related to fracture conductivity and proposed that the optimum fracture conductivity necessary to clean up the invaded zone should be much higher than that necessary to produce the reservoir. These authors proposed a dimensionless fracture conductivity (C_r) value of 40 to recover the fracturing fluid effectively. However, Soliman and Hunt did not consider non-Darcy flow effect, mobile reservoir water, and damage around the fracture.

Montgomery[6,7] studied factors that affect fracture fluid cleanup in hydraulically fractured wells. In his cleanup model, the fracture fluid leaked off as far as 7 ft into the reservoir. He investigated the effect of dimensionless fracture conductivity (C_r) values ranging from 0.001 to 100 on fracture fluid cleanup. He found that when the fracture conductivity is extremely low, the well behaves more like a well producing under radial flow conditions. However, when the fracture conductivity is high, the water and gas production occurs along the propped length evenly. He concluded that the optimum C_r value is 10 when considering the cumulative gas and water production. According to this paper, a temporary water block to gas flow into the fracture may occur after the fracture treatment, but only at early times.

Berthelot *et al.*[8,9] investigated the effects of post-fracture operating procedures on well productivity. Their study showed that the depth of fracture fluid invasion is 3 to 7 ft around the created fracture. One of their recommendations was the well should be placed on a smaller size choke (4/64" to 8/64") while the fracture is cleaning up in order to reduce proppant crushing so that a maximum volume of fracturing fluid around the fracture may be cleaned up prior to significant crushing of the proppant. Once the fracture has cleaned up, the well may be placed on a larger choke and the gas may be produced without being blocked by water; thus maximizing the effectiveness of the propped fracture.

Robinson *et al.*[10,11] presented two field cases where severe crushing and proppant flowback occurred as a result of flowing the well at high rates in an attempt to produce more gas or oil after the fracture treatment. They suggested that drastic reductions in fracture conductivity particularly near the wellbore often occur during well cleanup. Their conclusion was even when the correct proppant is selected for a particular well, severe damage can occur as a result of rapid increases in closure stress. As such, slow and controlled flowback procedures will minimize proppant crushing and proppant flowback into the wellbore.

The effect of damage around the fracture associated with the leakoff fracturing fluid has been reported.[12-15] This type of damage is commonly referred to as fracture face damage. While the results of the previous work are often contradictory; single-phase models showed that damage around the fracture up to 90% has minor effect on well productivity unless the damage extends several inches deep and reduces the formation permeability by a factor of a thousand or more. Holditch[13] studied the combined effects of damage, relative gas permeability reduction, and capillary pressure increase in the damaged zone on gas productivity. According to Holditch, the damage zone around the fracture can sometimes act like a water sink that traps water and blocks gas flow. He found that no serious water block occurs if the absolute reservoir permeability is not reduced and concluded that damage in the fracture is more important than damage around the fracture. However, if the fracturing fluid does cause damage on the formation permeability, severe reduction in gas production may occur particularly in low-pressure, water-sensitive reservoirs when the degree of damage and the level of capillary pressure in the damaged zone increase significantly.

Fox[14] used a single-phase, 2D simulator to investigate the effect of damage in and around the fracture on the long-term gas productivity. His study indicated that only minor effects on cumulative gas production are experienced at the end of a fifteen-year production period. Adegbola and Boney[15] recently conducted a study to determine the effect of fracture face damage on well productivity. They found that fracture face damage up to 90% resulted in a skin value of less than 0.0005 for low permeability gas wells. Accordingly, they concluded that damage around the fracture due to leakoff fluid has small effect on the productivity of the low permeability gas wells. However, the work of Adegbola and Boney was based on the assumption that damage through the fracture face is only caused by fluid saturation changes. They did not consider the capillary pressure increases in the damaged zone.

Schubarth *et al.*[16] proposed that there is a direct relationship between fracture conductivity and fracture fluid cleanup. **Fig. 2.2** shows a schematic that illustrates an ineffective fracture fluid cleanup after production.[16] They suggested that the portion of the fracture that does clean up will have a dimensionless fracture conductivity (C_r) value of 10 when considering just the length that cleaned up. Using this assumption, they used a simple relationship between fracture half-length, fracture conductivity, and formation permeability to estimate the "effective" fracture half-length (Eq. 2.1 and Eq. 2.2). Eq. 2.2 shows that the greater the fracture conductivity (wk_f), the longer the effective fracture length. While the fracture fluid recovery increases with increasing fracture conductivity, this empirical solution (Eq. 2.2) may not accurately predict the "true" effective fracture length. This is because the effective fracture length is also affected by such factors as capillary phase trapping in the reservoir and viscosity of the leakoff fluid in the invaded zone.

$$C_r = wk_f / \pi L_f k \quad \text{.....(2.1)}$$

Assuming $C_r = 10$,

$$(L_f)_{\text{eff}} = wk_f / 31.4\, k \quad \text{.....(2.2)}$$

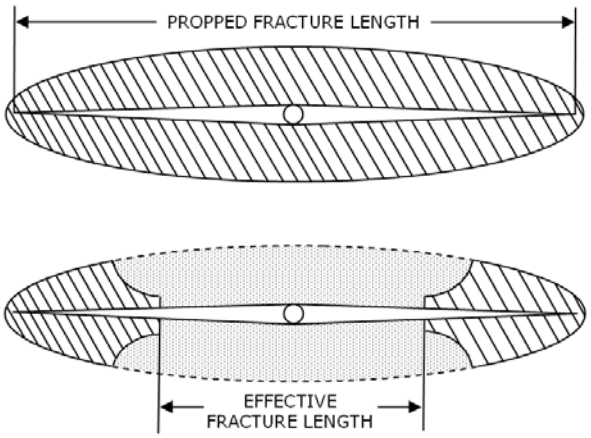

Fig. 2.2—Top view of ineffective fracture fluid cleanup,[16] $(L_f)_{\text{eff}} = wk_f/31.4k$.

2.2 Fracture Fluid Degradation

During the fracture treatment, a large volume of fluid is injected into the reservoir. Its main functions are to open the fracture and to transport the proppant along the length of the fracture. Therefore, the viscous properties of the fluid are usually considered the most important. Successful fracture treatments require that fracturing fluids should degrade rapidly after the treatment to allow the fluid to be easily removed from the formation and to prevent plugging the proppant pack with high viscous fluids.[17-23]

The parameters known to affect the degree of damage due to fracturing fluids include polymer type and concentration, crosslinking, fluid loss additive concentration, breaker concentration, and reservoir temperature.[24-29] Brannon and Pulsinelli[24] performed a laboratory study to investigate the proppant-pack permeability damage due to fracturing fluids. The study showed that gelling agents used in hydraulic fracture treatment are concentrated within the proppant-pack because the molecular sizes of the gelling agents are too large to be able to penetrate into the matrix of the formations during fluid leakoff. These gels reduce the in-situ permeability of the proppant packs. Their conclusion was that sufficient breaker concentrations are needed in the fracture treatment to reduce the fluid viscosity effectively.

Davidson *et al*.[25] presented results of intense quality control operations on 54 hydraulic fracture treatments in several geographic locations including Texas, Alabama, and Wyoming. They concluded that a low-viscosity fluid system with poor proppant transport properties will allow proppant to settle into the bottom of the fracture, reducing the amount of proppant placed across the pay interval, thus reducing fracture length and fracture conductivity. A fracture fluid that is too viscous can create a wide fracture, reducing the propped fracture length and, increase the amount of time for the fracture to clean up. They go on to say that it is critical for the polymer and chemical additives to be blended in the proper ratio because this mixing procedure will have impacts on the fracture geometry achieved. Even if the chemical additives are blended in the proper ratios, problems can occur if the additives are contaminated. They also concluded that fracture fluid viscosity measured in field could be a few thousand centipoises greater than the published values. Accordingly, design engineers must be cautious when choosing a fluid and predicting fracture geometry and proppant transport based on the published viscosity values.

Rahim *et al*.[26] investigated the effect of viscosity degradation on the fracture geometry in hydraulically fractured, low permeability reservoirs. They reported that designs with uncontaminated buffer result in higher cumulative gas production than those with a buffer contaminated with a borate crosslinker [Buffering agents are required in most fracture fluid systems to control gel hydration, crosslinking, and overall fluid stability]. Their study showed that cumulative gas production, based on published viscosity values, is too optimistic compared with the cumulative gas production based on measured viscosity data. This is because the highly viscous fluid from the actual measurements creates a taller and wider fracture and much of the proppant is carried to the non-productive intervals, whereas the design fluid based on published viscosity values yields less fracture height growth and increases the propped length.

Voneiff *et al*.[30] used a three-phase, 2D simulator to investigate the effects of unbroken fracture fluid on gas well performance. Their model consisted of formation gas, formation water, and unbroken fracture fluid. The fracture leakoff fluid was treated as the same phase as the formation water. The gel remaining in the proppant pack after closure was assigned as the third phase. The reservoir was assumed to have only two phases initially (gas and water) with the third phase (fracture fluid in the proppant pack) injected during the fracture treatment. The viscosity of the unbroken gel was assumed to be constant (i.e., Newtonian fluid

properties), for example 1,000 cp, 10,000 cp, and 15,000 cp. They found that the effective fracture length increases with time as the propped fracture cleans up. Their work also indicated that the unbroken fracture fluid could delay fracture fluid cleanup by weeks or months and flatten the gas production. **Fig. 2.3** portrays the performance of several hydraulic-fractured gas wells completed in the Frontier formation.[1,30] This type of production profile was attributed to the presence of unbroken fracture fluid in the proppant pack.

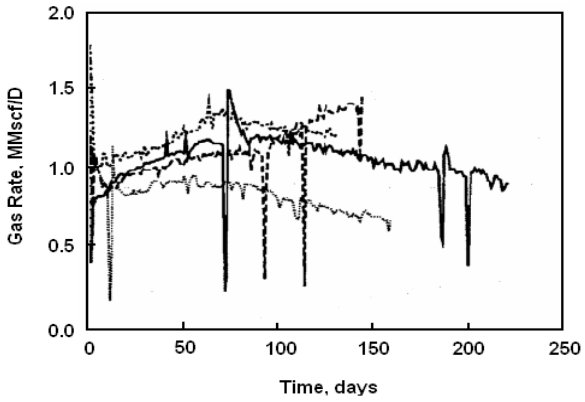

Fig. 2.3—Examples of production influenced by slow fracture fluid cleanup.[1,30]

A study by Cooke[31] indicated that the rock permeability will be in a range such that the polymer residue will be trapped in the fracture. Yet, some recent work suggested that polymer residue may leak off into the formation and is trapped in the invaded zone around the fracture. Siddiqui *et al.*[32] reported that a significant amount of polymer residue may come in contact with the reservoir rock during the fracture treatment. Based on tests conducted on core samples, they found some of the gel residue is present in the rock and cannot be displaced instantly by production; it degrades and is removed slowly. This residue occupies the pore spaces of the rock and reduces the rock permeability. They concluded that the structure and mineralogy of the formation rock play significant role in determining the amount of gel residue in the formation. It was found that the core plug with consolidated morphology exhibited less gel damage, whereas the core plug with lose and unconsolidated morphology showed higher degree of damage. Their work indicated that a certain portion of the gel residue (as high as 25%) remains in the core plug and cannot be recovered by cleanup process.

2.3 Post-Fracture Treatment Evaluation

To optimize the performance of hydraulically fractured, low permeability gas wells, reliable estimates of fracture length and fracture conductivity achieved are essential. A number of methods to estimate these parameters have been proposed in the literature.[33-57] In this section, I briefly summarize the previous work

and the current techniques used to determine the fracture and reservoir properties using the post-fracture treatment data.

Johansen[33] used a radial grid system, two-phase, 2D model to investigate the effect of fracture fluid on pressure transient data. In his model, the fracture was represented by an effective wellbore radius equal to half of the fracture half-length. The fracture fluid leakoff was modeled by manually inputting a water-saturated zone around the fracture. The well was produced for 1, 3, 6, and 12 months prior to fourteen and sixty day pressure buildup tests. He found that the analysis of the pressure buildup test after one-month cleanup resulted in calculated fracture lengths and conductivities that are significantly less than the actual values because the fracture fluid has not cleaned up completely. He concluded that several months of fracture fluid cleanup may be needed to ensure good estimates of fracture length, fracture conductivity, and formation permeability.

Lee and Holditch[34] presented the results of pressure transient analysis from 13 hydraulic-fractured, low-permeability gas wells. They discussed the major strengths and weaknesses of analysis methods including Horner analysis, linear flow analysis, type curves, and finite difference reservoir simulator. Their study showed that calculated fracture half-lengths average only 5% to 11% of the designed lengths, while fracture lengths determined from reservoir simulation history matching average about 68% of the designed lengths. Holditch *et al.*[35] and Gist[36] proposed an iterative technique to determine formation permeability, fracture length, and fracture conductivity. They used a semi-log graph of the buildup data and a square root of time graph of the buildup data. It was concluded that the iterative technique works best on high conductivity fractures because the correct straight line on the square root of time graph is reached at early times. For low conductivity fractures, the correct straight line is not obtained during the pressure buildup tests. These authors[34-36] advocated an independent measurement of formation permeability in order to calculate the "correct" fracture length using pressure transient analysis in hydraulic-fractured, low permeability wells.

The integration of available data such as well test, production data, fracturing data, well log, and core data is necessary in evaluating the fractured wells. Elbel and Ayoub[37] presented a variety of reasons for apparent shorter fracture lengths. Insufficient shut-in time, cleanup effects, use of homogeneous model when layers with high-permeability contrast exist, and non-Darcy flow effects are some of the reasons identified causing an apparent shorter fracture. They concluded that incorrect estimates of fracture length and fracture conductivity could lead to modifications of fracturing treatment designs that may or may not result in improved well productivity. Therefore, a proper identification of the models or techniques used in the evaluation of a fractured well is critical.

Barre *et al.*[38] used different methods (e.g., pressure buildup, production analysis, and fracture treatment evaluation) to determine effective fracture lengths from a low-pressure, tight-gas reservoir in the Rocky Mountain Region. The discrepancy in the analysis results was attributed to non-Darcy and multiphase

flow, and model applicability (i.e., infinite or finite fracture conductivity type curves). They proposed an empirical method for predicting the effective fracture lengths from proppant conductivity data. The procedure involved matching the observed bottomhole flowing pressure and gas flow rate history using the proppant pack conductivity data after accounting for conductivity losses due to non-Darcy flow, filter-cake, gel residue, multiphase flow, and tip plugging caused by insufficient pressure gradient to initiate cleanup. In the example cases presented, the apparent fracture lengths under non-flowing conditions, accounting for only static damage mechanisms such as width loss to filter-cake and spalling, are 12 to 20% of the designed lengths. The apparent fracture lengths under flowing conditions, accounting for all of the conductivity losses, are only 3% of the designed values. While this method was based on laboratory work performed at StimLab, the calculated fracture lengths may not be representative of the "true" effective length. [In Chapter IV, I will show that the entire propped length is generally effective within a reasonable amount of time for typical low permeability gas wells.]

Several other authors[39-42] reported that turbulence and fracture closure should be considered in the analysis of pressure buildup or drawdown data. If substantial non-Darcy flow occurs in the fracture, the calculation of fracture length using conventional techniques will result in values that are far too small. Hresko[39] suggested that if the fracture conductivity is high (C_r is greater than 1,000), non-Darcy flow has no effect on pressure drawdown and buildup type curve shapes. However, if the C_r value is less than 1,000, the solutions with non-Darcy flow are different from the solutions considering only Darcy flow. Holditch[40,41] and Alvarez *et al*.[42] concluded that non-Darcy flow in the fracture is the cause of the calculated fracture length that is significantly less than the designed length even after a long period of shut-in times. They suggested that non-Darcy flow should be considered in the analysis of drawdown tests, pressure buildup tests, and history matching of fractured gas wells. If substantial non-Darcy flow occurs in the fracture, the calculated fracture lengths using conventional techniques are less than designed lengths.

2.4 Research Objectives

Uncertainty in calculation of effective fracture length still exists despite various analysis techniques for fractured wells proposed in the literature. This dilemma often creates problems when trying to optimize a fracturing treatment program. If we used the incorrect values of fracture lengths from the available methods, the next fracture treatment designs will likely be incorrect. There has not been a single method that provides consistently correct estimates of the effective fracture length. In addition, almost all of the previous studies used single-phase models, which limit their applicability for multiphase flow.[33-55]

The relationship between fracture conductivity, fracturing fluid production, and effective fracture length has not been thoroughly discussed in the literature. The conventional wisdom in tight gas reservoirs is often too general (not specific); for instance, increasing fracture conductivity will lead to increased gas productivity because the fracture fluid recovery increases. A great number of studies have determined the effective fracture lengths by analysis of pressure transient and production data. However, none has tried to

model or simulate this problem and determine the effective fracture lengths by direct observation of the simulation results.

My research was aimed to gain a better understanding of the relationship between fracture conductivity, fracture fluid production, and effective fracture length. The state of the art when this study began was that the performance of hydraulic fractured wells is often less than optimal because the effective fracture length is less than designed values. This research is necessary to answer questions such as: Is there a better model that can predict the effective fracture length? What are the factors that most affect the effective fracture length? By knowing the factors that most affect the effective fracture length, we can design a better treatment for typical gas reservoirs.

The overall objectives of this research were:

- Determine the effect of fracture conductivity on fracture fluid production and effective fracture length.
- Resolve discrepancies between effective fracture length from design, buildup, and production analyses.
- Simulate fracturing fluid cleanup behavior and determine the factors that most affect fracture fluid production and gas productivity.
- Provide recommendations for future fracture treatments. A better understanding of the fluid production behavior will lead to better design which will reduce costs resulting from poorly designed fracture treatments.

CHAPTER III
METHODOLOGY

This chapter outlines the simulation technique used in this work. The reservoir and fracture properties used in this study were chosen after reviewing fracture treatment data from over 150 wells in the Moxa Arch Frontier formation, southwest Wyoming. This data set was provided by Norton Proppants Inc. and consists of injected fluid and estimated leakoff volume, average fluid viscosity, fracture gradient, reservoir permeability, pore pressure, and proppant concentration. In addition, I also used published data on tight gas wells that have exhibited slow cleanup after fracture treatment. The latter data was primarily based on previous studies[6,8,58-75] conducted at Texas A&M University. The reservoir simulator used in this research is capable of handling parameters such as non-Darcy and multiphase flow, closure stress effect, and damage around the fracture.

3.1 Reservoir and Fracture Properties

The basic reservoir and fracture properties used in this study are presented in **Table 3.1**. The initial reservoir pressures are 6,000 psia ("high" pressure cases) and 2,325 psia ("low" pressure cases). The effective permeability to gas investigated varies from 0.005 to 0.1 md (tight gas reservoirs). The values of fracture conductivity (wk_f) simulated range from 31.25 to 500 md-ft (i.e., $0.12 < C_r < 159$). Since I have no relative permeability and capillary pressure data from the Moxa Arch Frontier formation, I used the published relative permeability and capillary pressure data[6,8] from an east Texas tight gas reservoir. **Fig. 3.1** and **Fig. 3.2** show the relative permeability data used for the fracture and reservoir, respectively. The fracture relative permeability is represented by two 45° lines with the water relative permeability becoming zero at a 5% water saturation. The irreducible water saturation is assumed to be 40% in the reservoir.

Table 3.1—Basic Reservoir and Fracture Parameters

Drainage area (A), acres	640
Formation depth (D), ft	10,000
Initial reservoir pressure (p_i), psia	2,325 and 6,000
Reservoir net thickness (h), ft	100
Formation permeability (k), md	0.005-0.1
Reservoir porosity (ϕ), %	10
Reservoir temperature (T), ^{o}F	150
Water saturation (S_w), %	40
Rock compressibility (c_f), psi-1	4.0x10-6
Water compressibility (c_w), psi-1	3.26x10-6
Gas specific gravity (γ_g)	0.6
Fracture half-length (L_f), ft	200, 500, 800
Fracture width (w_f), ft	0.014
Fracture conductivity (wk_f), md-ft	31.25-500

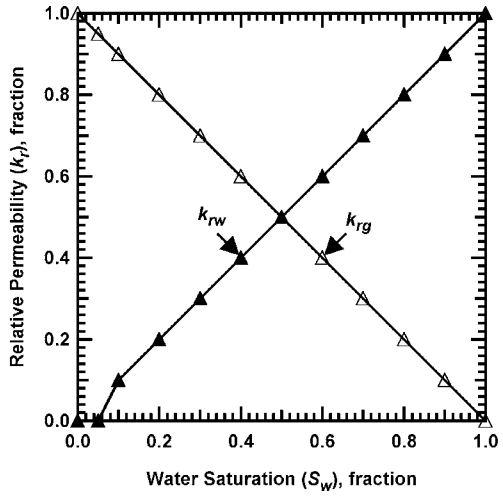

Fig. 3.1—Relative permeability curves for the fracture.[6,8]

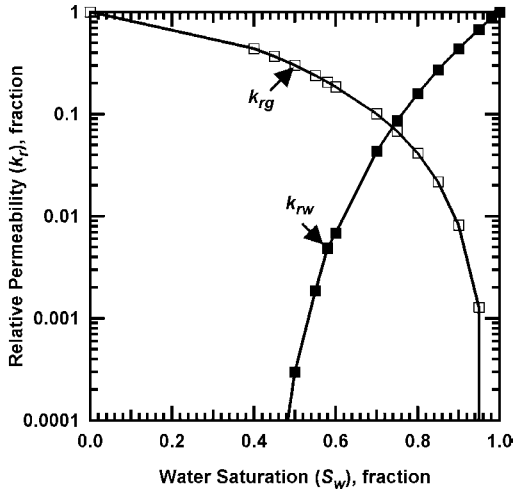

Fig. 3.2—Relative permeability curves for the reservoir.[6,8]

Fig. 3.3 shows the capillary pressure data used for the reservoir. This data was chosen after reviewing the work of Holditch.[13] The capillary forces in the fracture are assumed to be negligible. Fracture permeability reduction versus closure pressure is simulated assuming 20/40 mesh InterProp proppant. Changes in fracture permeability with closure pressure for this proppant type are shown in **Fig. 3.4**; where k_f is the permeability of the fracture at a given closure pressure and k_a is the fracture permeability at zero closure pressure.

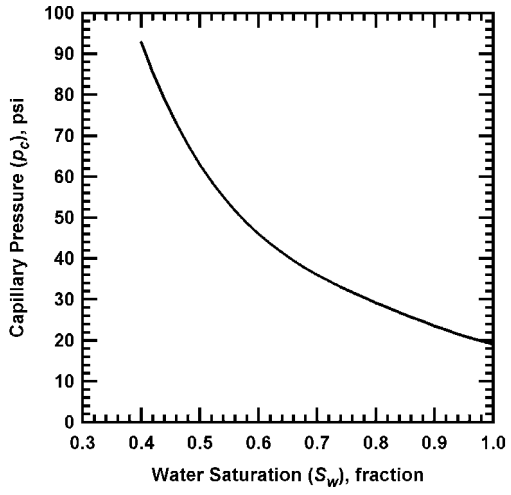

Fig. 3.3—Capillary pressure data for the reservoir.[13]

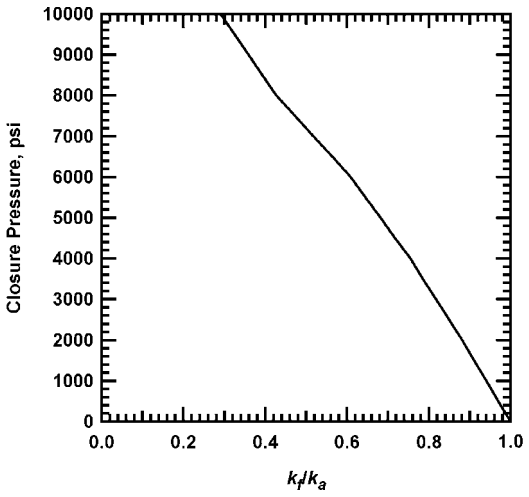

Fig. 3.4—Closure pressure versus change in fracture permeability for 20/40 InterProp proppant.

3.2 Fractured Well Model

Fig. 3.5 shows a schematic of the fractured well model used in this study. In our modeling, the fracture extends an equal distance on both sides of the wellbore and fully penetrates the vertical extent of the formation. The width of the fracture is assumed to be constant (0.014 ft) from the wellbore to the tip, while the porosity of the fracture is 30%. The model is single-layer, two-dimensional, and consists of two-phase (gas/water) flow. The reservoir is assumed to be homogeneous, horizontal, and isotropic. Only one-fourth of the square drainage area is modeled due to the symmetry of the system investigated.

To accurately model bottomhole pressure response in the wellbore, a large well constant/index is used in grid cell (1,1,1) such that the pressure in that cell represents the wellbore pressure. **Table 3.2** shows typical grid cell sizes used. Grid cell dimensions in the *x*-direction are varied such that the grids in the plane along the fracture are very small at the wellbore, increase towards the middle of the propped fracture half-length, decrease until the tip of the propped fracture, increase again towards the middle of the length between the propped fracture tip and the created fracture tip, decrease again until the tip of the created fracture, and then increase to the model boundary. In this study, the fracture length that is propagated during the fracture treatment is referred to as the "created" fracture length. The length supported by proppant after the fracture closes is defined as the "propped" fracture length. I assumed that the created fracture lengths are 50% greater than the propped fracture lengths. The total grid cells are 7,500 (150x50x1).

The model was verified by back-calculating the input parameters using pressure transient analysis. For validation I used single-phase models with Darcy flow only. I found that proper selection of time steps and grid-cell sizes is key to validating the simulated reservoir and fracture properties with pressure transient analysis.[76]

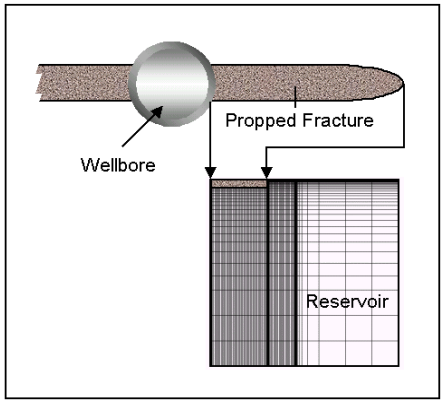

Fig. 3.5—Plan view of a hydraulically fractured reservoir model.

Table 3.2—Typical Grid Cell Sizes for A Case with L_f of 800 ft and w = 0.014 ft

Δx: 0.001 0.002 0.004 0.008 0.016 0.032 0.064 0.128 0.256 0.489 1. 1.8 2.8 3.4 2*5. 2*10. 36*20. 2*10. 2*5. 3.4 2.8 1.8 1. 0.489 0.256 0.128 0.064 0.032 0.016 0.008 0.004 0.002 2*0.001 0.002 0.004 0.008 0.016 0.032 0.064 0.128 0.256 0.489 1. 1.8 2.8 3.4 2*5. 2*10. 16*20. 2*10. 2*5. 3.4 2.8 1.8 1. 0.489 0.256 0.128 0.064 0.032 0.016 0.008 0.004 0.002 2*0.001 0.002 0.004 0.008 0.016 0.032 0.064 0.128 0.256 0.489 1. 1.8 2.8 3.4 5. 10. 20. 40. 80. 160. 5*180. 215.

Δy: 0.007 0.01 0.015 0.02 0.025 0.03 0.04 0.05 0.06 0.07 0.08 0.09 0.1 0.2 0.4 0.8 1. 2. 3. 4. 5. 6. 7. 8. 9. 10. 12. 14. 16. 18. 20. 25. 30. 35. 40. 45. 50. 60. 70. 80. 90. 100. 120. 140. 160. 180. 200. 3*359.334

3.3 Fracture Fluid Leakoff

Fracture fluid leakoff is simulated by injecting water at a constant pressure into cells representing the created fracture, which initially have zero water saturation. The injection pressures are 8,500 psi ("high" pressure cases) and 3,325 psi ("low" pressure cases). The fracture leakoff fluid is treated as the same phase as the water formation (i.e., water-based fracturing fluids). The water is injected first into the cell representing the wellbore, then the injection continues progressively outward until the tip of the created fracture. This injection technique represents the fracture growth and leakoff versus time during the hydraulic fracture treatment. The water is injected for 3 to 6 hours. The amount of water injected for given formation permeabilities and propped fracture lengths is presented in **Fig 3.6**. This plot shows that a higher permeability reservoir has a greater volume of water leaked off into the formation than a lower permeability reservoir. Likewise, the amount of water leaked off into the formation for a long fracture is greater than that for a short fracture. This leakoff volume is representative of the typical amount of the fracturing fluid leaked off during the fracture treatments in the Moxa Arch Frontier formation. At the end of the injection, I recorded the saturation and pressure distributions for use at the start of the succeeding stage. I investigated the effects of fracture conductivity and fracture fluid viscosity on the effective fracture length by varying the fracture permeability and water viscosity at the end of the injection.

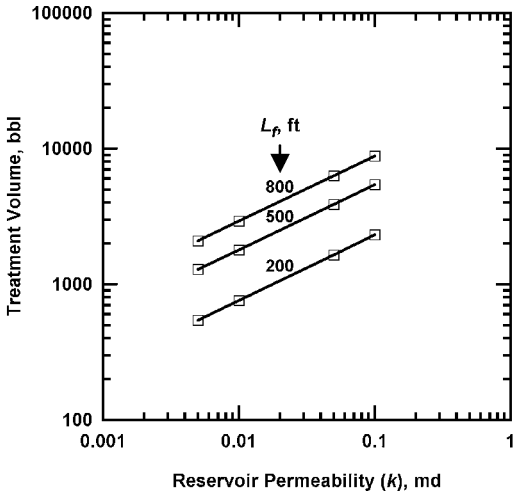

Fig. 3.6—Treatment volume as a function of fracture half-length and reservoir permeability.

The effect of unbroken fracture fluid was simulated by assuming that the formation water is immobile at all times. By varying the viscosity of the water namely 1, 50, 200, and 1,000 cp at the end of the injection, I assumed that the fracture fluid viscosity is constant after the treatment (i.e., Newtonian fluid properties). Except where noted, the well is producing at a constant gas rate of 1 MMscf/D and is subject to a minimum bottomhole pressure of 1,000 psi.

3.4 Non-Darcy Flow Modeling

In this work I considered non-Darcy flow effect in the fracture. At high fluid velocities, the pressure drop in the proppant pack increases more than the proportional increase in velocity. Forchheimer[77] proposed that the pressure gradient is the sum of the viscous forces ($\mu v/k$) and the inertial forces ($\beta\rho v^2$),

$$\Delta p/\Delta L = \mu v/k + \beta \rho v^2 \quad \text{.....(3.1)}$$

where β is referred to as beta factor or non-Darcy coefficient which is essentially a measure of the tortuosity of the flow path. For single-phase flow in the presence of irreducible water saturation, Geertsma[78] proposed the following equation for β:

$$\beta = 48511.34\ (k_g)^{-0.5}\ [\phi\,(1 - S_w)]^{-5.5} \quad \text{.....(3.2)}$$

where β is in 1/ft and k_g is effective gas permeability in md.

For multiphase flow, Frederick and Graves[79] proposed the following correlation for β:

$$\beta = 7.89 \times 10^{10}\ (k_g)^{-1.60}\ [\phi\,(1 - S_w)]^{-0.404} \quad \text{.....(3.3)}$$

This correlation was derived from laboratory measurements on core samples with permeabilities ranging from 0.00197 to 1,230 md. I used this correlation (Eq. 3.3) in modeling the non-Darcy flow in the fracture. Again, β is in 1/ft and k_g is effective gas permeability in md.

3.5 Fracture Face Damage Modeling

I modeled damage around the fracture by reducing the absolute formation permeability at a variety of degrees of damage near the created fracture face (**Fig. 3.7**). In this study, the capillary pressure in the damaged zone is increased to model the impact of formation permeability reduction due to damage. **Fig. 3.8** portrays the capillary pressure curves used for the fracture face damage investigations.

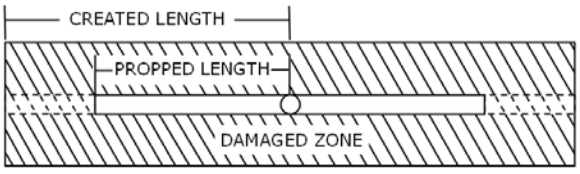

Fig. 3.7—Simulation of damaged zone along the created fracture.

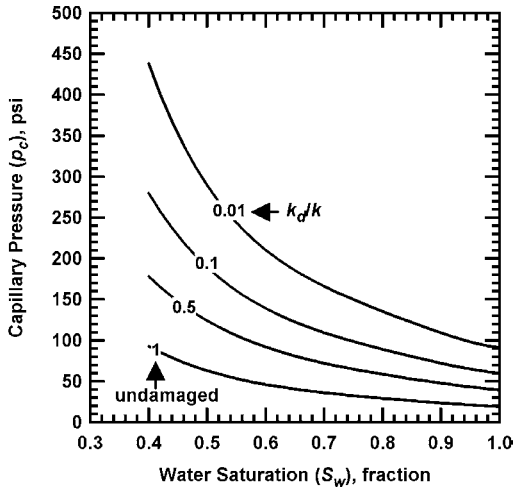

Fig. 3.8—Capillary pressure data used for the fracture face damage investigations.

CHAPTER IV
SIMULATION RESULTS

In this work, I have systematically investigated the effect of fracture conductivity on fracture fluid production and effective fracture length. The results of this investigation are presented in this chapter. The distribution of gas flow rate into the fracture and the percentages of the total gas being produced between each point and the wellbore cell were plotted. I analyzed the water saturation, the reservoir pressure, and the effective gas permeability profiles in the invaded zone after the fracture treatment and determined the effective fracture lengths by direct observation of the simulation results.

While the focus of this study was to determine the effect of fracture conductivity on the effective fracture length and gas productivity, I also investigated the effects of the following parameters on the fracture fluid production and effective fracture length: 1) actual propped length, 2) fracture fluid viscosity, 3) fracture closure effect, and 4) damage around the fracture. These factors can usually be controlled to some extent during the fracture treatment. The reservoir conditions affecting the fracture fluid production and effective fracture length are 1) formation permeability, 2) reservoir water mobility, 3) capillary forces, and 4) non-Darcy flow. These are the variables that engineers cannot influence. In this chapter, I present the results of our investigations for both single-phase and multiphase cases.

4.1 Single-Phase Simulation

4.1.1 Darcy Flow Cases

In this section, I present the profiles of cumulative gas flow rate into the fracture as a function of fracture conductivity (wk_f), formation permeability (k), and actual fracture half-length ($(L_f)_{actual}$) for cases with single-phase and Darcy flow only. **Fig. 4.1** through **Fig. 4.5** portray the profiles of cumulative gas flow rate into the fracture versus distance along the fracture for cases with wk_f of 500, 250, 125, 62.5, and 31.25 md-ft, respectively. For these runs, I assumed that the actual fracture half-length is 800 ft and the formation permeability is 0.01 md. The production time varying from 1 day to 365 days is shown in these graphs. Fig. 4.1 illustrates that when the wk_f is 500 md-ft (C_r = 19.89), 90% of the gas entering the fracture will occur 713 ft from the wellbore at 1 day. In comparison, when the wk_f is 31.25 md-ft (C_r = 1.24), 90% of the gas entering the fracture will occur 407 ft from the wellbore at 1 day (Fig. 4.5). Fig. 4.1 through Fig. 4.5 show that fracture conductivity affects the distribution of the gas flow rate along the propped fracture. The entire propped fracture will be accessible for gas flow quicker when the fracture conductivity is high. Note that the results presented in Figs. 4.1 to 4.5 are applicable for single-phase and Darcy flow only. I conclude that the entire propped length will be effective within a few days for the single-phase and Darcy flow cases. This is all due primarily to pressure transient effects.

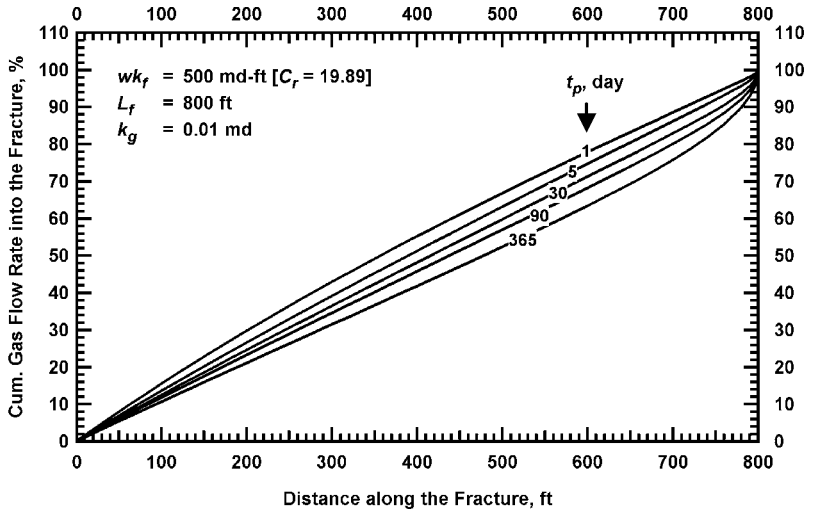

Fig. 4.1—Cumulative gas flow rate into the fracture versus distance along the fracture for a single-phase case with wk_f = 500 md-ft, L_f = 800 ft, and k_g = 0.01 md.

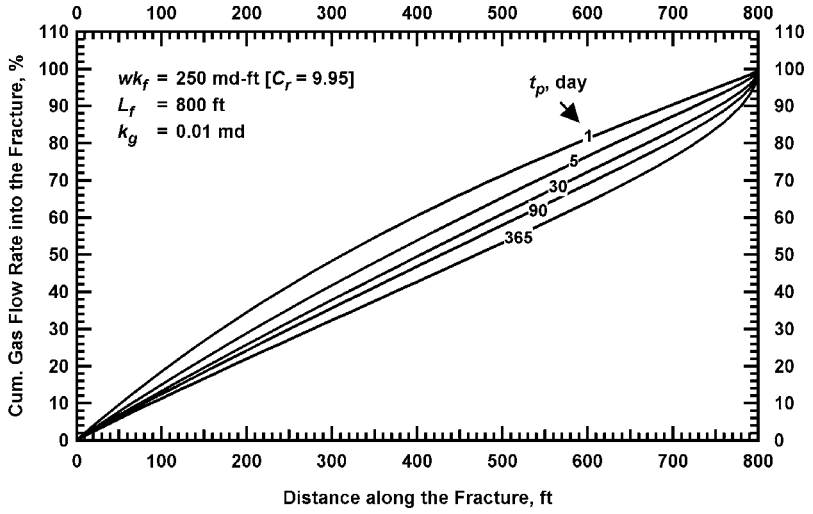

Fig. 4.2—Cumulative gas flow rate into the fracture versus distance along the fracture for a single-phase case with wk_f = 250 md-ft, L_f = 800 ft, and k_g = 0.01 md.

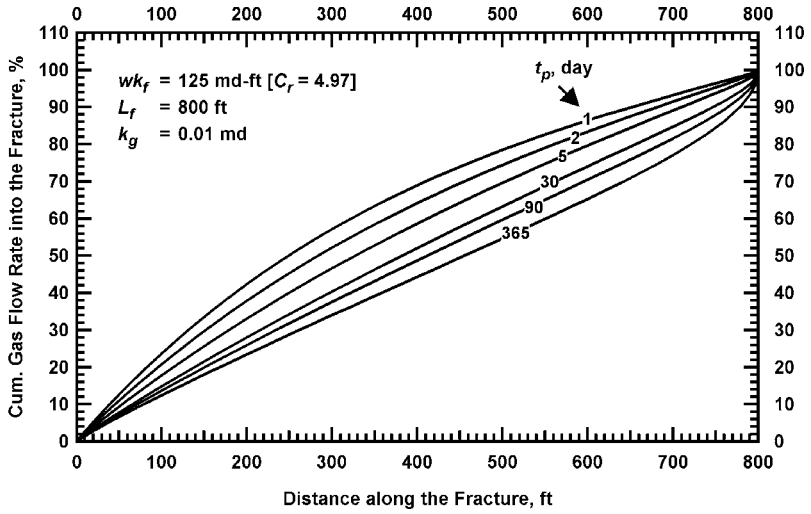

Fig. 4.3—Cumulative gas flow rate into the fracture versus distance along the fracture for a single-phase case with wk_f = 125 md-ft, L_f = 800 ft, and k_g = 0.01 md.

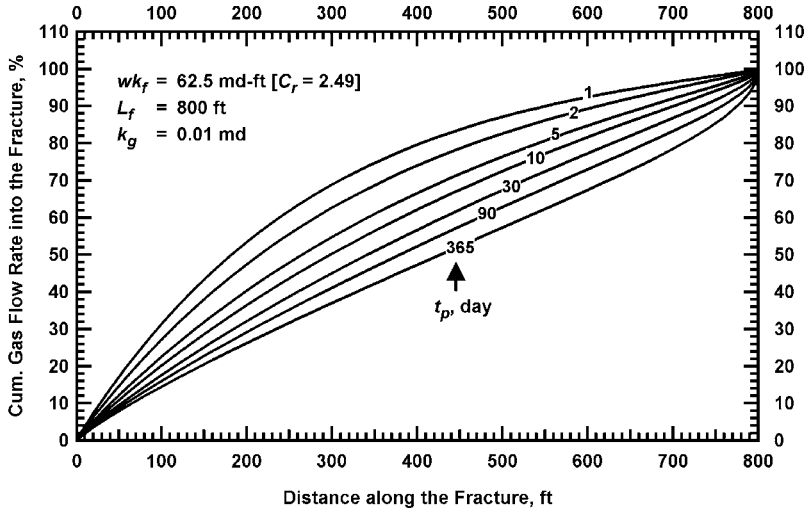

Fig. 4.4—Cumulative gas flow rate into the fracture versus distance along the fracture for a single-phase case with wk_f = 62.5 md-ft, L_f = 800 ft, and k_g = 0.01 md.

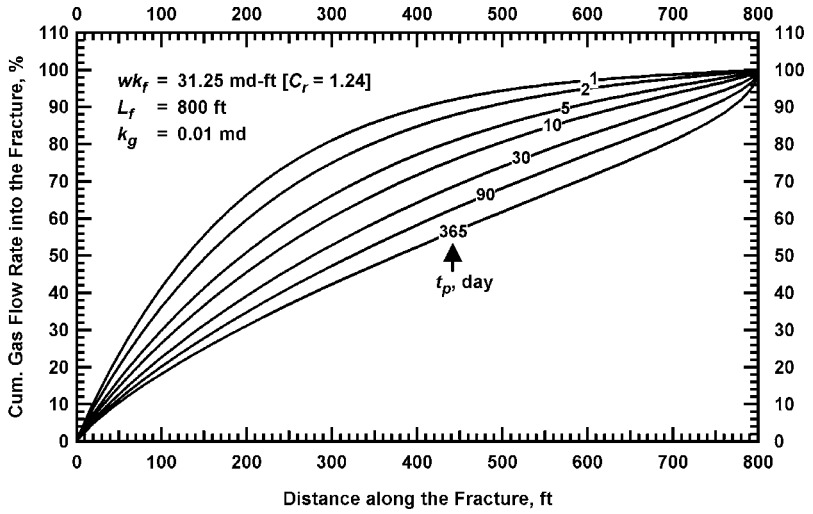

Fig. 4.5—Cumulative gas flow rate into the fracture versus distance along the fracture for a single-phase case with wk_f = 31.25 md-ft, L_f = 800 ft, and k_g = 0.01 md.

An effort was made to quantify the effective fracture length in hydraulically fractured gas wells as a function of time. Previous empirical model[16] suggests that the effective fracture half-length is proportional to wk_f and $1/k$

$$(L_f)_{\text{effective}} \approx wk_f / k \quad \text{.....(4.1)}$$

Dividing Eq. 4.1 by $(L_f)_{\text{actual}}$ on both sides of the equation gives

$$\frac{(L_f)_{\text{effective}}}{(L_f)_{\text{actual}}} \approx \frac{wk_f}{k}\frac{1}{(L_f)_{\text{actual}}} \quad \text{.....(4.2)}$$

Eq. 4.2 shows that the ratio of effective fracture half-length to actual fracture half-length is proportional to wk_f and inversely proportional to k and $(L_f)_{\text{actual}}$. There are various ways that effective fracture length can be described. The effective fracture length is often described as the fracture length obtained from pressure buildup tests or production data analysis. For this study the effective fracture length is described as (1) cleanup length, (2) effective length, and (3) apparent length.

I define the "cleanup" length as the fracture length corresponding to 90% cumulative gas flow rate into the fracture. For instance, the cleanup fracture half-length is 713 ft (89% of the actual fracture half-length) at 1 day for the case shown in Fig. 4.1 and 407 ft (51% of the actual fracture half-length) at 1 day for the case shown in Fig. 4.5. In this work, the "effective" length is the equivalent fracture length under single-phase flow conditions that gives similar performance as the actual propped fracture under multiphase conditions (i.e., same wk_f). Later, I define the "apparent" length as the fracture length in which the ratio of the

multiphase gas rate profile to the single-phase gas rate profile becomes unity. The use of the "effective" and "apparent" lengths will be given under the multiphase simulation section.

Fig. 4.6 portrays the ratio of the cleanup fracture half-length to the actual fracture half-length, $(L_f)_{cleanup}/(L_f)_{actual}$, versus time for the cases presented in Figs. 4.1 to 4.5. The $(L_f)_{cleanup}/(L_f)_{actual}$ approaches unity as the invaded zone is cleaned up and the entire propped length becomes accessible for gas flow. Fig. 4.6 indicates that the ratio of the cleanup fracture half-length to the actual propped length is close to unity at 1 day for the case with wk_f = 500 md-ft (C_r = 19.89). However, the ratio of the cleanup fracture half-length to the actual fracture half-length becomes unity after 100 days if the wk_f = 31.25 (C_r = 1.24). This reduced and changing cleanup length for the single-phase cases is due to transient flow in the fracture and reservoir. Transient flow effects are faster (i.e., cleanup length is greater), when fracture conductivity is high. The cleanup length increases as the fracture conductivity (wk_f) increases. Note that I assumed there is no damage in and/or around the fracture for these cases. Also, we have not considered multiphase flow. The entire propped fracture is generally cleaned up within 365 days for all conductivities presented in Fig. 4.6; the difference is the time required.

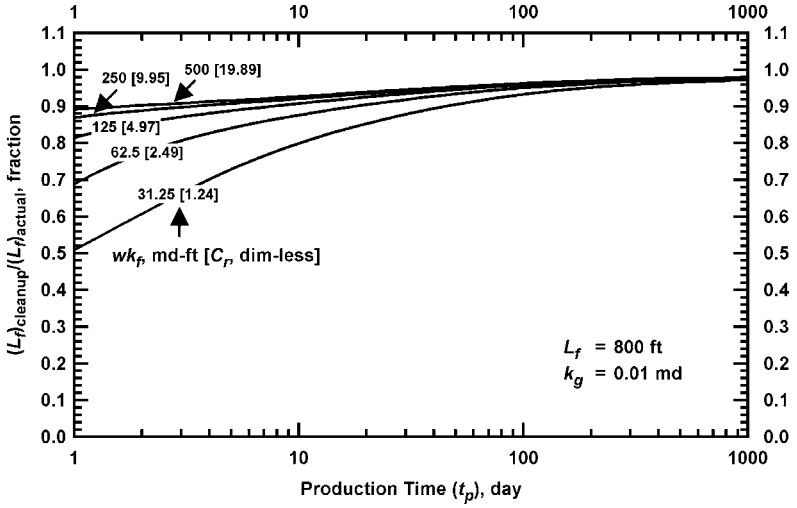

Fig. 4.6—Ratio of cleanup fracture half-length to actual fracture half-length for single-phase and Darcy flow cases with L_f = 800 ft and k_g = 0.01 md.

Next, I present the effect of formation permeability on the cleanup length. **Fig. 4.7** and **Fig. 4.8** show the ratio of the cleanup fracture half-length to the actual fracture half-length versus time for the cases where the formation permeabilities are 0.05 and 0.1 md, respectively. Again, the $(L_f)_{actual}$ is 800 ft for these cases. Recall that when the wk_f is 31.25 md-ft (C_r = 1.24), the cleanup length is 51% of the actual propped length at 1 day for the case shown in Fig. 4.6 (k = 0.01 md). For the same conductivity (wk_f is 31.25 md-ft), the cleanup length is 34% of the actual propped length at 1 day if the k = 0.05 md (Fig. 4.7) and only 29% of the actual propped length at 1 day if the k = 0.1 md (Fig. 4.8).

Assuming the fracture conductivity is constant, the resultant C_r value is much lower when the formation permeability is higher. For instance, if the wk_f = 31.25 md-ft, L_f = 800 ft, and k = 0.01 md, the C_r value is 1.24 and decreases to 0.25 and 0.12 if the formation permeabilities are 0.05 and 0.1 md. These results suggest that the cleanup length is more a function of C_r than formation permeability. Recall that C_r is nothing else but the ratio of the fluid flow capacity along the fracture relative to that delivered by the reservoir. When the formation permeability is higher, the capacity of the reservoir to deliver fluid increases, while the capacity of the fracture to handle the fluid is held constant. Fig. 4.8 shows that the ratio of the cleanup fracture half-length to the actual fracture half-length may not reach unity after a long time if the C_r value is extremely low (e.g., C_r = 0.12). Accordingly, the cleanup length is affected directly by the wk_f and is inversely proportional to 1/k. Greater wk_f means greater C_r, which results in better well cleanup.

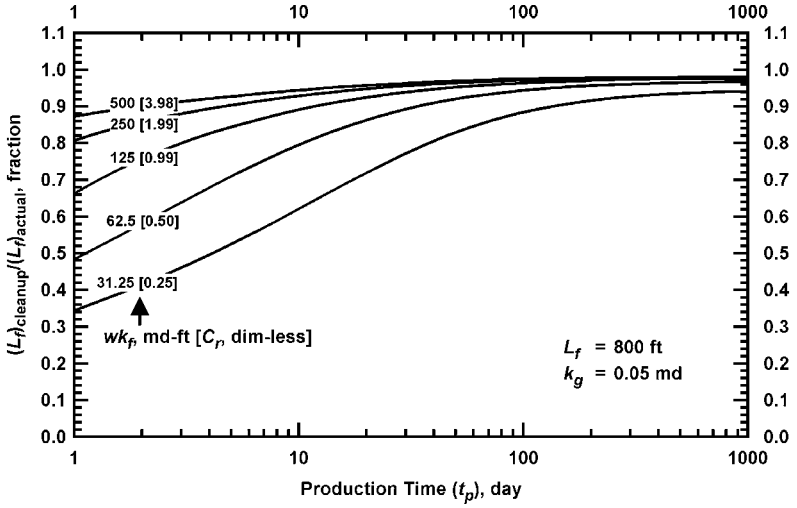

Fig. 4.7—Ratio of cleanup fracture half-length to actual fracture half-length for single-phase and Darcy flow cases with L_f = 800 ft and k_g = 0.05 md.

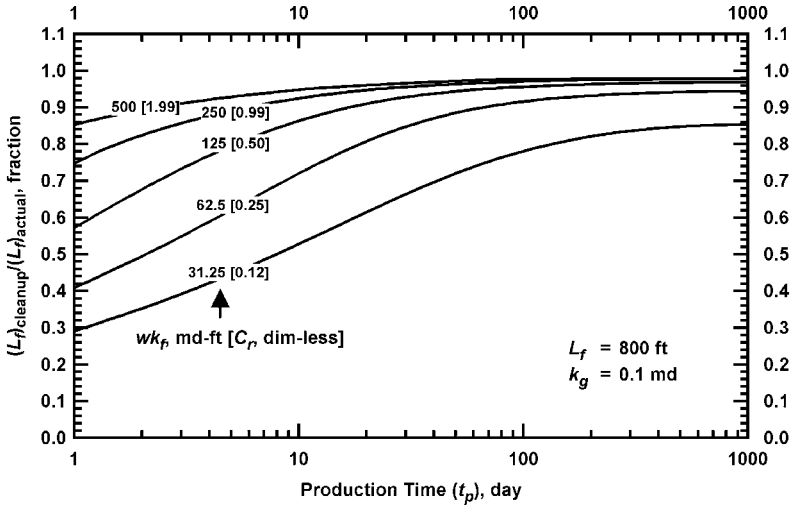

Fig. 4.8—Ratio of cleanup fracture half-length to actual fracture half-length for single-phase and Darcy flow cases with L_f = 800 ft and k_g = 0.1 md.

As noted previously (Eq. 4.2), the ratio of the cleanup fracture half-length to the actual fracture half-length is inversely proportional the $(L_f)_{actual}$. The cleanup length is 29% of the actual propped length at 1 day for the case shown in Fig. 4.8 if the wk_f = 31.25 md-ft, L_f = 800 ft, and k = 0.1 md. For this case, the cleanup length is 46% of the actual propped length at 1 day if the L_f = 500 ft (**Fig. 4.9**) and 89% of the actual fracture length at 1 day if the L_f = 200 ft (**Fig. 4.10**). Therefore, the ratio of the cleanup fracture half-length to the actual fracture half-length increases as the actual fracture half-length decreases.

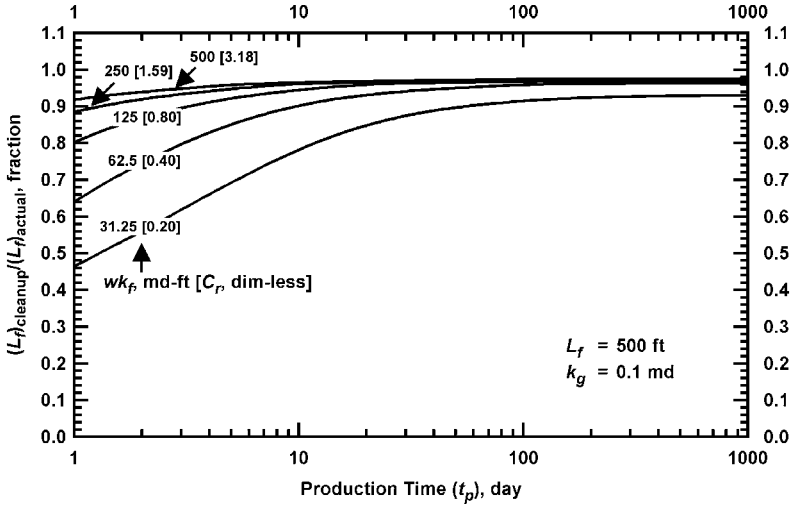

Fig. 4.9—Ratio of cleanup fracture half-length to actual fracture half-length for single-phase and Darcy flow cases with L_f = 500 ft and k_g = 0.1 md.

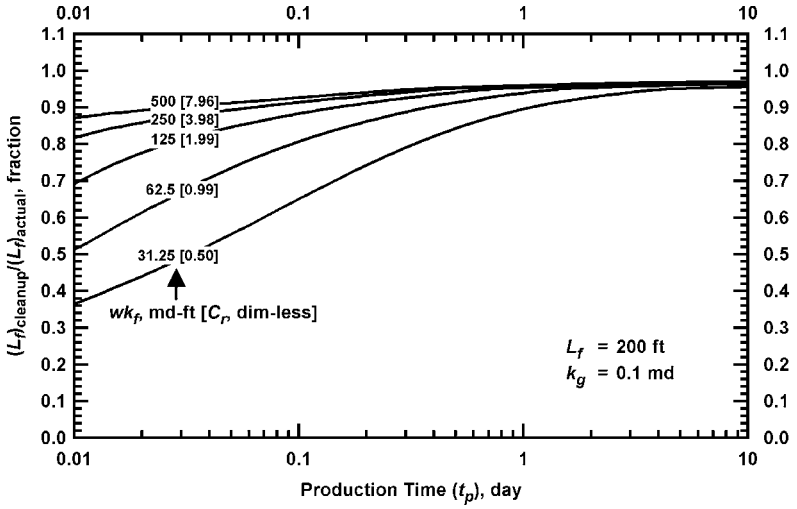

Fig. 4.10—Ratio of cleanup fracture half-length to actual fracture half-length for single-phase and Darcy flow cases with L_f = 200 ft and k_g = 0.1 md.

Now, I have shown that there is a relationship between cleanup length, fracture conductivity, formation permeability, and actual fracture length (Eq. 4.2). Our next question is: Are there other factors that affect the cleanup length?

4.1.2 Non-Darcy Flow Cases

In this section, I present the effect of fracture non-Darcy flow on the cleanup length. The ratio of the cleanup fracture half-length to the actual fracture half-length versus time for the single-phase and non-Darcy flow cases is presented in **Fig. 4.11**. The cleanup fracture length is 38% of the actual propped length at 1 day when the wk_f = 31.25 md-ft (C_r = 1.24) for the case shown in Fig. 4.11. This value is slightly lower than that presented in Fig. 4.6 for the case with Darcy flow only in which the cleanup length is up to 51% of the actual propped length at 1 day.

When the fracture non-Darcy flow is present, the pressure drop in the fracture increases. As a result, more gas enters the fracture near the wellbore because the bottomhole flowing pressure is reduced to a minimum. Fig. 4.11 shows that the cleanup length may be reduced significantly particularly at early times if the non-Darcy flow effect in the fracture is significant. For instance, in Fig. 4.11, the ratio of the cleanup fracture half-length to the actual fracture half-length becomes unity after 365 days if the wk_f = 31.25 md-ft (C_r = 1.24). This emphasizes the need for higher wk_f values to reduce the impact of non-Darcy flow in the fracture. Again, multiphase flow effects have not been included in these cases.

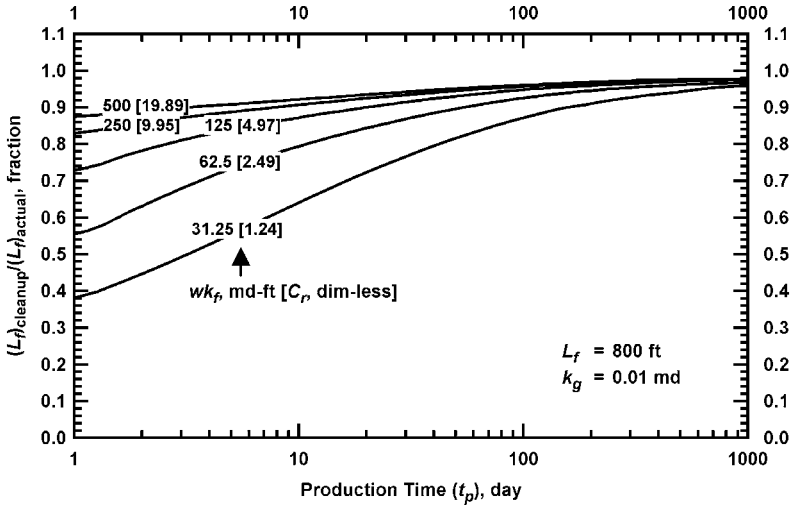

Fig. 4.11—Ratio of cleanup fracture half-length to actual fracture half-length for single-phase and non-Darcy flow cases with L_f = 800 ft and k_g = 0.01 md.

4.1.3 Fracture Face Damage Cases

The effect of fracture face damage on the cleanup length was investigated by reducing the absolute formation permeability 0.5 ft around the fracture. For these runs, the L_f = 800 ft and k = 0.01 md. Three different scenarios, namely no damage, 50% damage, and 99% damage, were investigated. **Fig. 4.12** shows the ratio of the cleanup fracture half-length to the actual fracture half-length for the cases without fracture face damage (this plot is similar to Fig. 4.6, except that the *x*-axis scale is from 0.01 to 10 to enable comparison between cases). **Fig. 4.13** depicts the ratio of the cleanup fracture half-length to the actual fracture half-length for cases where the absolute formation permeability is reduced by 50%. Such damage could be caused by swelling clays, movement of fines, or chemical reactions between injected and formation materials.[12-15] Comparing Fig. 4.12 and Fig. 4.13, note that the ratio of the cleanup fracture half-length to the actual fracture half-length seems to be identical for both cases. Based on these results, I conclude that absolute permeability damage around the fracture up to 50% does not affect the cleanup length. **Fig. 4.14** presents the ratio of the cleanup fracture half-length to the actual fracture half-length for cases where the absolute formation permeability is reduced by 99%. For these cases, the ratio of the cleanup fracture half-length to the actual fracture half-length becomes unity faster than that for the cases without fracture face damage or with a reasonable degree of fracture face damage.

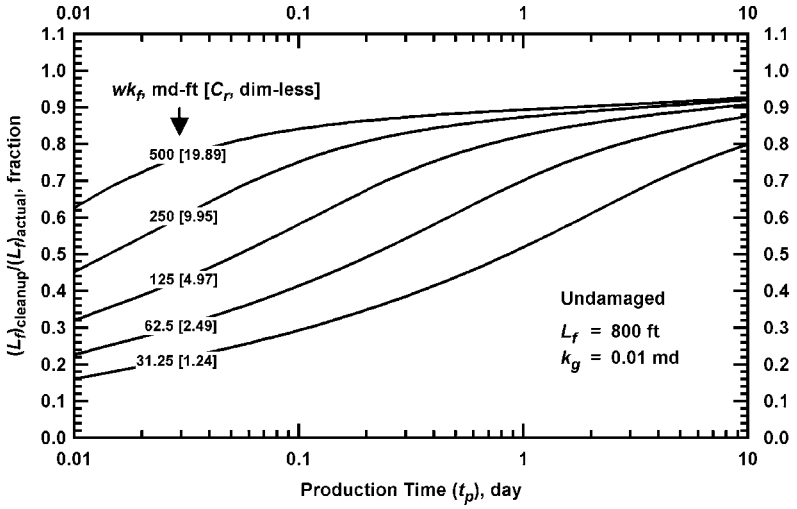

Fig. 4.12—Ratio of cleanup fracture half-length to actual fracture half-length for single-phase and Darcy flow cases without fracture face damage.

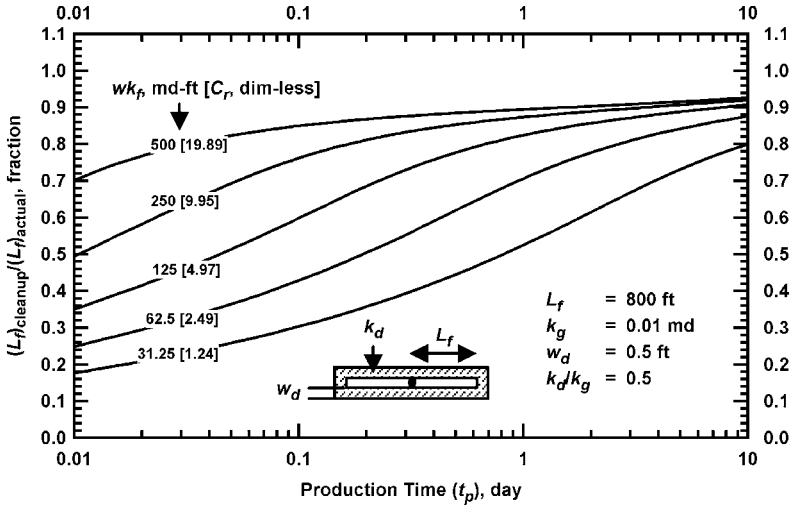

Fig. 4.13—Ratio of cleanup fracture half-length to actual fracture half-length for single-phase and Darcy flow cases with fracture face damage (k_d/k_g = 0.5).

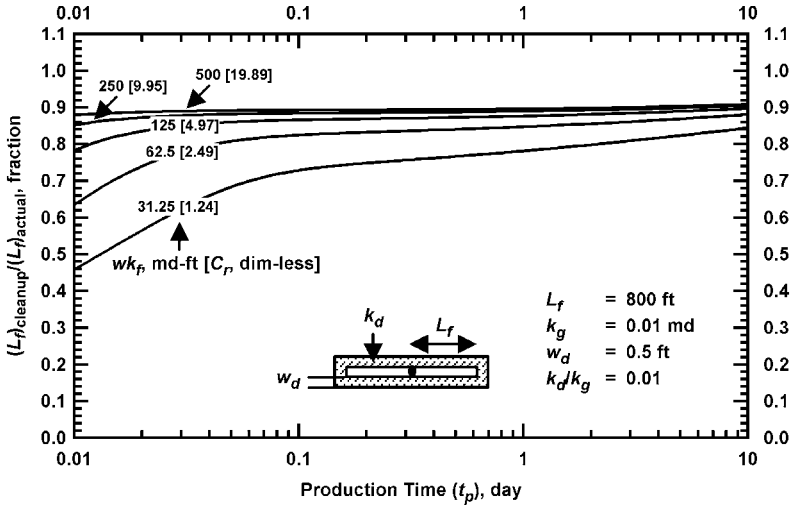

Fig. 4.14—Ratio of cleanup fracture half-length to actual fracture half-length for single-phase and Darcy flow cases with fracture face damage (k_d/k_g = 0.01).

Fig. 4.15 shows the pressure distribution in the reservoir at 1 day for the cases shown in Figs. 4.12 to 4.14. In the direction perpendicular to the fracture, the area shown in Fig. 4.15 is 2 ft into the formation. Again, the absolute reservoir permeability damage is assumed 0.5 ft around the fracture. In Fig. 4.15, I assumed that the wk_f = 500 md-ft. The pressure distribution in the reservoir for the undamaged case and 50% damage case is identical. However, when the absolute reservoir permeability is reduced by 99%, the transient flow in the formation along the fracture occurs quicker (i.e., the band of the light color along the fracture in the bottom of Fig. 4.15 indicates lower pressures in the damaged zone). This explains why the ratio of the cleanup fracture half-length to the actual fracture half-length achieves unity quicker when the absolute reservoir permeability around the fracture is reduced by 99%. Cinco and Samaniego[45] concluded that fracture face damage makes the flux distribution along the fracture more uniform. Thus, our results are consistent with the work of Cinco and Samaniego namely that the gas entry rate along the propped fracture is distributed evenly for the cases with fracture face damage.

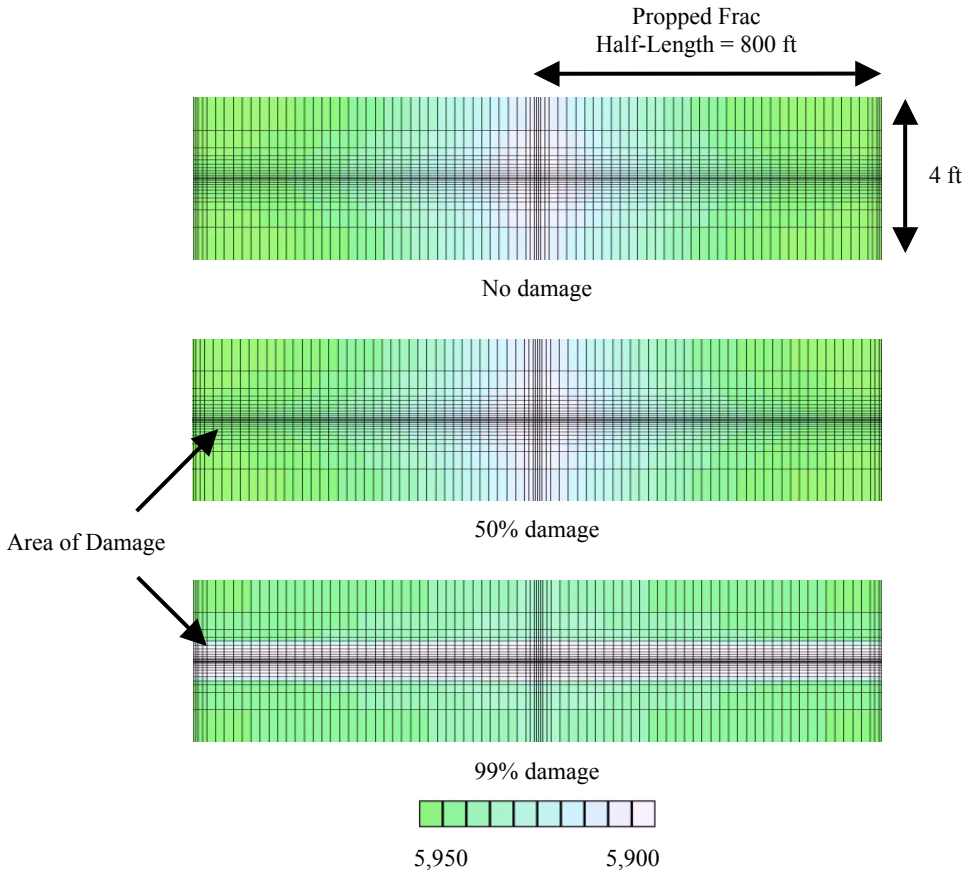

Fig. 4.15—Pressure distribution (psi) in the reservoir at 1 day for single-phase and Darcy flow cases with wk_f = 500 md-ft, L_f = 800 ft, and k_g = 0.01 md.

4.2 Multiphase Simulation

4.2.1 "High" Pressure Reservoirs

The entire propped length is practically accessible for gas flow within a relatively short period of time for all conductivities for the single-phase cases. **Fig. 4.16** through **Fig. 4.20** show the percentages of the total gas being produced along the fracture for cases with multiphase and non-Darcy flow. Again, I assumed that the L_f = 800 ft and k = 0.01 md. For all cases presented in Figs. 4.16 to 4.20, the amount of water injected is 2,923 bbls (see Fig. 3.6). The viscosity of the fluid injected is 1 cp. Fig. 4.16 indicates that, when the wk_f is 500 md-ft (C_r = 19.89), 90% of the gas entering the fracture will occur 299 ft from the wellbore at 1 day (about 37% of the actual fracture half-length), compared to 93 ft from the wellbore at 1 day (about 12% of the actual fracture half-length) for the case with the wk_f = 31.25 md-ft (C_r = 1.24) presented in Fig. 4.20.

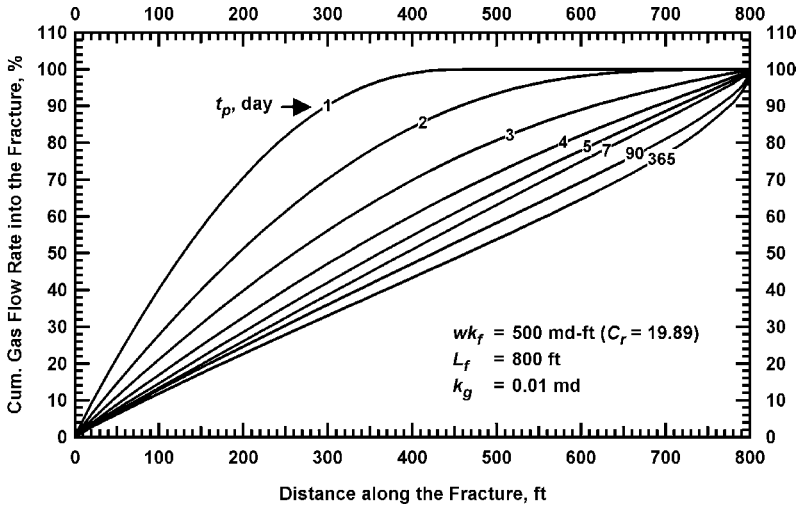

Fig. 4.16—Cumulative gas flow rate into the fracture versus distance along the fracture for a multiphase case with wk_f = 500 md-ft, L_f = 800 ft, and k_g = 0.01 md.

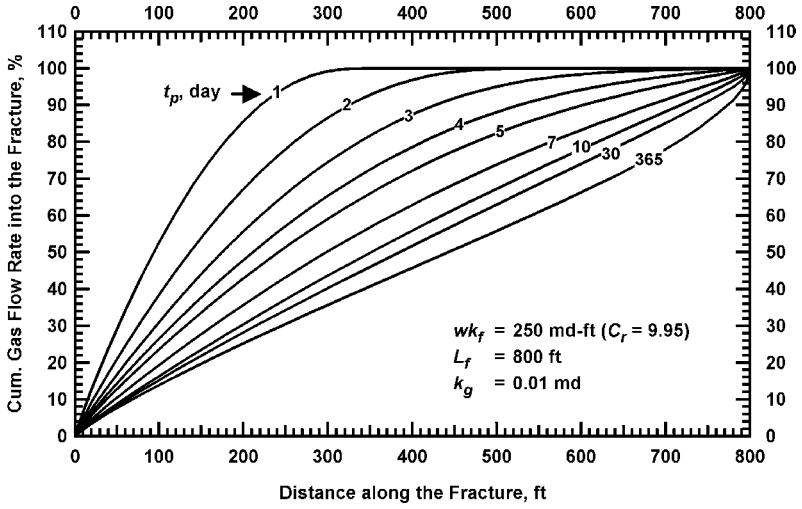

Fig. 4.17—Cumulative gas flow rate into the fracture versus distance along the fracture for a multiphase case with wk_f = 250 md-ft, L_f = 800 ft, and k_g = 0.01 md.

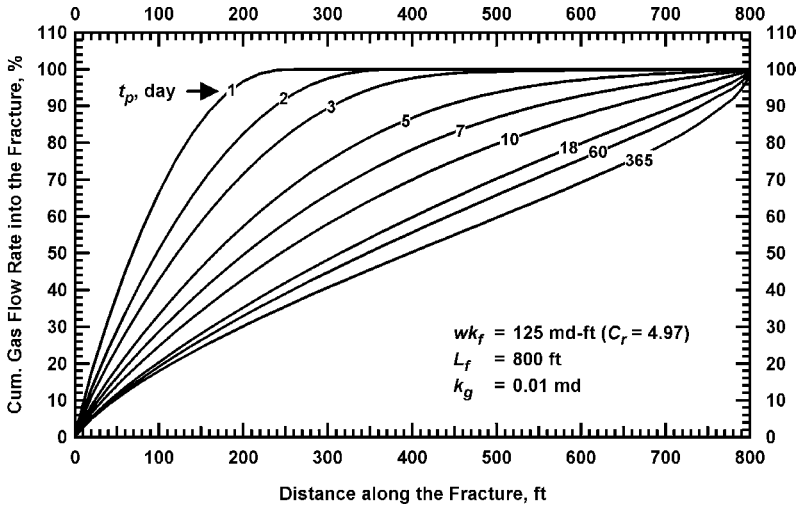

Fig. 4.18—Cumulative gas flow rate into the fracture versus distance along the fracture for a multiphase case with wk_f = 125 md-ft, L_f = 800 ft, and k_g = 0.01 md.

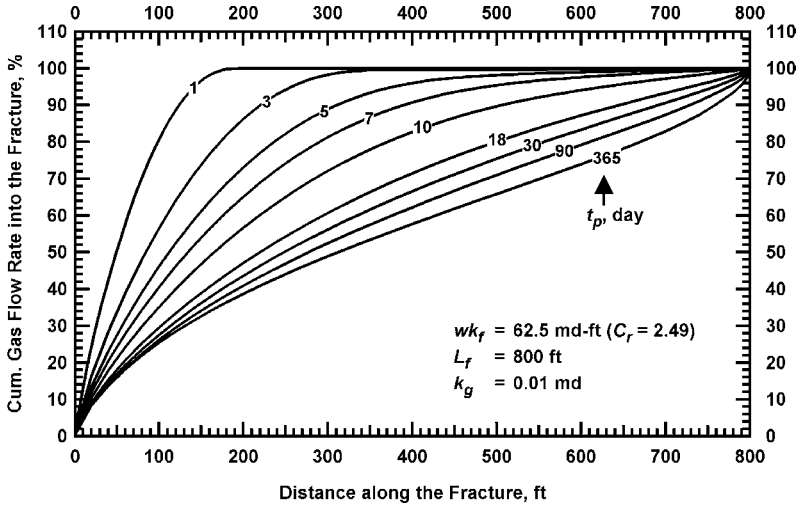

Fig. 4.19—Cumulative gas flow rate into the fracture versus distance along the fracture for a multiphase case with wk_f = 62.5 md-ft, L_f = 800 ft, and k_g = 0.01 md.

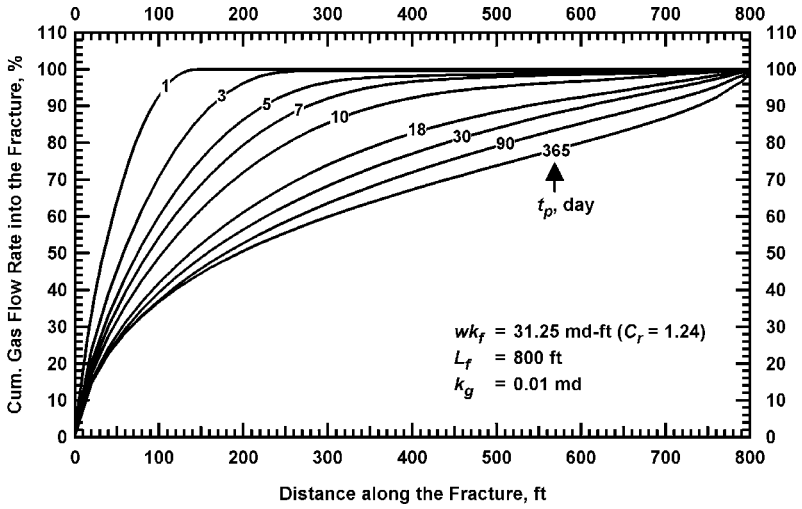

Fig. 4.20—Cumulative gas flow rate into the fracture versus distance along the fracture for a multiphase case with wk_f = 31.25 md-ft, L_f = 800 ft, and k_g = 0.01 md.

Fig. 4.21 presents the ratio of the cleanup fracture half-length to the actual fracture half-length versus time for the cases shown in Figs. 4.16 to 4.20. Recall that the ratio of the cleanup fracture half-length to the actual fracture half-length versus time when plotted on a semilog plot exhibits a smooth increase versus time for the single-phase cases (ignoring cleanup effects, Figs. 4.6 to 4.14). However, when the cleanup effects are considered, the cleanup length increases rapidly at early times, then continues to increase smoothly. This is because the resistance to gas flow is greatest at early times and decreases rapidly as the fracturing fluid is removed. Returning to Fig. 4.21, the ratio of the cleanup fracture half-length to the actual fracture half-length is 37% at 1 day and levels off after 4 to 5 days if the wk_f = 500 md-ft. If the wk_f = 31.25 md-ft, the ratio of the cleanup fracture half-length to the actual fracture half-length is 12% at 1 day and approaches unity after 365 days. Therefore, I conclude that, for a given propped length, greater fracture conductivity results in longer cleanup lengths versus time and more effective stimulation of the well.

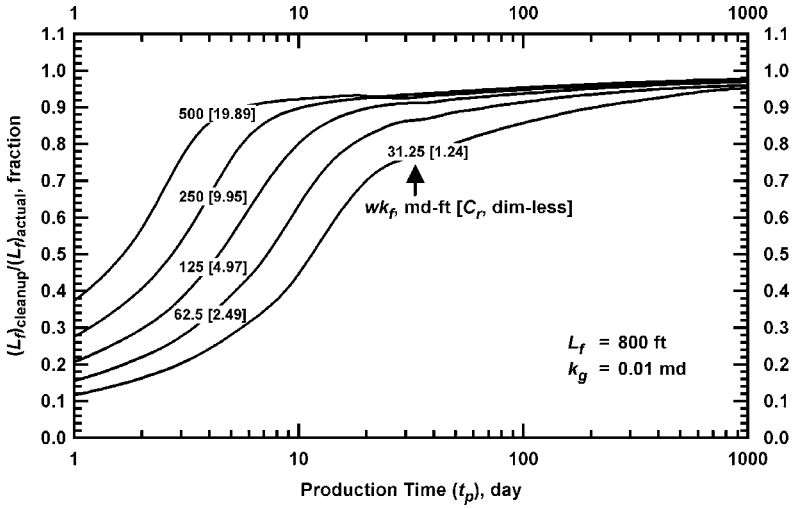

Fig. 4.21— Ratio of cleanup fracture half-length to actual fracture half-length for multiphase and non-Darcy flow cases with L_f = 800 ft and k_g = 0.01 md.

Fig. 4.22 shows the pressure distribution in the reservoir at 365 days for the cases shown in Fig. 4.21. The reservoir pressure is 6,000 psi (shown by the red color). The light color indicates low reservoir pressures. The bottomhole flowing pressure has not reached the minimum bottomhole flowing pressure (1,000 psi) at 365 days. Fig. 4.22 shows that the pressure drops are distributed evenly along the fracture when the fracture conductivity is high. As such, the fracture will drain the reservoir more effectively because the pressure drop inside the fracture is reduced to a minimum. However, when the fracture conductivity is low, the pressure drop inside the fracture is large.[76] For the latter case, the greatest pressure drops in the reservoir occur near the wellbore. Fig. 4.22 suggests that the "effective" fracture length is much different depending on fracture conductivity when considering the pressure distribution around the fracture. If the fracture conductivity is very low (e.g., $C_r < 1$), the pressure drops in the reservoir will appear to be "radial" even though the actual propped length is several hundred feet.

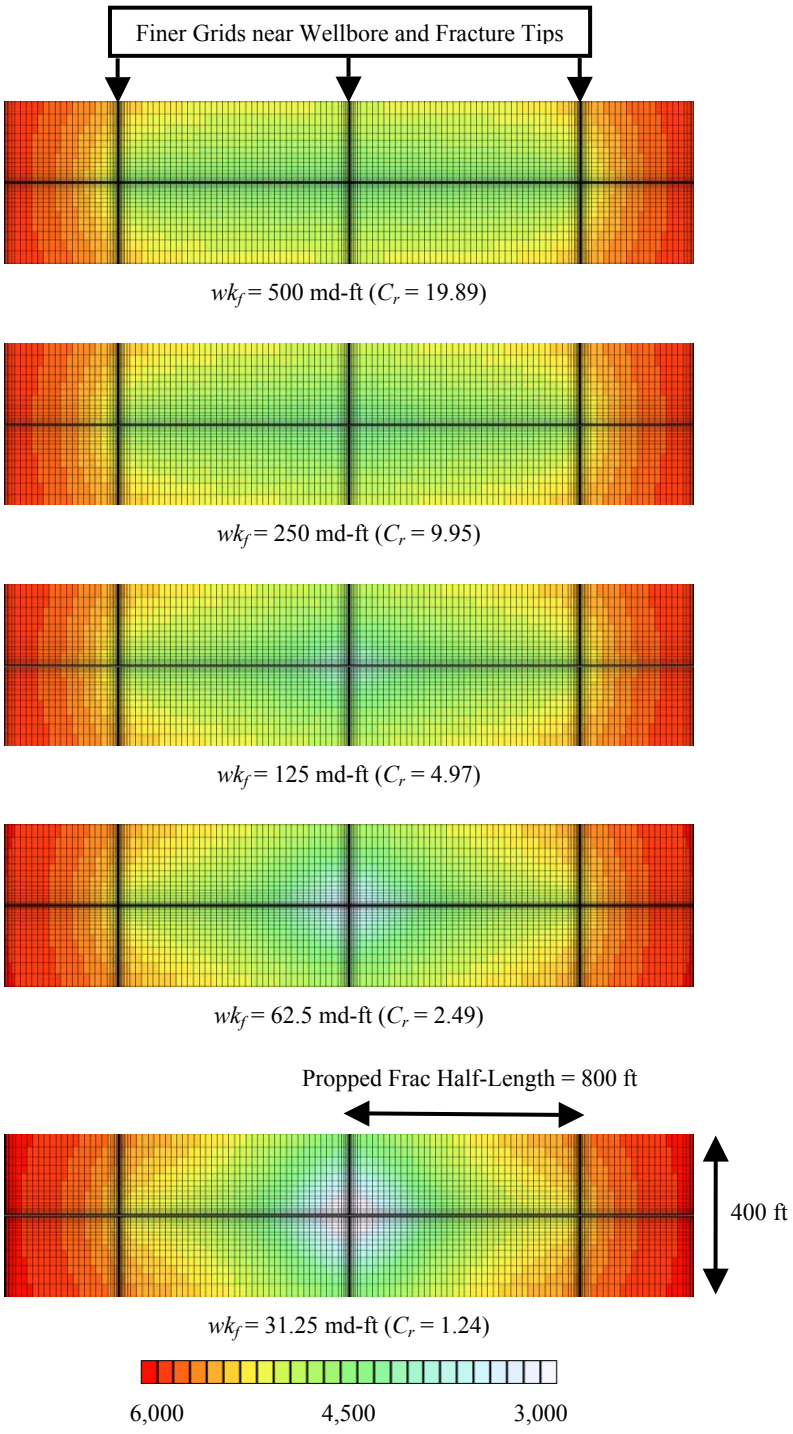

Fig. 4.22—Pressure distribution (psi) in the reservoir at 365 days for multiphase and non-Darcy flow cases with L_f = 800 ft and k_g = 0.01 md.

Fig. 4.23 and **Fig. 4.24** present the water saturation profiles around the fracture at 1 day and 365 days after the treatment for the cases above. The water saturation in the invaded zone near the fracture is 100% at the end of the injection (shown by the red color). The initial water saturation (prior to fracturing) is 40% and is displayed by the light color. Fig. 4.23 compares the rate of fracture fluid cleanup for different conductivities. The fracturing fluid cleans up faster if the fracture conductivity is high. Changing nothing else but the fracture conductivity, the fracturing fluid in the invaded zone is "partially" cleaned up along 30% of the propped length at 1 day if the wk_f = 500 md-ft (C_r = 19.89) and only 10% of the propped length at 1 day if the wk_f = 31.25 md-ft (C_r = 1.24). Fig. 4.24 shows that even though the gas enters the entire propped fracture at a reasonable period of time (e.g., 365 days), the water saturation in the invaded zone does not completely decrease to the initial water saturation. The water saturation near the fracture remains 60 to 70% at 365 days, whereas the initial water saturation is only 40%. Accordingly, multiphase effects may still linger after fracture cleanup. If one performs pressure buildup tests or analyze production data at 365 days, the calculated fracture lengths will be 40 to 50% of the actual lengths.[76] This is because both conventional pressure transient analysis (PTA) and production data analysis (PDA) ignore the major factors of non-Darcy and multiphase flow effects. I found that the cleanup length is generally longer than the effective lengths (i.e., calculated lengths) determined from pressure buildup tests or production data analysis.

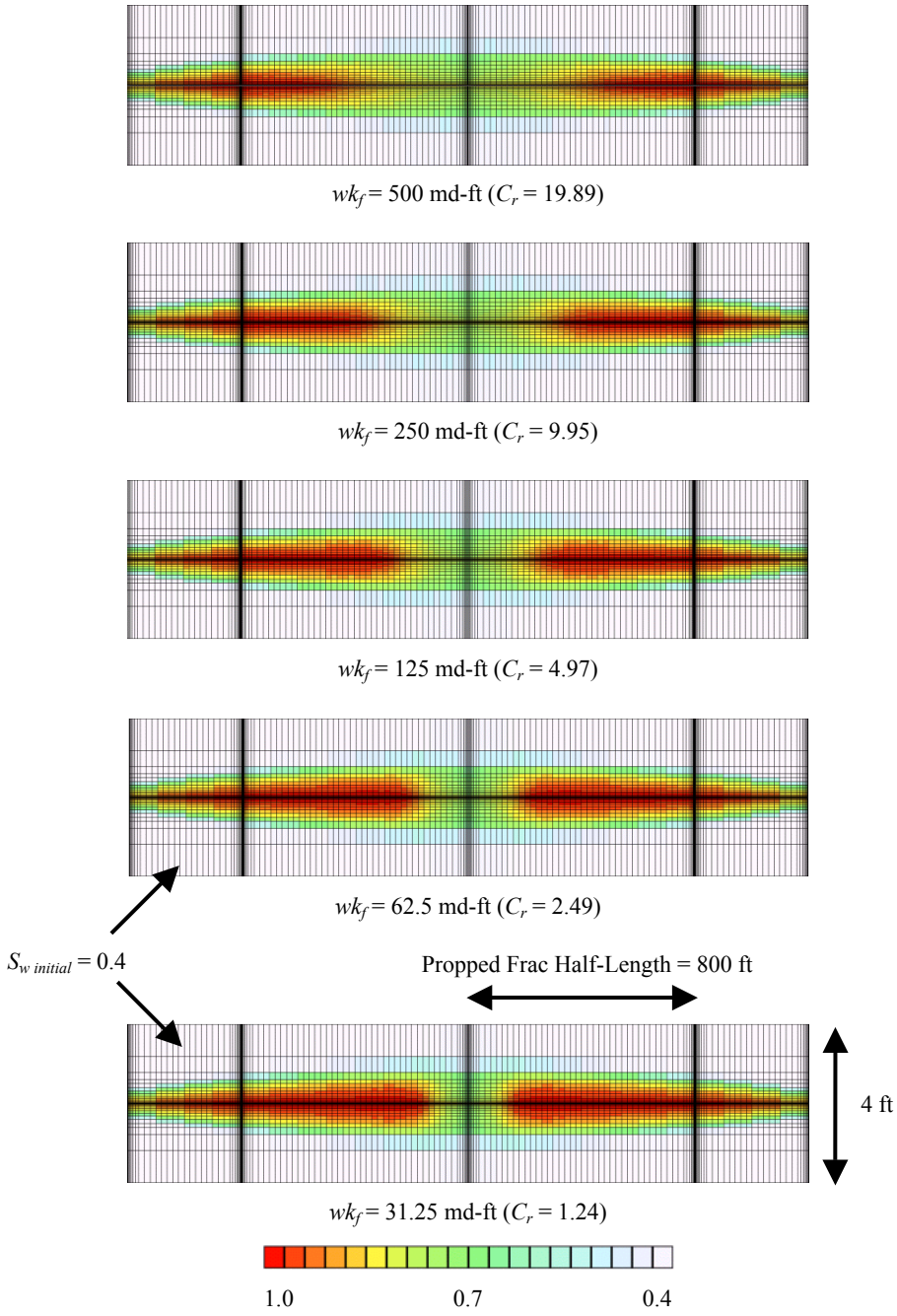

Fig. 4.23—Water saturation (fraction) in the reservoir at 1 day for multiphase and non-Darcy flow cases with L_f = 800 ft and k_g = 0.01 md.

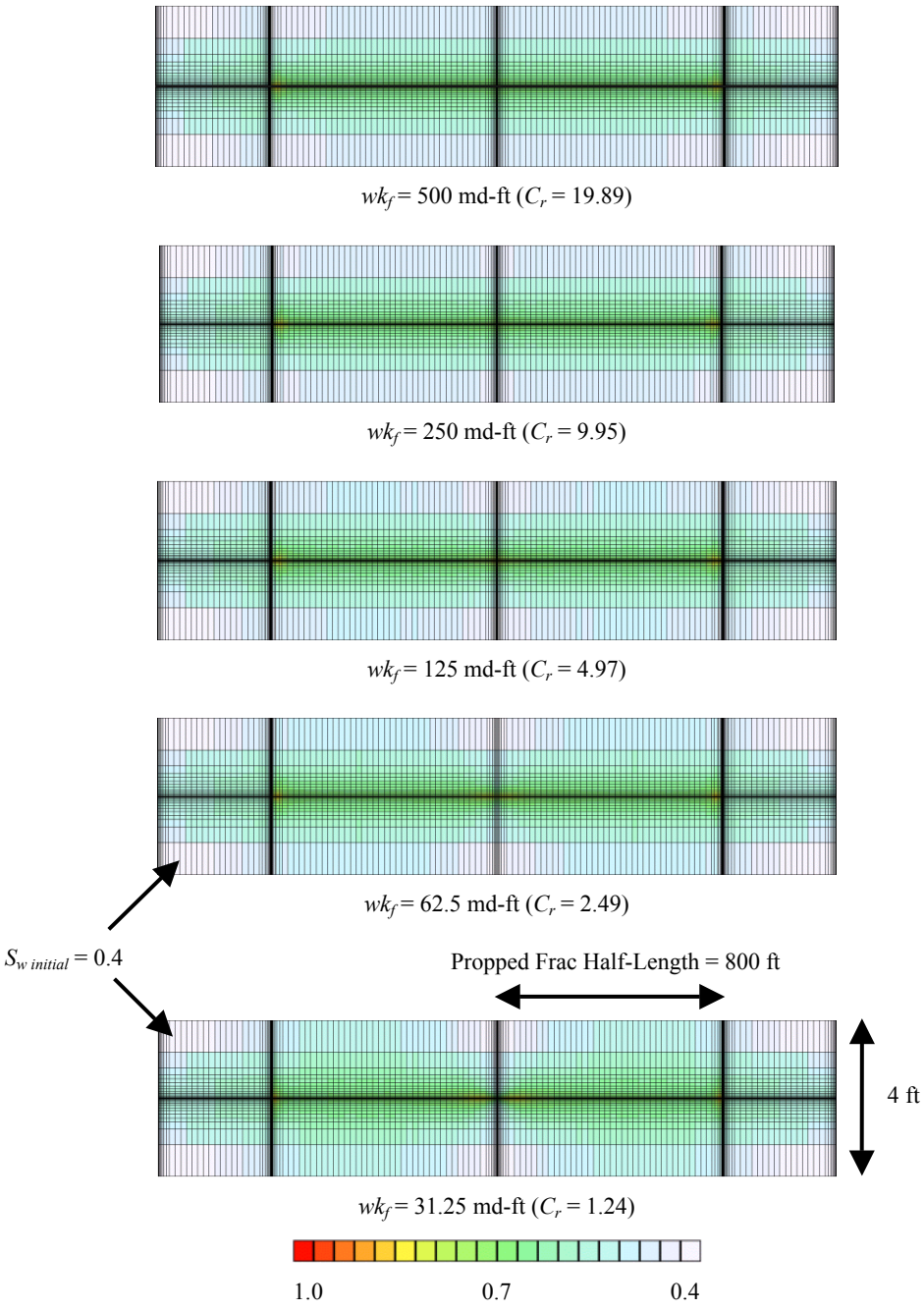

Fig. 4.24—Water saturation (fraction) in the reservoir at 365 days for multiphase and non-Darcy flow cases with L_f = 800 ft and k_g = 0.01 md.

The productivity of hydraulically fractured gas wells is often not optimal because the relative permeability to gas in the invaded zone around the fracture is reduced by the leakoff fluid. **Fig. 4.25** shows the effective gas permeability around the fracture at 365 days for the high and low fracture conductivities. The initial gas permeability in the formation (prior to fracturing) is 0.01 md and is shown by the red color. Fig. 4.25

shows that the reduction in the effective gas permeability occurs more uniformly along the fracture if the fracture conductivity is high. However, the effective gas permeability in the invaded zone will be much higher near the wellbore if the fracture conductivity is low. Greater fracture conductivity improves the effectiveness of the propped fracture because the gas enters the entire portion of the propped fracture between the wellbore and fracture tip more evenly.

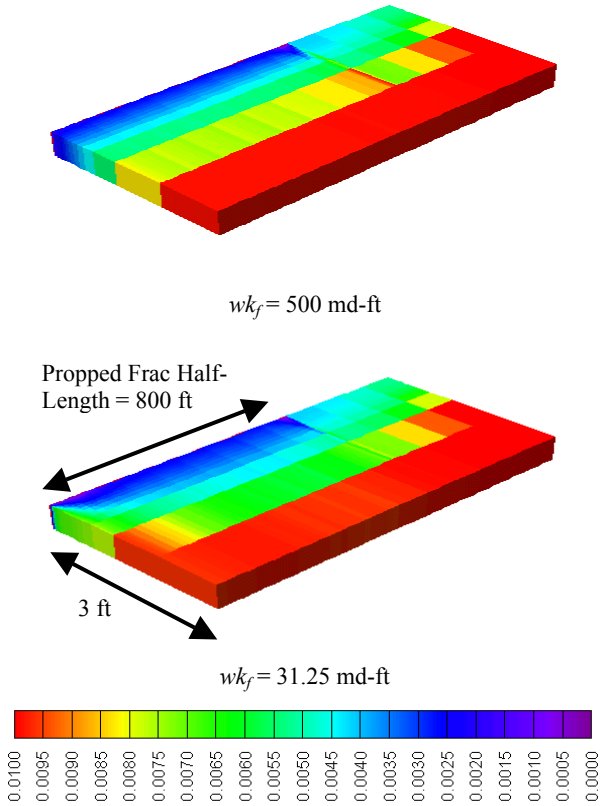

Fig. 4.25—Effective gas permeability map at 365 days for multiphase and non-Darcy flow cases with L_f = 800 ft and k_g = 0.01 md.

The fracture fluid recovery versus production time for these cases is presented in **Fig. 4.26**. Recall that the formation water is immobile; thus, the water produced is injected water. Fig. 4.26 shows that the fracture fluid production rates begin to level off at 30 to 60 days. At 365 days, the fluid recovery is 46% for the case with wk_f = 500 md-ft (C_r = 19.89) and 21% for the case with wk_f = 31.25 md-ft (C_r = 1.24). The cumulative gas recovery versus production time for these cases is given in **Fig. 4.27**. The Initial Gas In Place (IGIP) is 45,586 MMscf. The case with wk_f = 500 md-ft yields a cumulative gas recovery that is approximately twice as much as the case with wk_f = 31.25 md-ft. The results presented in Figs. 4.26 and 4.27 are consistent with prior studies[6-8] that show that higher fracture conductivity promotes higher fracture fluid recovery and cumulative gas recovery.

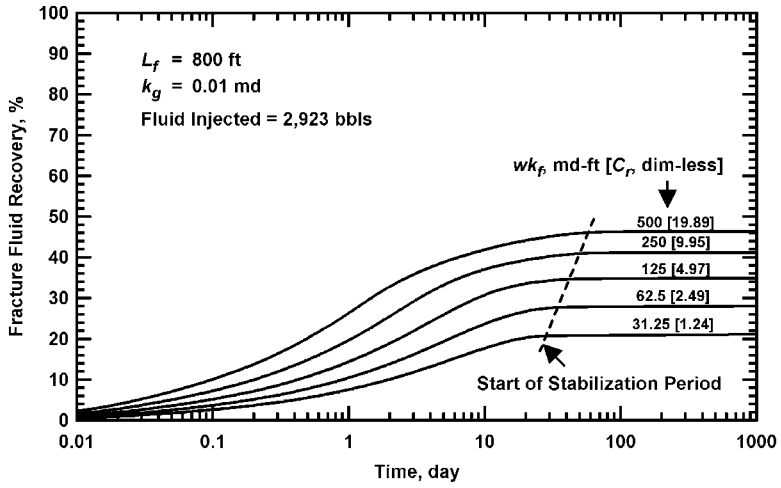

Fig. 4.26—Fracture fluid recovery versus production time for multiphase and non-Darcy flow cases with L_f = 800 ft and k_g = 0.01 md.

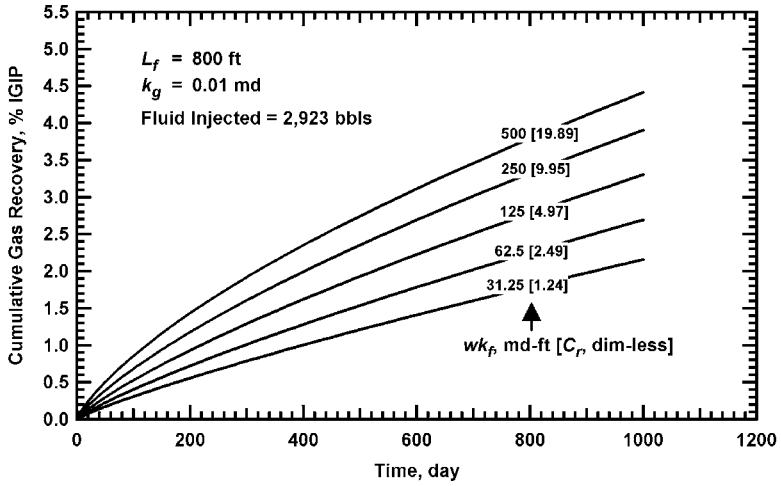

Fig. 4.27—Cumulative gas recovery versus production time for multiphase and non-Darcy flow cases with L_f = 800 ft and k_g = 0.01 md.

Fig. 4. 28 presents the performance of a multiphase case (considering cleanup effects) with L_f = 800 ft and corresponding single-phase cases (ignoring cleanup effects) with different fracture lengths, all with wk_f = 500 md-ft. For the multiphase case, the effective fracture half-length appears to be 660 ft. This is the equivalent fracture half-length under single-phase flow conditions that gives similar performance (i.e., cumulative gas recovery) as for multiphase flow conditions. The residual fracturing fluid in the formation does not seem to affect the after cleanup production performance of the multiphase case significantly, since the cumulative gas recoveries for the multiphase case (L_f = 800 ft) and the single-phase case with $(L_f)_{\text{effective}}$ = 660 ft are practically parallel after an extended period of time. The difference in the ultimate gas

recovery between the two cases is due to reduced gas production during fracture fluid cleanup (i.e., at early times). However, if the fracture conductivity is low, the performance of the well can be affected significantly by the residual fracturing fluid in the formation. **Fig. 4.29** indicates that the performance of this well (considering cleanup effects, wk_f = 31.25 md-ft) is equivalent to the performance of a well with a shorter effective fracture length, $(L_f)_{effective}$ = 220 ft when ignoring cleanup effects. The data in Fig. 4.29 indicate that the well is acting like a "single-phase" 220 ft long fracture.

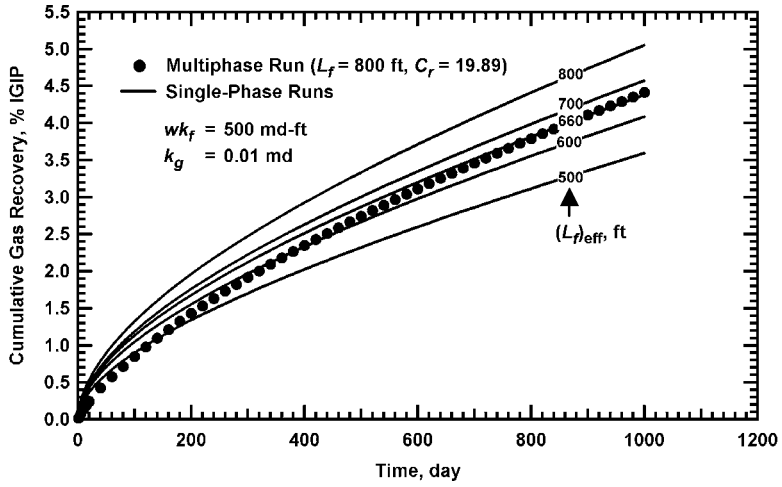

Fig. 4.28—Cumulative gas recovery versus production time for a multiphase case with wk_f = 500 md-ft (C_r = 19.89), L_f = 800 ft, and k_g = 0.01 md, and corresponding single-phase cases with different fracture lengths.

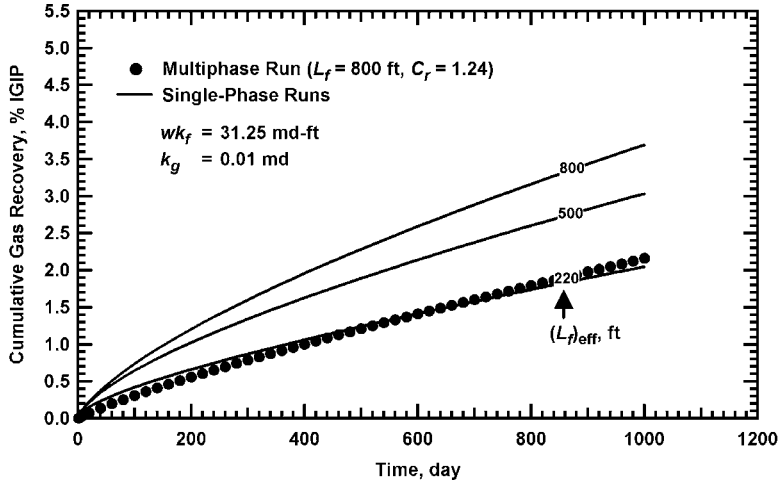

Fig. 4.29—Cumulative gas recovery versus production time for a multiphase case with wk_f = 31.25 md-ft, L_f = 800 ft, and k_g = 0.01 md, and corresponding single-phase cases with different fracture lengths.

The problem is not the well, but the analysis technique. If the engineer analyzes this problem with 2P flow models, the effective fracture half-length would have been close to 800 ft. **Fig. 4.30** and **Fig. 4.31** present the ratio of the multiphase gas rate profile to the single-phase gas rate profile versus distance along the propped fracture for cases given in Fig. 4.28 and Fig. 4.29, respectively. While not exact, the points where the profiles intersect (i.e., the ratio of the multiphase to single-phase gas entry profile is unity) correlate well with the effective single-phase fracture lengths presented in Figs. 4.28 and 4.29. The apparent fracture half-lengths (i.e., the points where the curves intersect) are 600 ft for the case with the wk_f = 500 md-ft and 180 ft for the case with the wk_f = 31.25 md-ft.

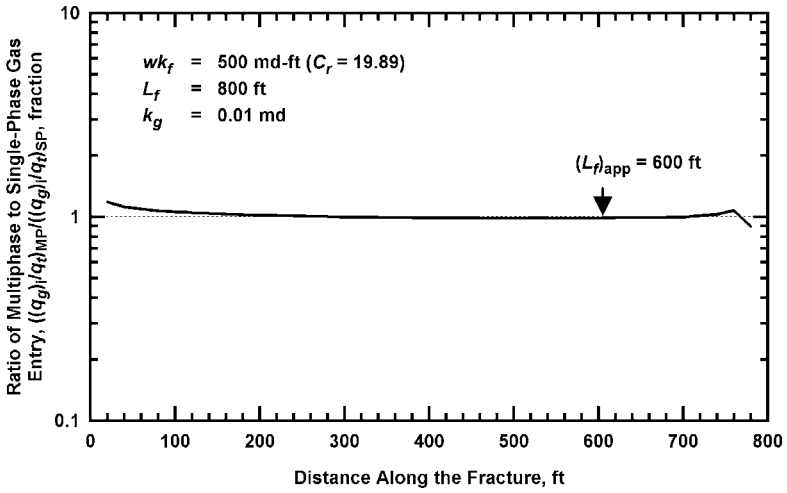

Fig. 4.30—Ratio of multiphase to single-phase gas entry profile for a case with wk_f = 500 md-ft, L_f = 800 ft, and k_g = 0.01 md.

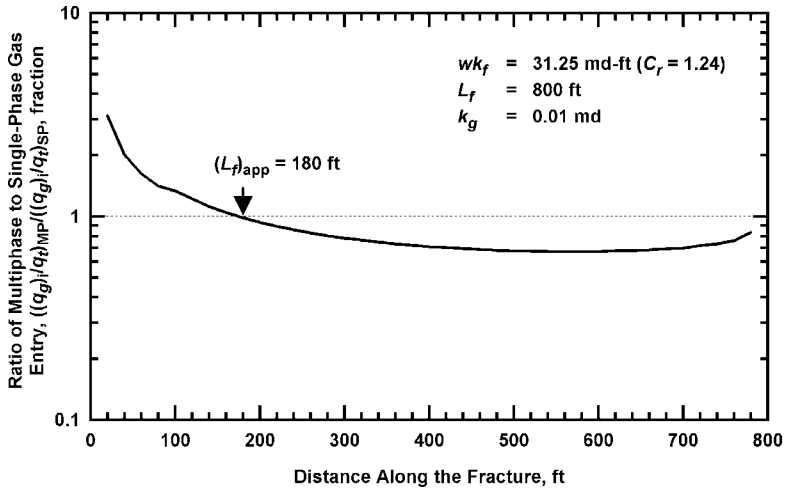

Fig. 4.31—Ratio of multiphase to single-phase gas entry profile for a case with wk_f = 31.25 md-ft, L_f = 800 ft, and k_g = 0.01 md.

4.2.2 "Low" Pressure Reservoirs

In low-permeability reservoirs, the fractures often take a long time to cleanup. In this section, I present the simulation results for cases with low reservoir pressure. For these runs, the reservoir pressure is assumed to be 2,325 psi. The capillary pressure used for the reservoir is presented in **Fig. 4.32**. To investigate the relationship between pressure drawdown and capillary pressure, two bottomhole flowing pressures (p_{wf}'s) were used in these runs namely 1,000 and 2,000 psi. The formation water saturation is at irreducible condition (40%). When the bottomhole flowing pressure is 1,000 psi, the total pressure drawdown in the reservoir is 1,325 psi and is greater than the capillary pressure at 40% water saturation. For the cases when the bottomhole flowing pressure is 2,000 psi, the pressure drop in the reservoir is only 325 psi and is less than the value of capillary pressure at 60% water saturation (345 psi). Therefore, when the bottomhole flowing pressure is 2,000 psi, the water saturation in the formation near the fracture (i.e., 100% at the end of the injection) will decrease to a minimum 60% water saturation after the treatment. For these cases, it is impossible for the water to migrate toward the fracture if the water saturation is less than 60%. These reservoir conditions were chosen after reviewing the example of the low-pressure reservoir cases presented by Holditch[13] (i.e., the formation pressure is less than the reservoir pressure for the Moxa Arch Frontier formation). The cumulative water injected is 2,930 bbls for these cases assuming that the injection pressure is 3,325 psi.

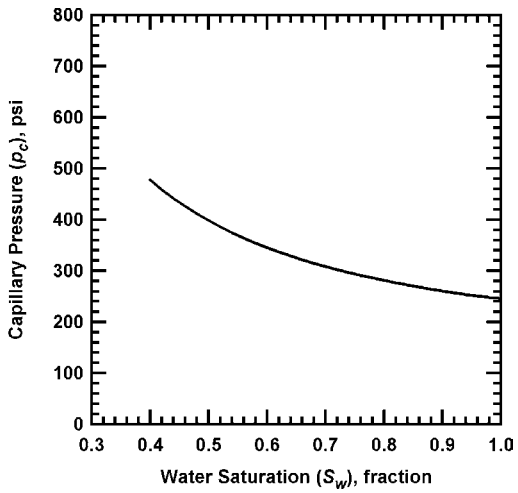

Fig. 4.32—Capillary pressure data for the low-pressure reservoir investigation.[13]

Fig. 4.33 and **Fig. 4.34** show the profiles of cumulative gas flow rate into the fracture versus distance along the fracture for the high and low fracture conductivities when the initial reservoir pressure is 2,325 psi and the bottomhole flowing pressure is 1,000 psi. For these runs, the L_f = 800 ft, k = 0.01 md, and μ_w = 1 cp. The results presented in Figs. 4.33 and 4.34 suggest that the gas will eventually enter along the entire propped fracture within 1 day to 10 days.

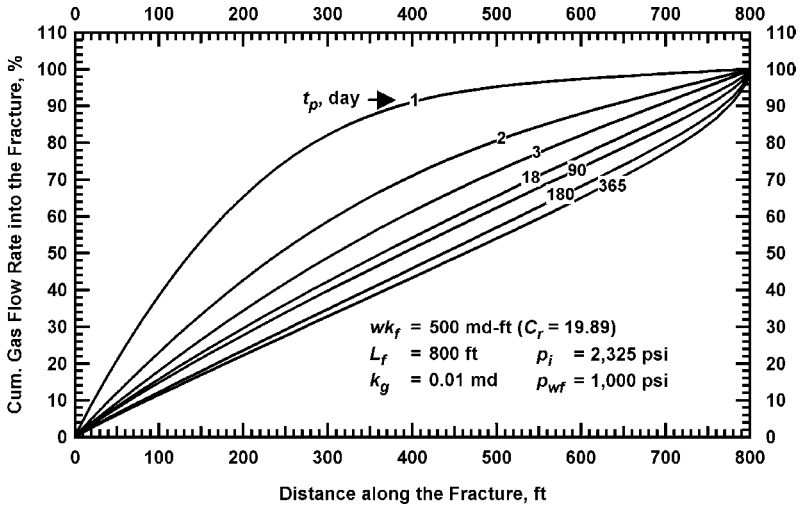

Fig. 4.33—Cumulative gas flow rate into the fracture versus distance along the fracture for the low-pressure reservoir investigation (p_i = 2,325 psi, p_{wf} = 1,000 psi, and wk_f = 500 md-ft).

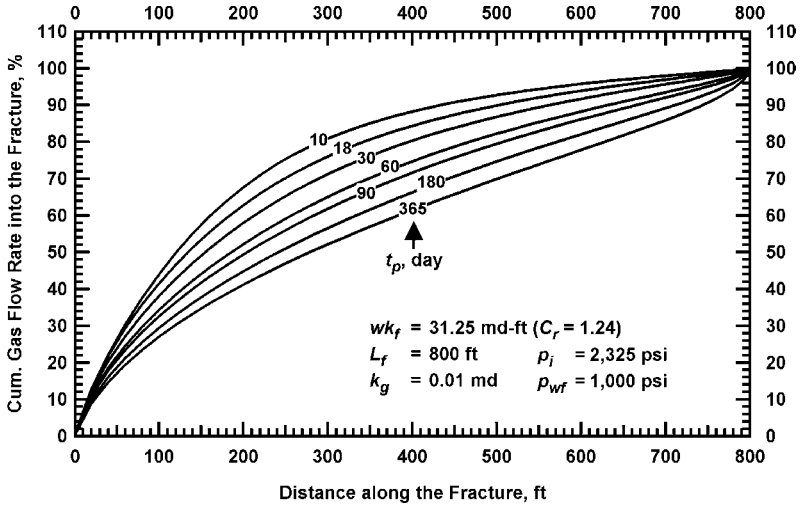

Fig. 4.34—Cumulative gas flow rate into the fracture versus distance along the fracture for the low-pressure reservoir investigation (p_i = 2,325 psi, p_{wf} = 1,000 psi, and wk_f = 31.25 md-ft).

The ratio of the cleanup fracture half-length to the actual fracture half-length versus time for these cases is presented in **Fig. 4.35.** As before, greater fracture conductivity results in longer cleanup fracture lengths versus time. The ratio of the cleanup fracture half-length to the actual fracture half-length generally approaches unity within 365 days for all conductivities even when the reservoir pressure is low.

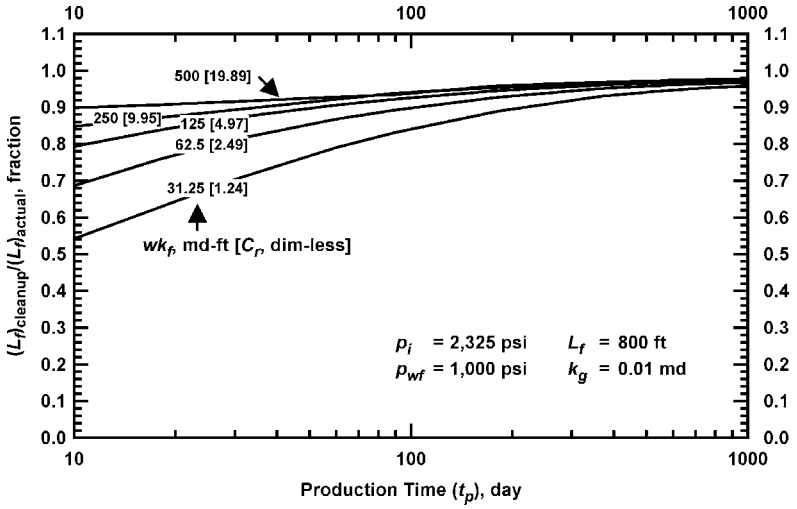

Fig. 4.35— Ratio of cleanup fracture half-length to actual fracture half-length for the low-pressure reservoir investigation (p_i = 2,325 psi and p_{wf} = 1,000 psi).

Fig. 4.36 and **Fig. 4.37** show the profiles of cumulative gas flow rate into the fracture versus distance along the fracture for the cases above when the bottomhole pressure is 2,000 psi. At 365 days, 90% of the gas entering the fracture will occur at 778 ft from the wellbore if the wk_f = 500 md-ft (Fig. 4.36) and 757 ft from the wellbore if the wk_f = 31.25 md-ft (Fig. 4.37). Again, the entire propped length is generally accessible for gas flow after a relatively short period of time (less than 10 days) even for the reservoirs where the pressure drawdown is small. The ratio of the cleanup fracture half-length to the actual fracture half-length versus time for the cases with the p_{wf} = 2,000 psi is presented in **Fig. 4.38**. Note that the cleanup length is also close to the actual propped length for these cases.

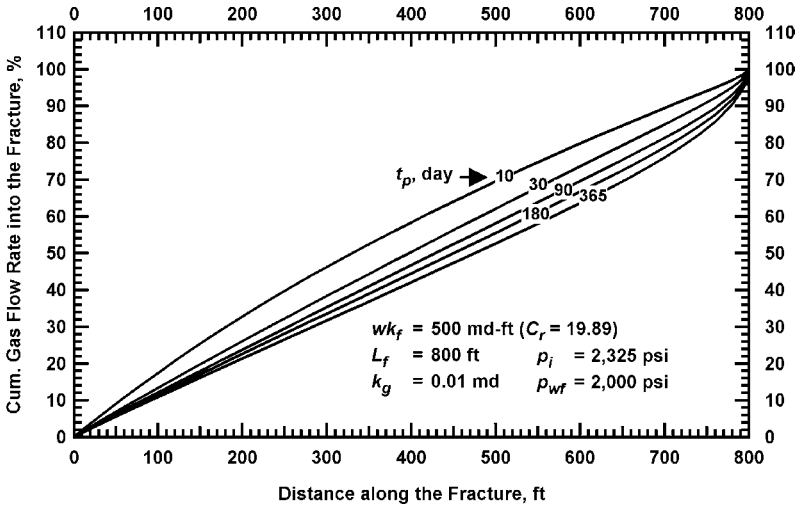

Fig. 4.36—Cumulative gas flow rate into the fracture versus distance along the fracture for the low-pressure reservoir investigation (p_i = 2,325 psi, p_{wf} = 2,000 psi, and wk_f = 31.25 md-ft).

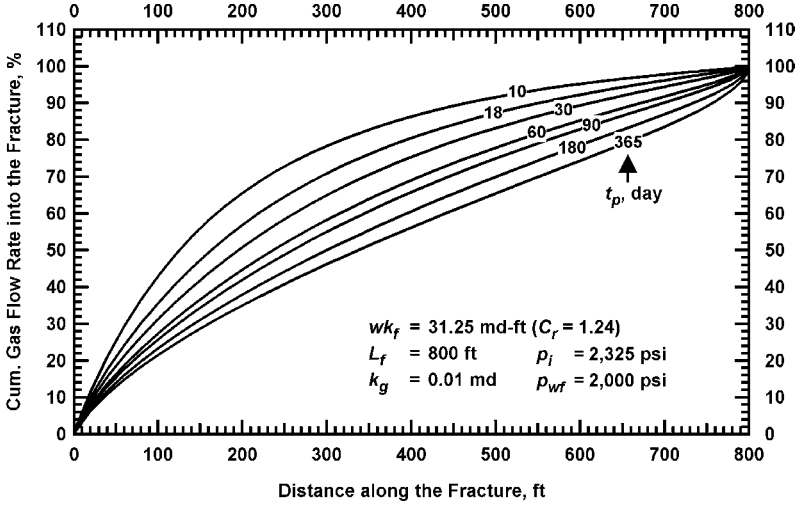

Fig. 4.37—Cumulative gas flow rate into the fracture versus distance along the fracture for the low-pressure reservoir investigation (p_i = 2,325 psi, p_{wf} = 2,000 psi, and wk_f = 31.25 md-ft).

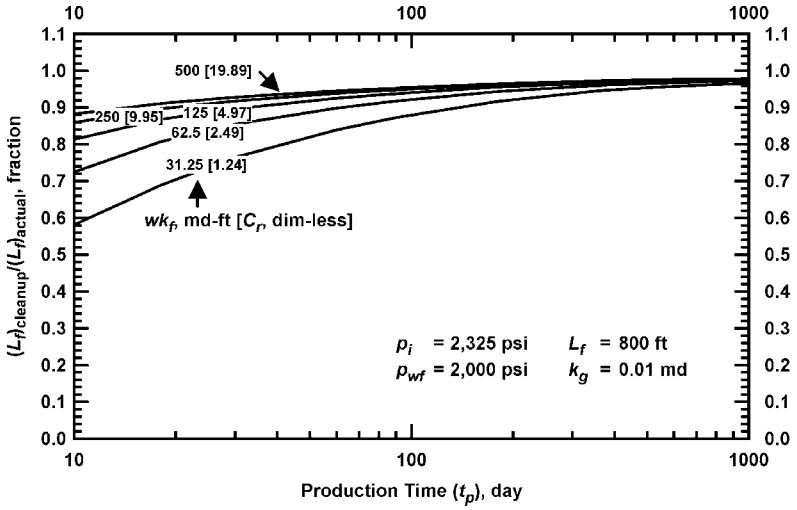

Fig. 4.38— Ratio of cleanup fracture half-length to actual fracture half-length for the low-pressure reservoir investigation (p_i = 2,325 psi and p_{wf} = 2,000 psi).

Fig. 4.39 shows the pressure distribution in the reservoir at 365 days for the cases presented in Figs. 4.33 to 4.35. The reservoir pressure is 2,325 psi (shown by the red color). The bottomhole flowing pressure is 1,000 psi (shown by the light color). As before, the pressure drops in the reservoir are distributed more equally along the fracture when the fracture conductivity is high. In comparison, if the fracture conductivity is low, the reservoir pressures vary along the fracture and the largest pressure drops occurring near the wellbore.

Fig. 4.40 and **Fig. 4.41** show the water saturation profiles around the fracture at 1 day and 365 days for the cases where the p_{wf} = 1,000 psi. The water saturation is 100% in the formation near the fracture at the end of the injection (shown by the red color). The initial water saturation (prior to fracturing) is 40% and is displayed by the light color. Fig. 4.40 indicates that the cleanup of fracture fluid is quicker if the fracture conductivity is high. After the treatment, imbibition will begin to alter the fluid distribution in the reservoir. Some of the fluid injected flow from the formation into the fracture and some imbibe deeper into the formation. The depth of the invasion is approximately 1 ft at the end of the injection for these cases. At 365 days, the injected fluid imbibes as far as 3 to 10 ft into the formation. Fig. 4.41 shows that the water saturation in the invaded zone does not completely decrease to the initial water saturation. At 365 days, the average water saturations in the invaded zone near the fracture are 62% for the case with the wk_f of 500 md-ft (C_r = 19.89) and 68% for the case with the wk_f of 31.25 md-ft (C_r = 1.24).

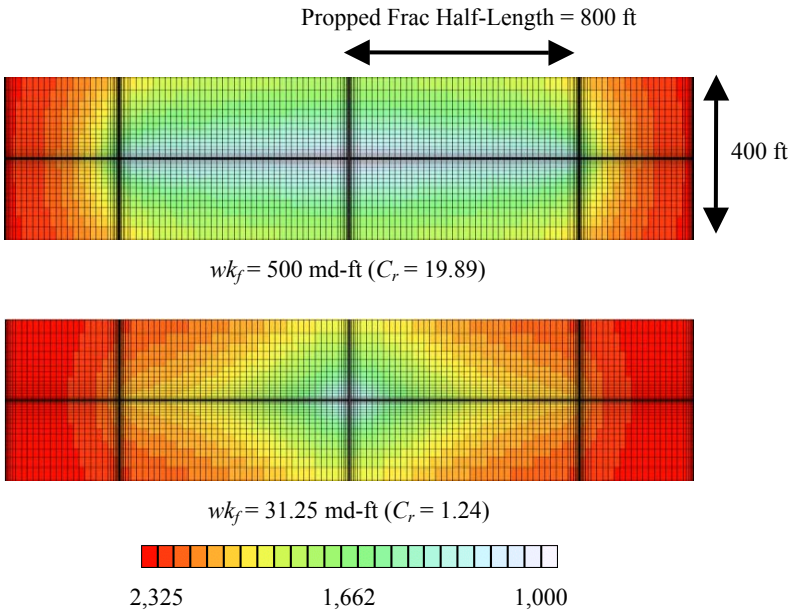

Fig. 4.39—Pressure distribution (psi) in the reservoir at 365 days for the low-pressure reservoir investigation (p_i = 2,325 psi, p_{wf} = 1,000 psi, L_f = 800 ft, and k_g = 0.01 md).

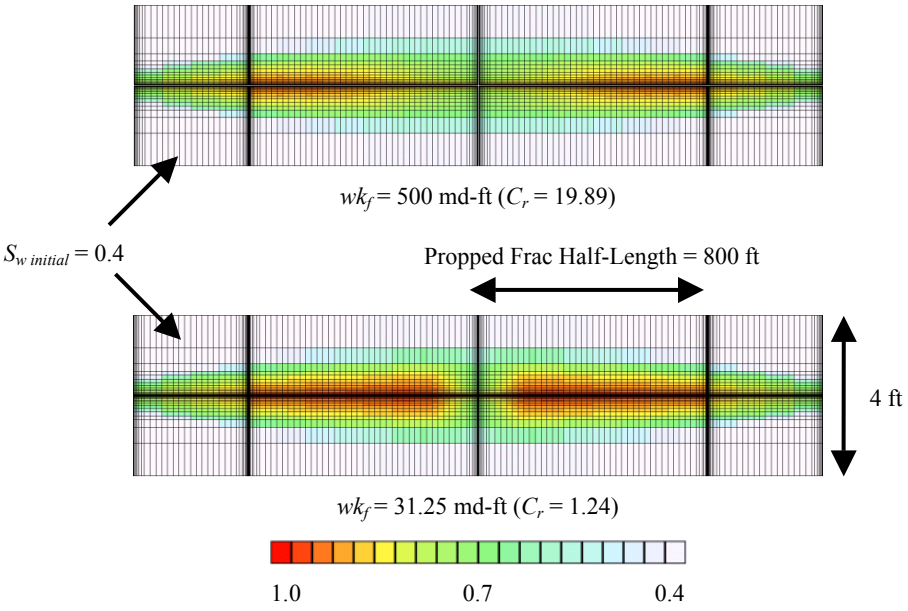

Fig. 4.40—Water saturation (fraction) in the reservoir at 1 day for the low-pressure reservoir investigation (p_i = 2,325 psi, p_{wf} = 1,000 psi, L_f = 800 ft, and k_g = 0.01 md).

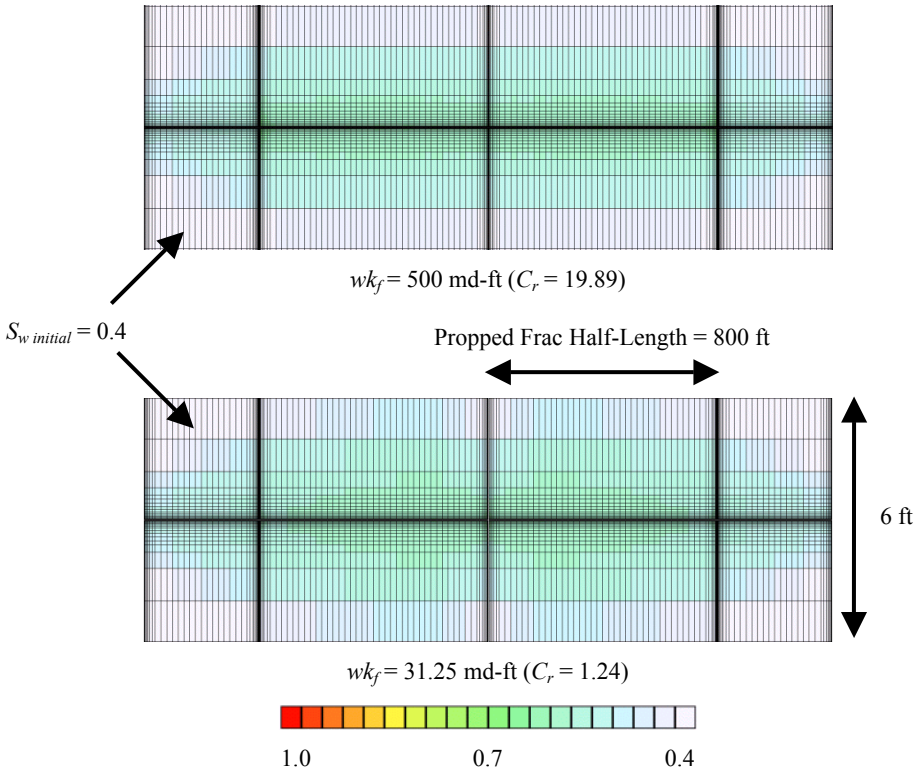

Fig. 4.41—Water saturation (fraction) in the reservoir at 365 days for the low-pressure reservoir investigation (p_i = 2,325 psi, p_{wf} = 1,000 psi, L_f = 800 ft, and k_g = 0.01 md).

Fig. 4.42 presents the effective gas permeability around the fracture at 365 days for the high and low conductivity fractures presented in Figs. 4.39 to 4.41. The effective gas permeability displayed by the red color represents a high value. The effective gas permeability shown by the dark blue color represents a low value. In Fig. 4.42, the effective gas permeability in the formation (prior to fracturing) is 0.01 md. The graphs show that the effective gas permeability decreases more uniformly along the fracture if the fracture conductivity is high. However, if the fracture conductivity is low, the effective gas permeability is much lower in the invaded zone between the wellbore and the fracture tip. Comparing Fig. 4.42 and Fig. 4.25, we see that the area, where the effective gas permeability is reduced by the residual fracturing fluid, is deeper into the formation for the "low" reservoir pressure cases than that for the "high" reservoir pressure cases.

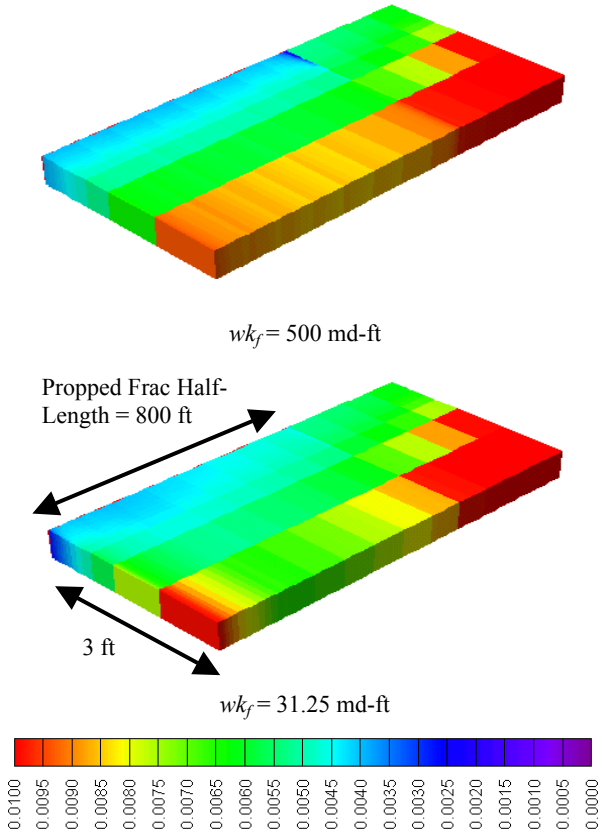

Fig. 4.42—Effective gas permeability map at 365 days for the low-pressure reservoir investigation (p_i = 2,325 psi, p_{wf} = 1,000 psi, L_f = 800 ft and k_g = 0.01 md).

Fig. 4.43 shows the pressure distribution in the reservoir for the "low" reservoir pressure cases where the p_{wf} = 2,000 psi. The pressure drops are distributed uniformly along the fracture for the high fracture conductivity case and appear to be "radial" near the wellbore for the low fracture conductivity case. **Fig. 4.44** and **Fig. 4.45** illustrate the water saturation profiles around the fracture at 1 day and 365 days for the cases presented in Fig. 4.43. Fig. 4.44 shows that the fracturing fluid cleans up more rapidly when the fracture conductivity is high. At 365 days, the water saturation in the invaded zone does not decrease to the initial water saturation. The depth of the imbibition is much deeper for these cases than that for the cases with the p_{wf} of 1,000 psi (Fig. 4.41).

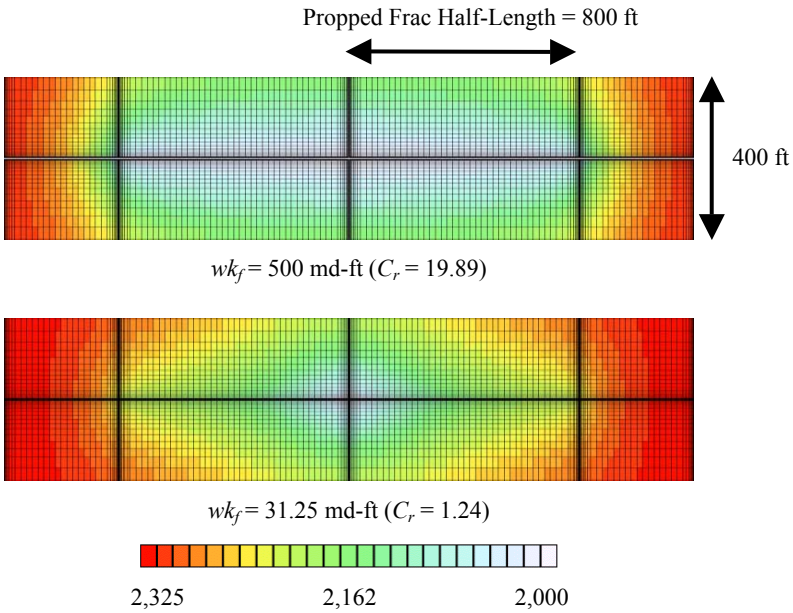

Fig. 4.43—Pressure distribution (psi) in the reservoir at 365 days for the low-pressure reservoir investigation (p_i = 2,325 psi, p_{wf} = 2,000 psi, L_f = 800 ft, and k_g = 0.01 md).

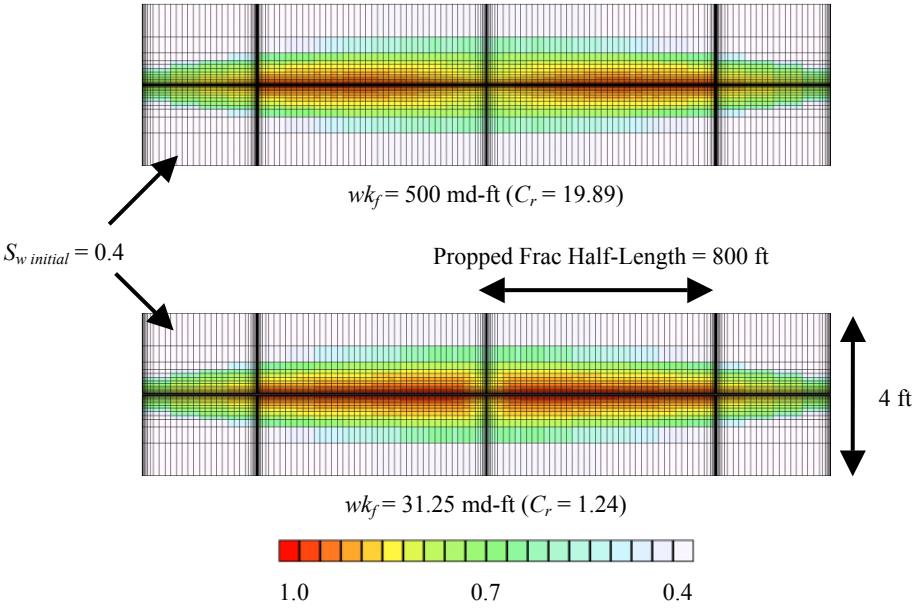

Fig. 4.44—Water saturation (fraction) in the reservoir at 1 day for the low-pressure reservoir investigation (p_i = 2,325 psi, p_{wf} = 2,000 psi, L_f = 800 ft, and k_g = 0.01 md).

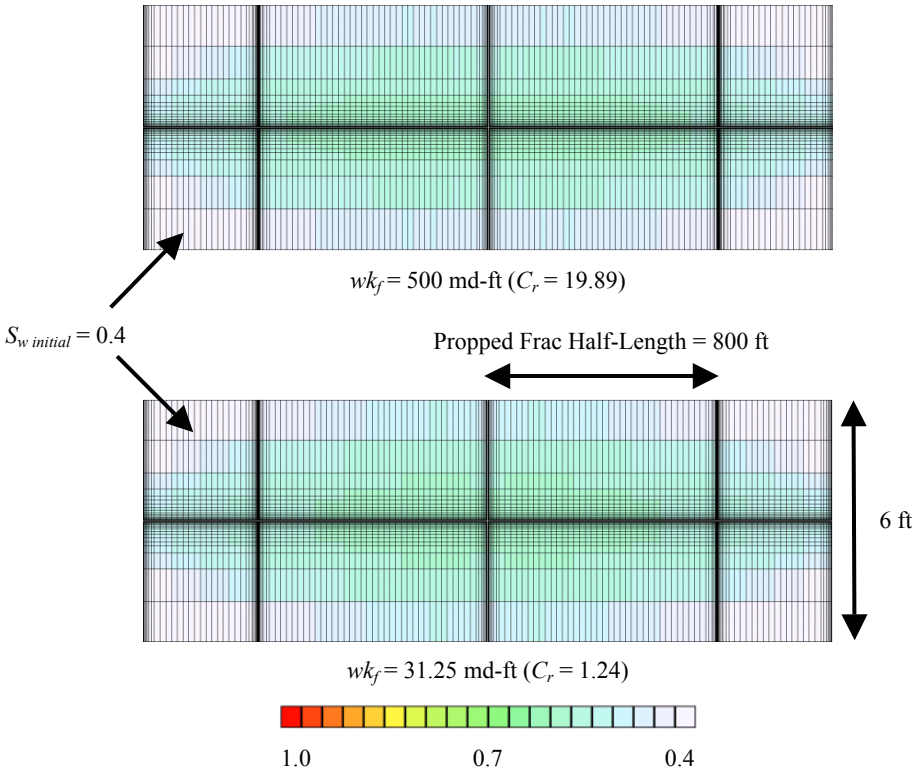

Fig. 4.45—Water saturation (fraction) in the reservoir at 365 days for the low-pressure reservoir investigation (p_i = 2,325 psi, p_{wf} = 2,000 psi, L_f = 800 ft, and k_g = 0.01 md).

Fig. 4.46 shows the effective gas permeability around the fracture at 365 days for the high and low conductivity fractures where the p_{wf} = 2,000 psi. Again, the red color shows high effective gas permeabilities and the dark blue color indicates low effective gas permeabilities. The effective gas permeability in the formation (prior to fracturing) is 0.01 md. The graphs show that the effective gas permeability in the invaded zone is significantly lower than the initial value even after 365 days. I conclude that, when the pressure drawdown is small relative to the capillary forces in the reservoir, the effective gas permeability in the invaded zone will be reduced severely and may limit the gas productivity significantly.

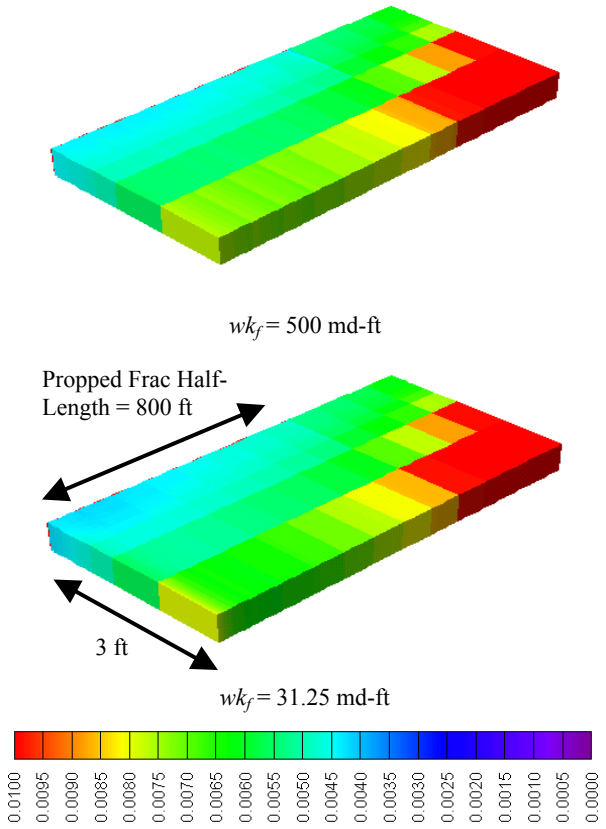

Fig. 4.46—Effective gas permeability map at 365 days for the low-pressure reservoir investigation (p_i = 2,325 psi, p_{wf} = 2,000 psi, L_f = 800 ft, and k_g = 0.01 md).

The fracture fluid recovery versus production time for the cases with the p_{wf} of 1,000 psi is presented in **Fig. 4.47**. Recall that the formation water is immobile; therefore, the water produced is injected water. The fracture fluid production rates presented in Fig. 4.47 begin to level at 3 to 5 days. At 365 days, the fluid recovery is 20% for the case with wk_f = 500 md-ft (C_r = 19.89) and only 6% for the case with wk_f = 31.25 md-ft (C_r = 1.24). Thus, greater fracture conductivity helps to improve the fracture fluid recovery. The cumulative gas recovery versus production time for these cases is given in **Fig. 4.48**. For these cases, the IGIP is 20,437 MMscf. At 365 days, the case with wk_f = 500 md-ft yields a cumulative gas recovery that is approximately 100% higher than that for the case with wk_f = 31.25 md-ft. For these results, I varied the fracture conductivity only; other parameters including the amount of water injected and the minimum flowing bottomhole pressure are the same.

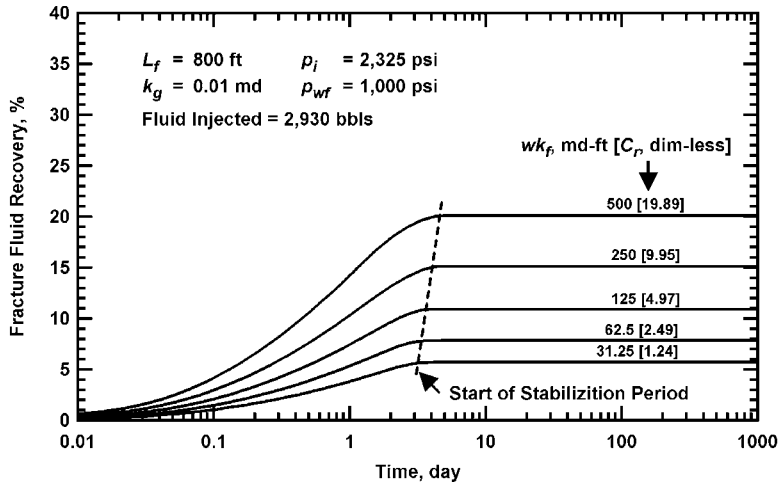

Fig. 4.47—Fracture fluid recovery versus production time for the low-pressure reservoir investigation (p_i = 2,325 psi, p_{wf} = 1,000 psi, L_f = 800 ft, and k_g = 0.01 md).

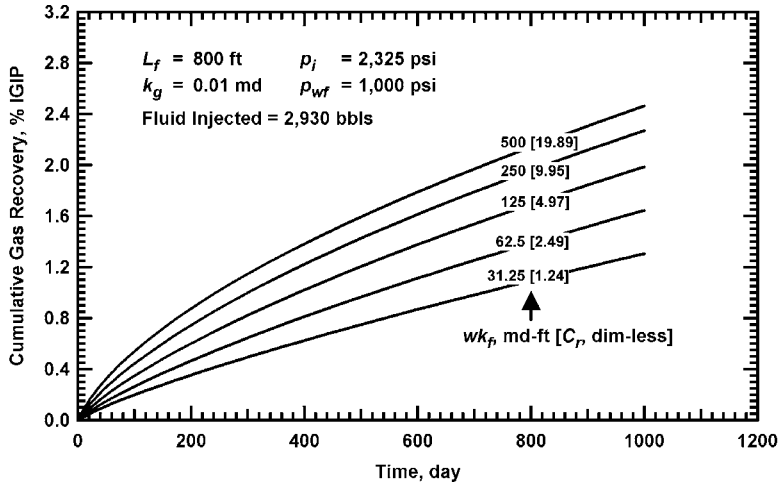

Fig. 4.48—Cumulative gas recovery versus production time for the low-pressure reservoir investigation (p_i = 2,325 psi, p_{wf} = 1,000 psi, L_f = 800 ft, and k_g = 0.01 md).

The fracture fluid recovery versus production time for the cases with the p_{wf} of 2,000 psi is presented in **Fig. 4.49**. For these cases, the fracture fluid production rates begin to level at 1 day to 2 days. Note that the fracturing fluid will be produced only if the pressure drawdown in the invaded zone is large enough to overcome the capillary forces in the reservoir. The results presented in Fig. 4.49 show that the fracture fluid recovery is very low due to low-pressure drawdown. The fluid recovery is 6% for the case with wk_f = 500 md-ft (C_r = 19.89) and only 1.6% for the case with wk_f = 31.25 md-ft (C_r = 1.24)). This suggests that more than 94% of the water injected is still present in the formation. **Fig. 4.50** presents the cumulative gas

recovery versus production time for these cases. The cumulative gas recovery is less than 1% for all conductivities simulated because the pressure drawdown is small. The case with the wk_f of 500 md-ft yield a cumulative gas recovery that is almost twice as much as that for the case with the wk_f of 31.25 md-ft.

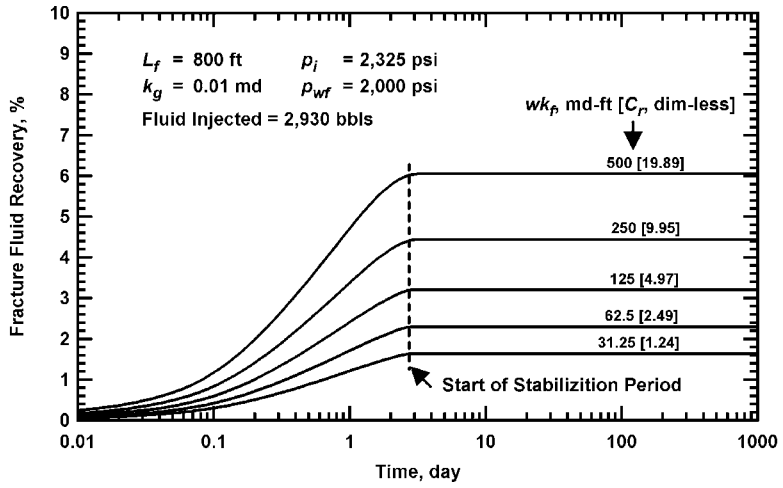

Fig. 4.49—Fracture fluid recovery versus production time for the low-pressure reservoir investigation (p_i = 2,325 psi, p_{wf} = 2,000 psi, L_f = 800 ft, and k_g = 0.01 md).

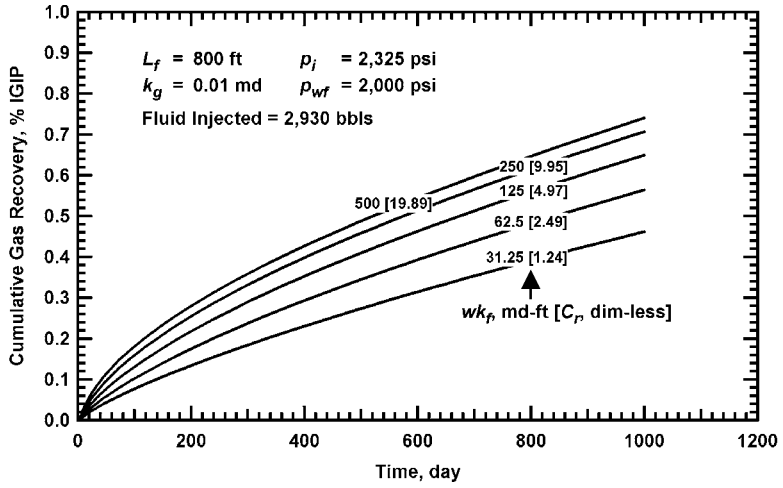

Fig. 4.50—Cumulative gas recovery versus production time for the low-pressure reservoir investigation (p_i = 2,325 psi, p_{wf} = 2,000 psi, L_f = 800 ft, and k_g = 0.01 md).

Fig. 4.51 and **Fig. 4.52** present the cumulative gas recovery of the multiphase cases (considering cleanup effects) with L_f = 800 ft and the corresponding single-phase cases (ignoring cleanup effects) with different fracture lengths for the cases where the p_i = 2,325 psi and p_{wf} = 1,000 psi. Fig. 4.47 indicates that more than 80% of the injected water still remains in the formation at 365 days for these cases. However, Fig. 4.51 shows that the residual fracturing fluid in the invaded zone does not affect the after cleanup production performance significantly once the fracture fluid production rates have leveled off. The reason for this is probably because enough fracturing fluid has been produced and sufficient gas permeability in the invaded zone has been achieved. The productivity is limited more by the pressure drawdown than by the residual fluid in the formation. The difference in the cumulative gas recovery between the single-phase and multiphase cases (Fig. 4.51) is caused by fracture fluid cleanup, which decreases the gas production rates at early times. Fig. 4.51 suggests that the effective fracture length is close to the designed length if the fracture conductivity is high. Recall that we define the "effective" fracture length as the fracture length under single-phase flow conditions that gives similar performance as for multiphase flow conditions. However, if the fracture conductivity is low, the residual fracturing fluid in the invaded zone has a significant effect on the long-term gas production (Fig. 4.52). The cumulative gas recovery for the latter case (L_f = 800 ft) is equivalent to that of a well with a shorter effective fracture half-length ($(L_f)_{\text{effective}}$ = 400 ft) when ignoring the cleanup effects. The cumulative gas recovery is 2.46% at 1,000 days for the case with wk_f = 500 md-ft when considering the cleanup effects (Fig. 4.51). However, the cumulative gas recovery is only 1.31% at 1,000 days for the case with wk_f = 31.25 md-ft when ignoring the cleanup effects (Fig. 4.52). For these cases, the cumulative gas recovery is affected more by the fracture conductivity than by the residual fracturing fluid in the formation.

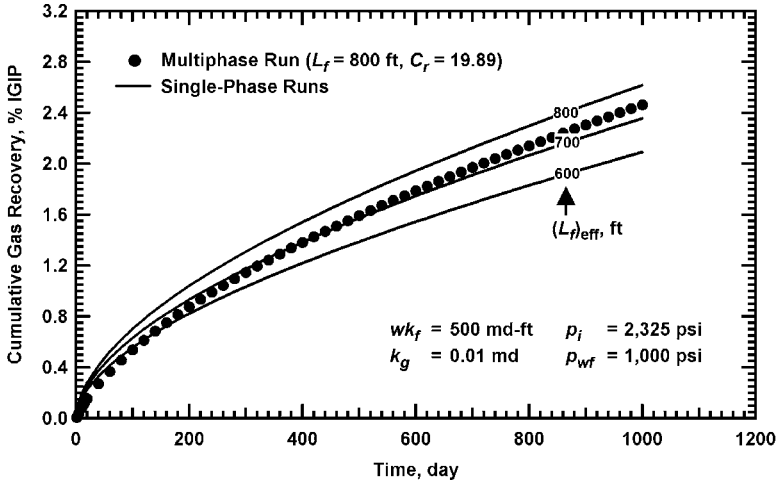

Fig. 4.51— Cumulative gas recovery versus production time for a multiphase, low-pressure reservoir (p_i = 2,325 psi and p_{wf} = 1,000 psi) with wk_f = 500 md-ft, L_f = 800 ft, and k_g = 0.01 md and corresponding single-phase cases with different fracture lengths.

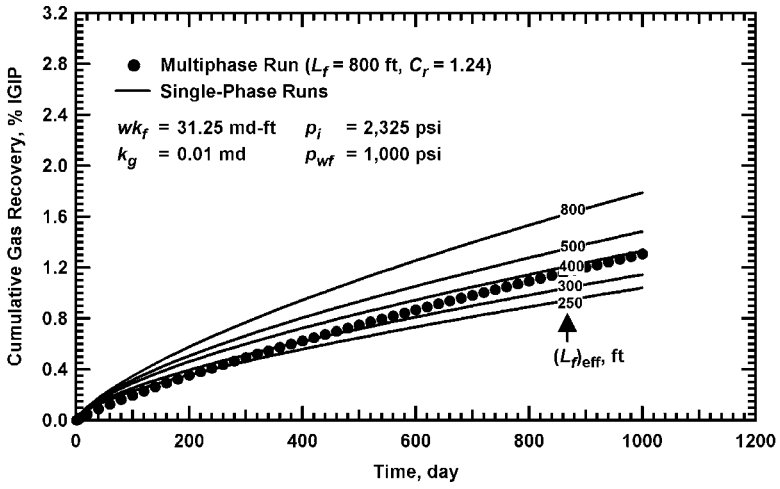

Fig. 4.52— Cumulative gas recovery versus production time for a multiphase, low-pressure reservoir (p_i = 2,325 psi and p_{wf} = 1,000 psi) with wk_f = 31.25 md-ft, L_f = 800 ft, and k_g = 0.01 md and corresponding single-phase cases with different fracture lengths.

Fig. 4.53 and **Fig. 4.54** present the cumulative gas recovery of the multiphase cases (considering cleanup effects) with L_f = 800 ft and the corresponding single-phase cases (ignoring cleanup effects) with different fracture lengths for the cases where the p_i = 2,325 psi and p_{wf} = 2,000 psi. According to Fig. 4.49, the fracture fluid recovery at 365 days is 6% for the case presented in Fig. 4.53 and 1.6% for the case presented in Fig. 4.54. Comparing these plots to Figs. 4.51 and 4.52 (where the p_{wf} = 1,000 psi), the cumulative gas recovery is reduced significantly for both the single-phase and multiphase cases because the pressure drawdown is not large enough to overcome the capillary forces in the formation. Fig. 4.53 indicates that, if the fracture conductivity is high, the cumulative gas recovery for the single-phase and multiphase cases is almost identical. This suggests that even if the fracture fluid recovery was much higher for these cases, the cumulative gas recovery will not increase significantly unless the pressure drawdown was increased (i.e., by reducing the bottomhole flowing pressure). However, the residual fracturing fluid may affect the long-term gas production significantly particularly if the fracture conductivity is low (Fig. 4.54). In summary, greater pressure drawdown results in higher fracture fluid recovery and higher cumulative gas recovery. These results are consistent with the work of Holditch;[13] however I did not only determine the cumulative gas recovery and fracture fluid recovery, but also show the water saturation and pressure distribution profiles around the fracture versus time after the treatment.

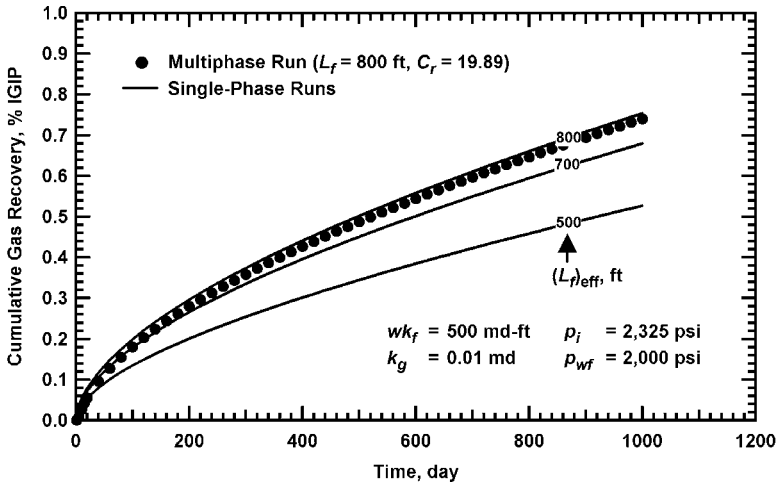

Fig. 4.53— Cumulative gas recovery versus production time for a multiphase, low-pressure reservoir (p_i = 2,325 psi and p_{wf} = 2,000 psi) with wk_f = 500 md-ft, L_f = 800 ft, and k_g = 0.01 md and corresponding single-phase cases with different fracture lengths.

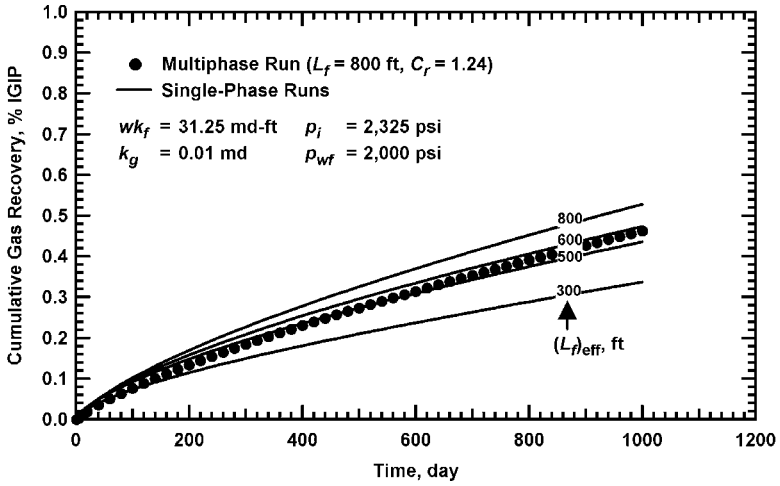

Fig. 4.54— Cumulative gas recovery versus production time for a multiphase, low-pressure reservoir (p_i = 2,325 psi and p_{wf} = 2,000 psi) with wk_f = 31.25 md-ft, L_f = 800 ft, and k_g = 0.01 md and corresponding single-phase cases with different fracture lengths.

Fig. 4.55 through **Fig. 4.58** present the ratio of the multiphase to single-phase gas entry profile for these cases. Again, the points where the curves intersect (i.e., the ratio of the multiphase to single-phase gas entry profile is unity) generally correlate well with the effective single-phase fracture lengths presented in Figs. 4.51 to 4.54. The apparent fracture half-lengths (i.e., where the curves intersect) are 400 ft for the case with the wk_f of 500 md-ft (C_r = 19.89) and 210 ft for the case with the wk_f of 31.25 md-ft (C_r = 1.24) if the p_{wf} = 1,000 psi. When the p_{wf} = 2,000 psi, the apparent fracture half-lengths are 500 ft for the case with the wk_f of 500 md-ft and 250 ft for the case with the wk_f of 31.25 md-ft.

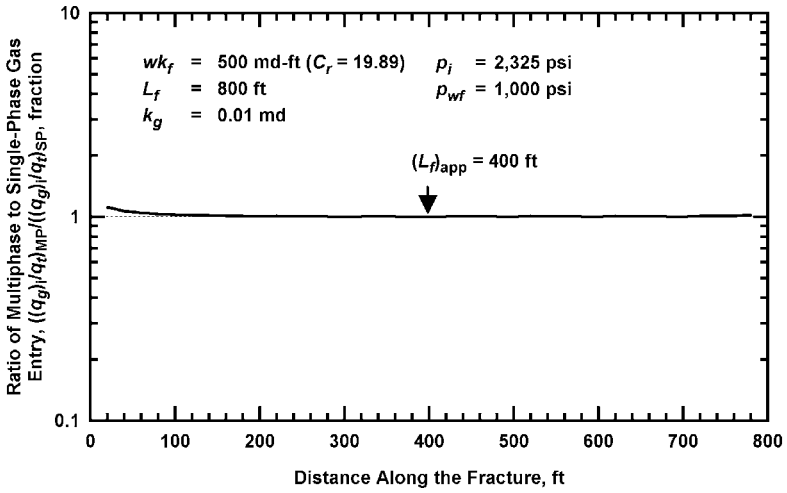

Fig. 4.55—Ratio of multiphase to single-phase gas entry profile for the low-pressure reservoir investigation (p_i = 2,325 psi, p_{wf} = 1,000 psi, wk_f = 500 md-ft, L_f = 800 ft, and k_g = 0.01 md).

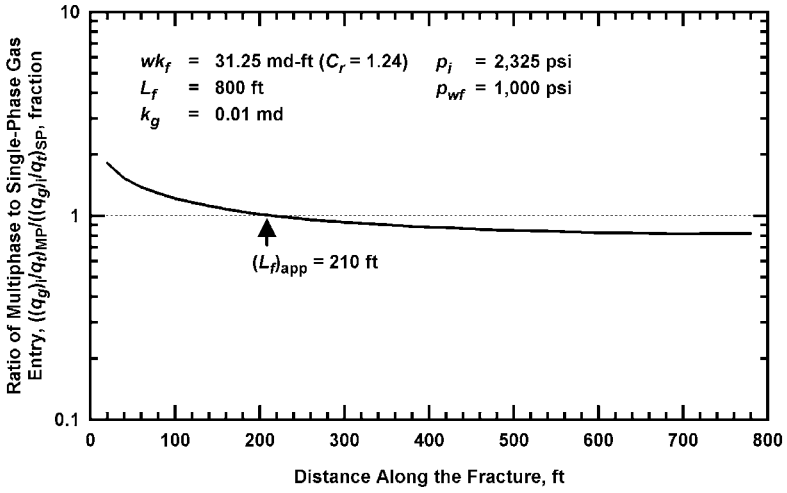

Fig. 4.56—Ratio of multiphase to single-phase gas entry profile for the low-pressure reservoir investigation (p_i = 2,325 psi, p_{wf} = 1,000 psi, wk_f = 31.25 md-ft, L_f = 800 ft, and k_g = 0.01 md).

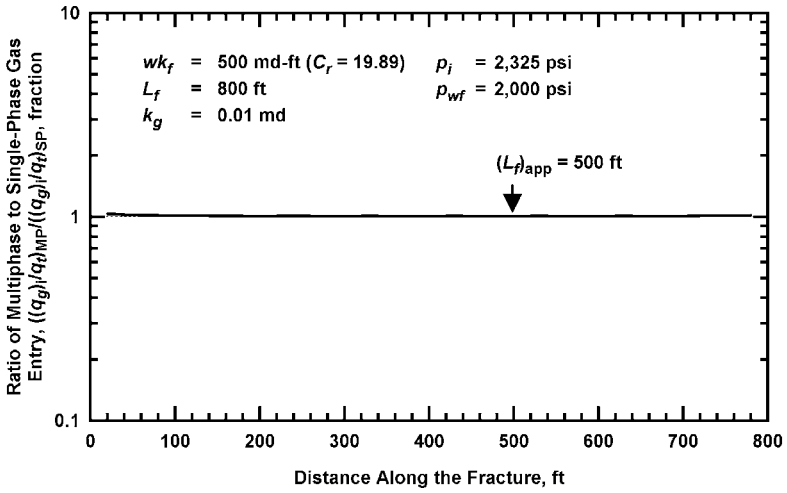

Fig. 4.57—Ratio of multiphase to single-phase gas entry profile for the low-pressure reservoir investigation (p_i = 2,325 psi, p_{wf} = 2,000 psi, wk_f = 500 md-ft, L_f = 800 ft, and k_g = 0.01 md)

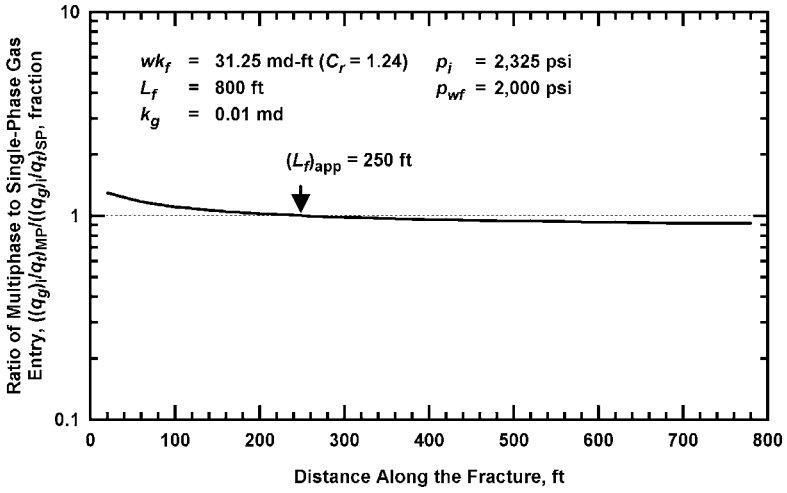

Fig. 4.58—Ratio of multiphase to single-phase gas entry profile for the low-pressure reservoir investigation (p_i = 2,325 psi, p_{wf} = 2,000 psi, wk_f = 31.25 md-ft, L_f = 800 ft, and k_g = 0.01 md)

4.2.3 Viscous Fracturing Fluid

While the gas cumulative gas recovery and fracture fluid recovery are affected significantly by fracture conductivity, the results presented so far indicate that the entire propped fracture is generally "effective" at 365 days for typical hydraulically fractured, low permeability reservoirs if the viscosity of the fluid in the invaded zone is 1 cp or less (i.e., water-based fracturing fluids). Field data often show that cleanup will proceed more slowly if the fluid to be displaced has a high viscosity. Thus, it is very important for the fluid to break under reservoir conditions to give a fluid with low viscosity. The average viscosity of the fluid used in the Moxa Arch Frontier formation is 30.6 cp (for the fracture treatments after 1992). I have no information if this value is representative of the fluid in the tubulars, perforations, fracture, or formation. In this section, I present the simulation results where the fracture fluid viscosity is greater than 1 cp.

Fig. 4.59 through **Fig. 4.61** present the ratio of the cleanup fracture half-length to the actual fracture half-length when the leakoff fluid viscosities are 50, 200, and 1,000 cp, respectively. For these runs, the actual fracture half-length is 800 ft and the formation permeability is 0.01 md. Fig. 4.59 (μ_w = 50 cp) shows that the cleanup length is 66% of the actual propped length at 30 days if the wk_f = 500 md (C_r = 19.89) and 16% of the actual propped length at 30 days if the wk_f = 31.25 md (C_r = 1.24). The ratio of the cleanup fracture half-length to the actual fracture half-length is close to unity within 2 months if the wk_f = 500 md-ft (assuming μ_w = 50 cp). However, if the wk_f = 31.25 md-ft, this ratio is close to unity within approximately one year. The results presented in Figs. 4.59 and 4.61 indicate that the cleanup length may be only a small fraction of the actual propped lengths even after a long time when the viscosity of the fracture fluid is greater than 50 cp. The greater the viscosity of the fracturing fluid to be displaced in the proppant pack and invaded zone, the lower the cleanup length versus time.

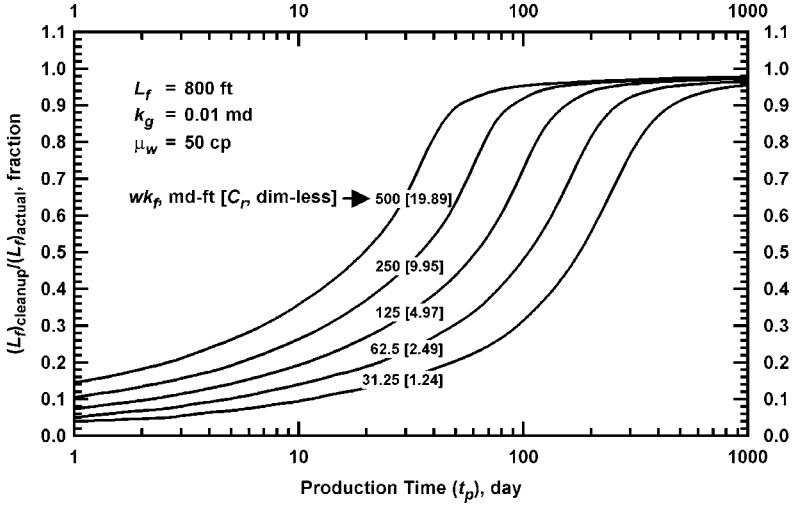

Fig. 4.59—Ratio of cleanup fracture half-length to actual fracture half-length for multiphase and non-Darcy flow cases with L_f = 800 ft, k_g = 0.01 md, and μ_w = 50 cp.

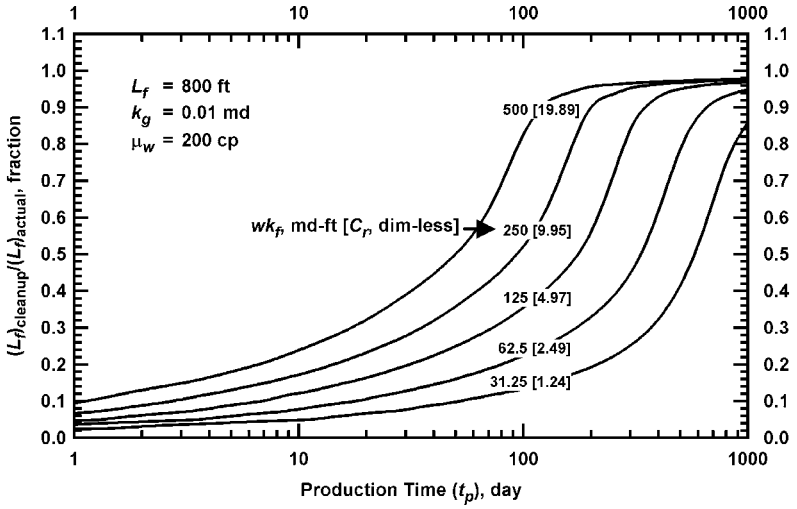

Fig. 4.60—Ratio of cleanup fracture half-length to actual fracture half-length for multiphase and non-Darcy flow cases with L_f = 800 ft, k_g = 0.01 md, and μ_w = 200 cp.

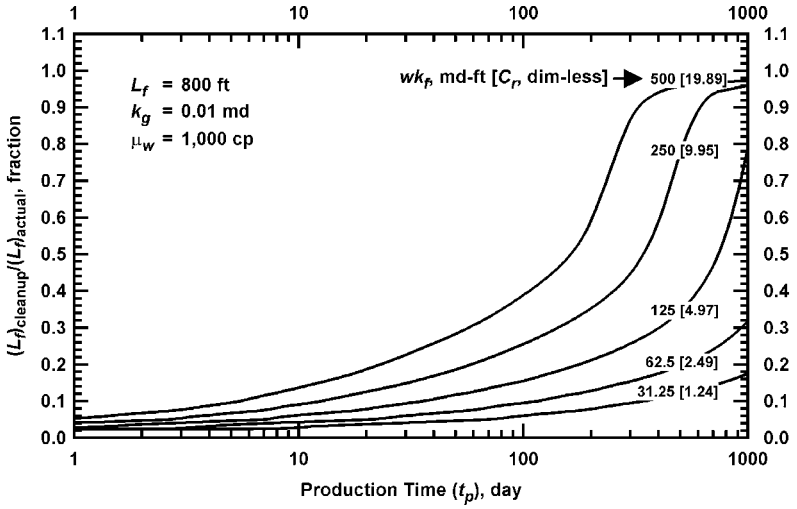

Fig. 4.61—Ratio of cleanup fracture half-length to actual fracture half-length for multiphase and non-Darcy flow cases with L_f = 800 ft, k_g = 0.01 md, and μ_w = 1,000 cp.

Fig. 4.62 through **Fig. 4.64** show the pressure distribution in the reservoir at 365 days for the cases shown in Figs. 4.59 to 4.61. As before, the pressure drops are greatest near the wellbore when the fracture conductivity is low. These pressure profiles in the reservoir show that the "effective" fracture length is reduced as the fracture fluid viscosity increases. In Fig. 4.64 (μ_w = 1,000 cp), the pressure drops are greatest near the wellbore despite having a C_r of 19.89. Note that the 50, 200, or 1,000 cp denotes the viscosity of the fracture fluid that remains in the proppant pack and invaded zone after the treatment. Even though prior work such as that by Voneiff, Robinson, and Holditch[30] reported that the viscosity of the fracture fluid can be several thousand centipoises and the viscous fracturing fluid is present in the proppant pack only, a recent published work[32] based on laboratory tests indicated that a significant amount of polymer residue may come in contact with the reservoir rock during the fracture treatment. The tests conducted on core samples showed that some of the gel residue is present in the rock and cannot be displaced instantly by production; it degrades and is removed slowly. This residue occupies the pore spaces of the rock and thereby reduces the permeability. The simulation results presented in Fig. 4.59 (μ_w = 50 cp) may be more likely than the ones portrayed in Figs.4.60 and 4.61 (μ_w's = 200 and 1,000 cp). This is because the gelling agents used in the fracture treatment will concentrate more within the proppant-pack than in the formation (i.e., the molecular sizes of the gelling agents are often too large to be able to penetrate into the matrix of the formations during fluid leakoff).

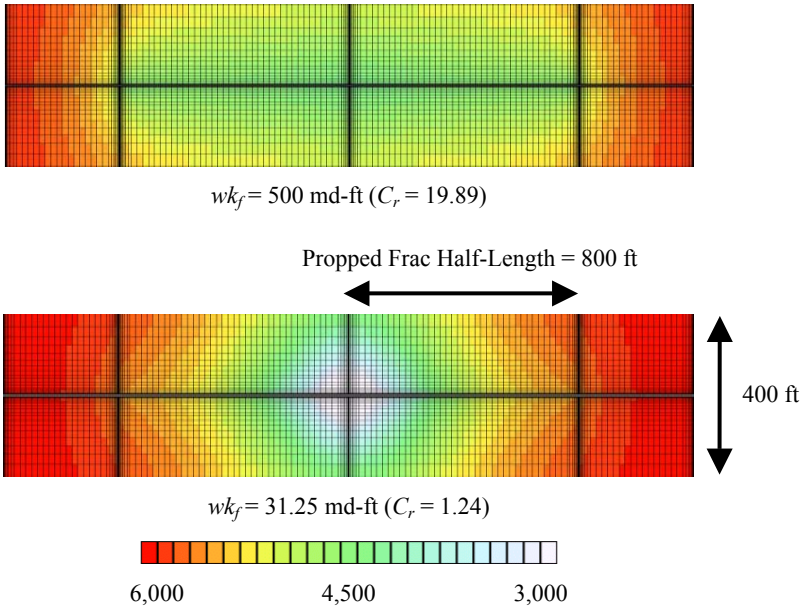

Fig. 4.62—Pressure distribution (psi) in the reservoir at 365 days for multiphase and non-Darcy flow cases with L_f = 800 ft, k_g = 0.01 md, and μ_w = 50 cp.

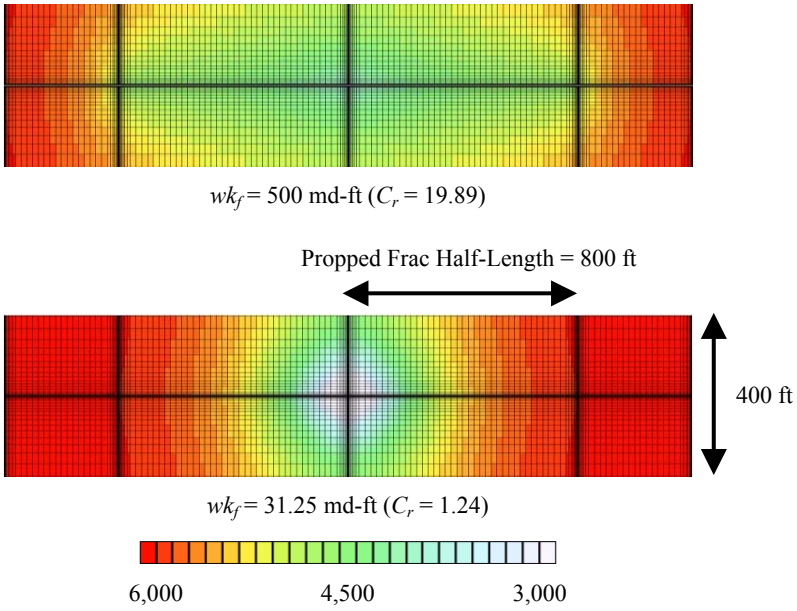

Fig. 4.63—Pressure distribution (psi) in the reservoir at 365 days for multiphase and non-Darcy flow cases with L_f = 800 ft, k_g = 0.01 md, and μ_w = 200 cp.

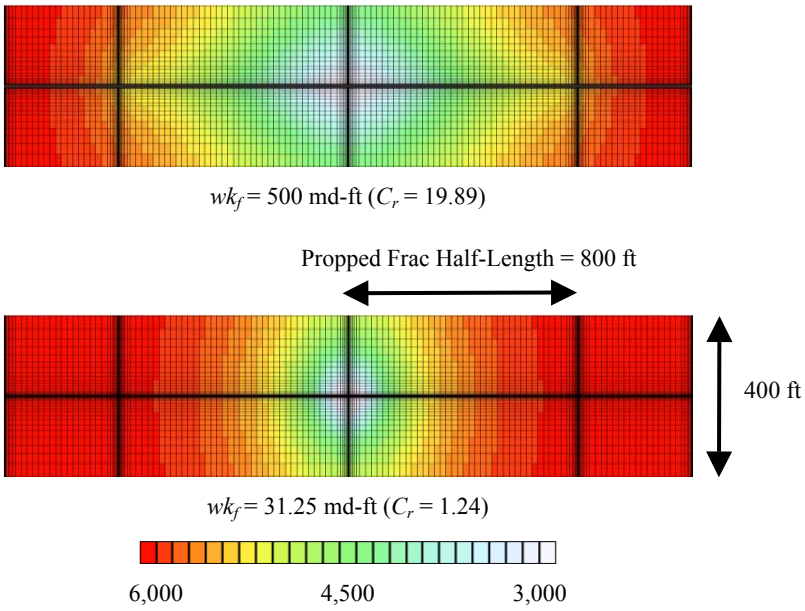

Fig. 4.64—Pressure distribution (psi) in the reservoir at 365 days for multiphase and non-Darcy flow cases with L_f = 800 ft, k_g = 0.01 md, and μ_w = 1,000 cp.

Fig. 4.65 through **Fig. 4.67** show the water saturation profiles at 365 days for the cases where the μ_w's = 50, 200, and 1,000 cp, respectively. The graphs show that the invaded zone is not cleaned up even after one year if the viscosity of the fluid to be displaced is a few hundred centipoises. The water saturation profiles shown in Fig. 4.65 (μ_w = 50 cp) indicate that the water saturation remains 70 to 80% around the fracture after 365 days if the wk_f = 500 md-ft and 90% if the wk_f = 31.25 md-ft. The injected water for these cases does not imbibe deeper into the formation, but it is either produced or stationary in the invaded zone for practical purposes. For the cases presented in Fig. 4.67 (μ_w = 1,000 cp), the gas enters the fracture near the wellbore and, the cleanup length is more like 20 to 50 ft instead of 800 ft. Therefore, when the viscous fracture fluid remains in the invaded zone, the cleanup length and gas productivity will be less than optimal.

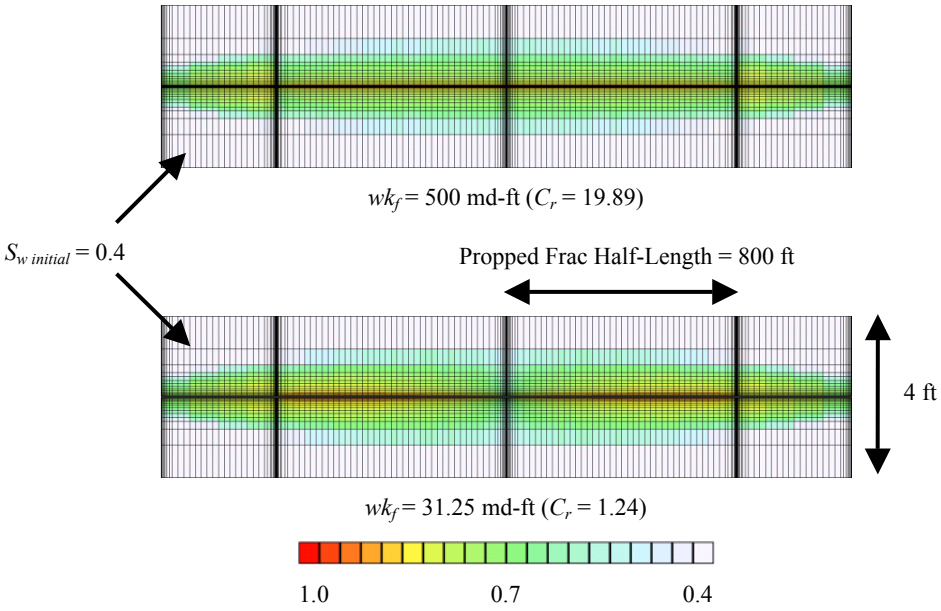

Fig. 4.65—Water saturation (fraction) in the reservoir at 365 days for multiphase and non-Darcy flow cases with L_f = 800 ft, k_g = 0.01 md, and μ_w = 50 cp.

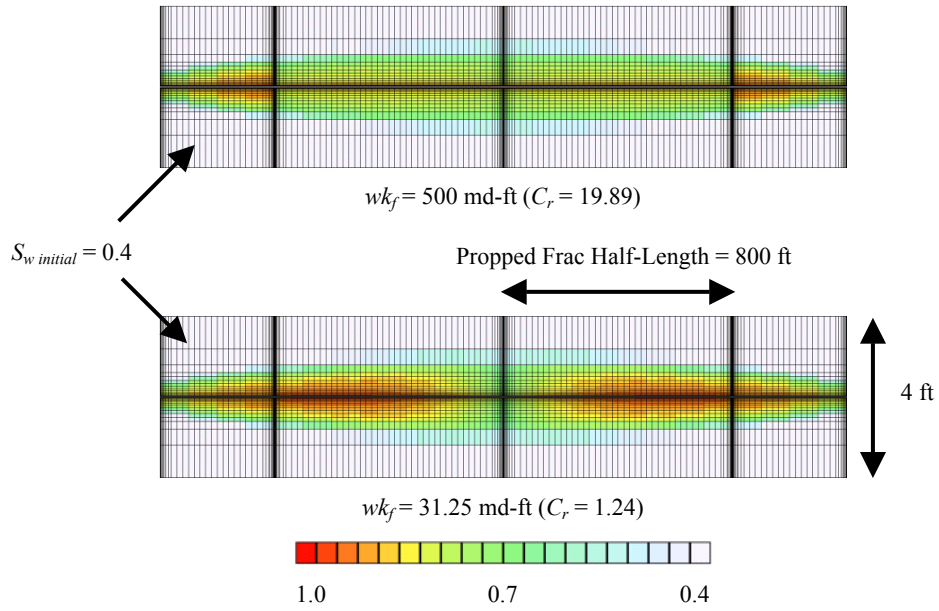

Fig. 4.66—Water saturation (fraction) in the reservoir at 365 days for multiphase and non-Darcy flow cases with L_f = 800 ft, k_g = 0.01 md, and μ_w = 200 cp.

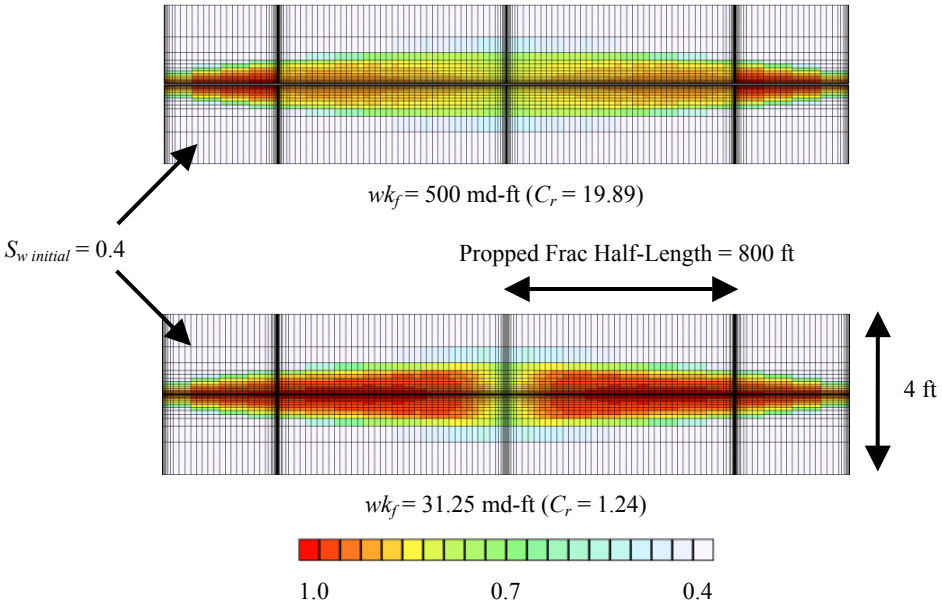

Fig. 4.67—Water saturation (fraction) in the reservoir at 365 days for multiphase and non-Darcy flow cases with L_f = 800 ft, k_g = 0.01 md, and μ_w = 1,000 cp.

Fig. 4.68 through **Fig. 4.70** show the effective gas permeability around the fracture at 365 days when the fracturing fluid viscosities are 50, 200, and 1,000 cp, respectively. The initial gas permeability in the formation (prior to fracturing) is 0.01 md (shown by the red color). All of these graphs indicate that the effective gas permeability is reduced more uniformly along the fracture if the fracture conductivity is high. However, if the fracture conductivity is low, the effective gas permeability is relatively higher near the wellbore and lower in the invaded zone away from the wellbore.

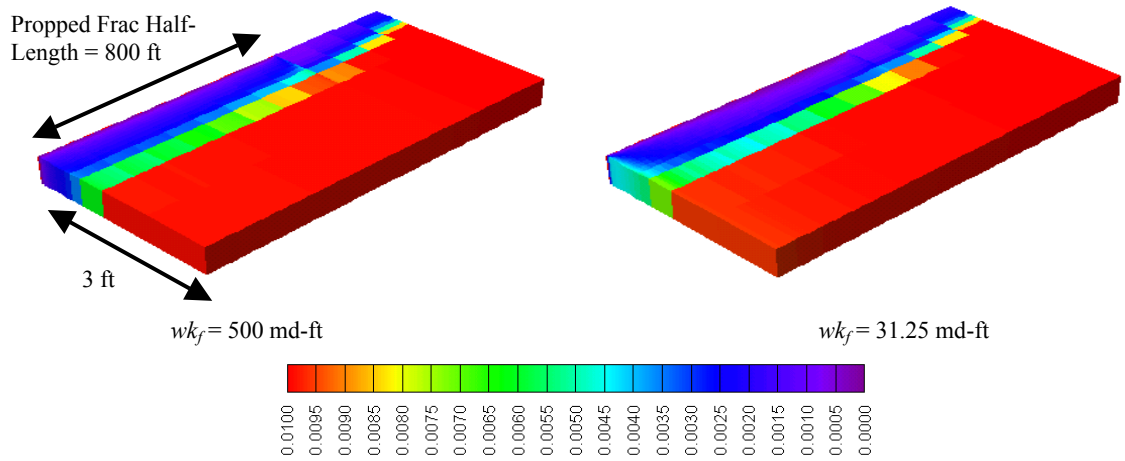

Fig. 4.68—Effective gas permeability map at 365 days for multiphase and non-Darcy flow cases with L_f = 800 ft, k_g = 0.01 md, and μ_w = 50 cp.

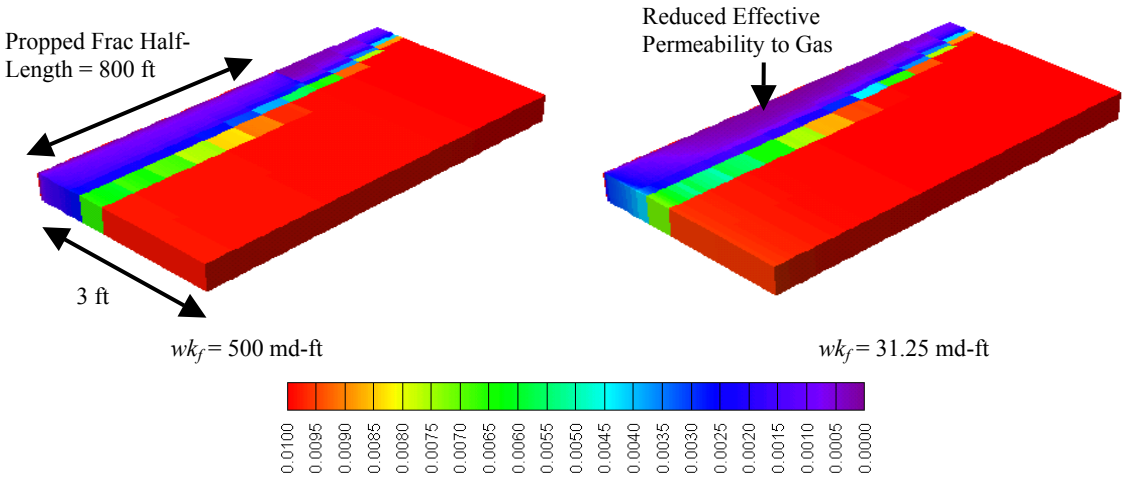

Fig. 4.69—Effective gas permeability map at 365 days for multiphase and non-Darcy flow cases with L_f = 800 ft, k_g = 0.01 md, and μ_w = 200 cp.

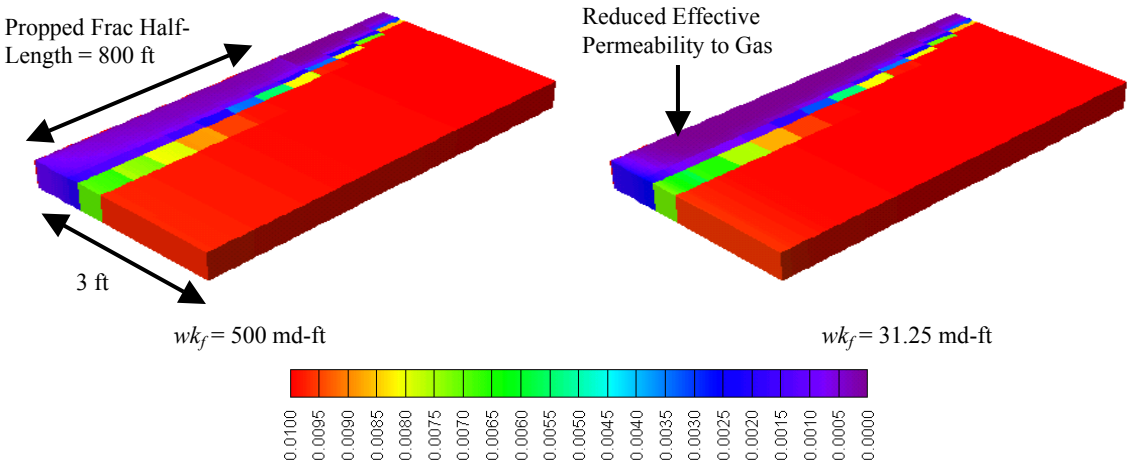

Fig. 4.70—Effective gas permeability map at 365 days for multiphase and non-Darcy flow cases with L_f = 800 ft, k_g = 0.01 md, and μ_w = 1,000 cp.

The fracture fluid recovery versus production time for these cases is presented in **Fig. 4.71** through **Fig. 4.73**. When the viscosity of the fluid to be displaced in the proppant pack and invaded zone is 1 cp, Fig. 4.26 indicates that about one-half the fracturing fluid is recovered within 30 to 60 days if the wk_f = 500 md-ft (C_r = 19.89). However, according to Fig. 4.71, the fracture is still cleaning up at 365 days. For the cases presented in Fig. 4.71, the fluid recovery at 365 days is 38% if the wk_f = 500 md-ft (C_r = 19.89) and 18% if the wk_f = 31.25 md-ft (C_r = 1.24). I conclude that the fractures will take a longer time to clean up if the fracturing fluid does not break properly. The fracture fluid production rates that require months or years to level off may be an indicative of the presence of the viscous fracture fluid in the proppant pack and/or the invaded zone around the fracture.

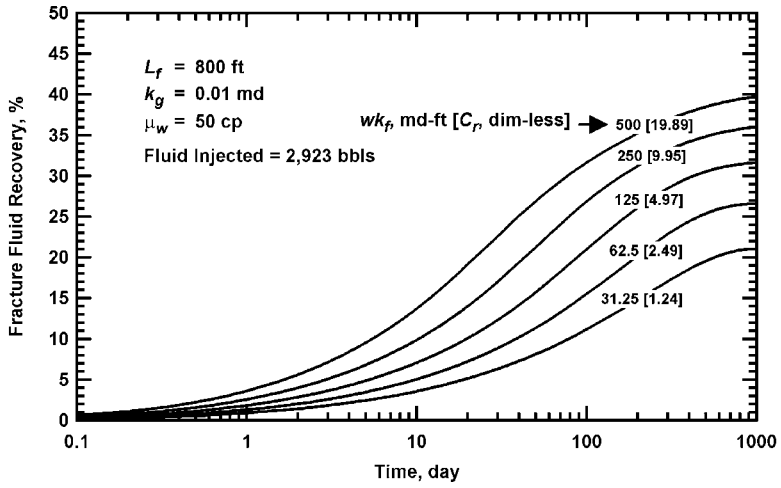

Fig. 4.71—Fracture fluid recovery versus production time for multiphase and non-Darcy flow cases with L_f = 800 ft, k_g = 0.01 md, and μ_w = 50 cp.

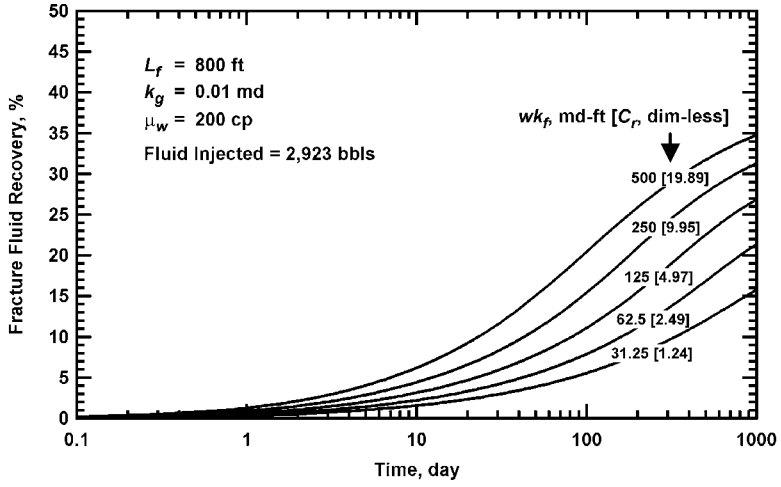

Fig. 4.72—Fracture fluid recovery versus production time for multiphase and non-Darcy flow cases with L_f = 800 ft, k_g = 0.01 md, and μ_w = 200 cp.

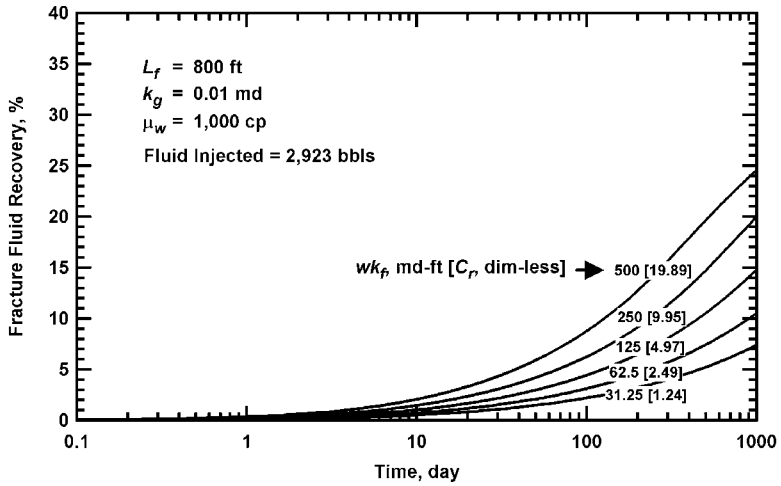

Fig. 4.73—Fracture fluid recovery versus production time for multiphase and non-Darcy flow cases with L_f = 800 ft, k_g = 0.01 md, and μ_w = 1,000 cp.

Fig. 4.74 and **Fig. 4.75** present the cumulative gas recovery and the gas flow rate for the cases with wk_f = 500 md-ft. The cumulative gas recovery and gas flow rate for the cases with wk_f = 31.25 md-ft are given in **Fig. 4.76** and **Fig. 4.77**. In Fig. 4.74 (wk_f = 500 md-ft), the cumulative gas recovery at 1,000 days is 3.3% for the case with the fluid viscosity of 1000 cp. In comparison, the cumulative gas recovery at 1,000 days is 2.2% for the case presented in Fig. 4.76 if the wk_f = 31.25 md-ft for the fluid viscosity of 1 cp. Thus for this case, the long-term gas production is affected more by fracture conductivity than by fluid viscosity. According to Voneiff *et al*.,[30] the fracturing fluids must break to a viscosity of 50 cp to ensure that gas flow rates are maximized. Figs. 4.74 and 4.75 indicate that the fracture fluid viscosity must be at least 50 cp if the fracture conductivity is high. However, if the fracture conductivity is low, the fracture fluid viscosity as low as 1 cp may be necessary to maximize the cumulative gas production (Figs. 4.76 and 4.77).

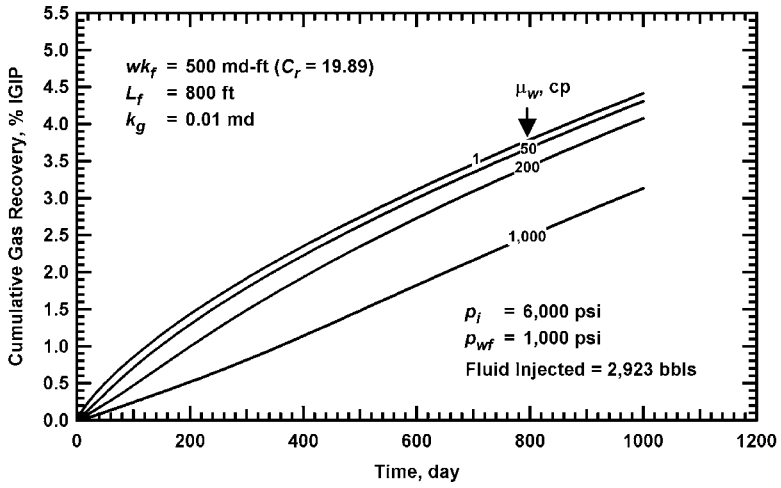

Fig. 4.74—Cumulative gas recovery versus production time for multiphase and non-Darcy flow cases with wk_f = 500 md-ft L_f = 800 ft, and k_g = 0.01 md.

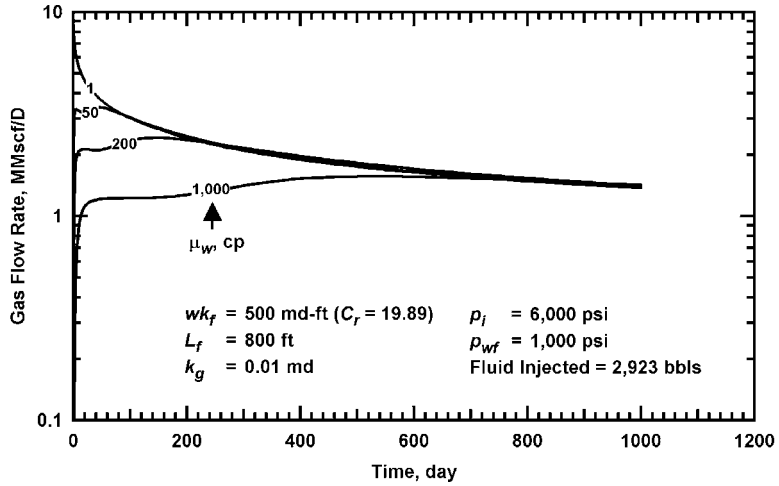

Fig. 4.75—Gas flow rate versus production time for multiphase and non-Darcy flow cases with wk_f = 500 md-ft, L_f = 800 ft, and k_g = 0.01 md.

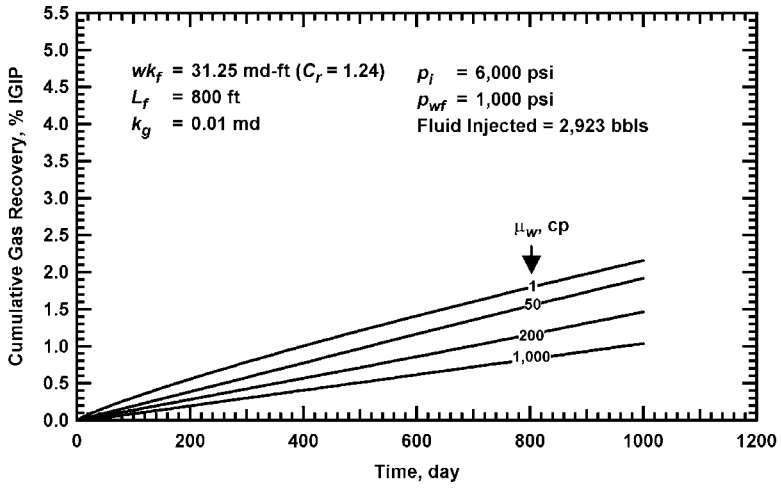

Fig. 4.76—Cumulative gas recovery versus production time for multiphase and non-Darcy flow cases with wk_f = 31.25 md-ft, L_f = 800 ft, and k_g = 0.01 md.

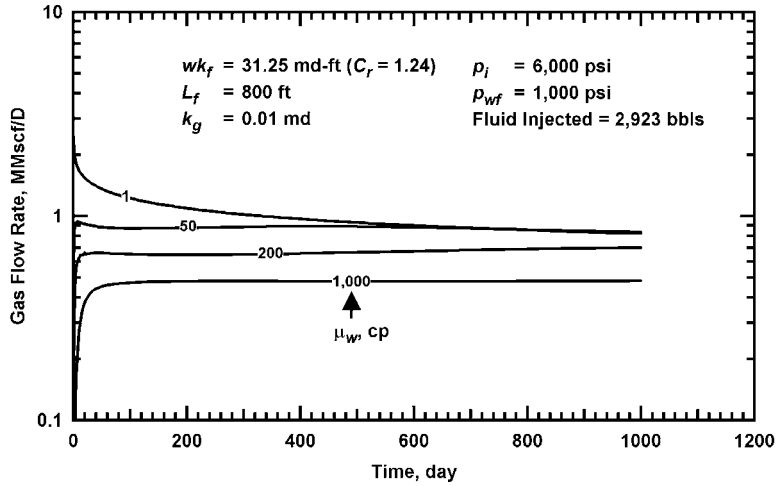

Fig. 4.77—Gas flow rate versus production time for multiphase and non-Darcy flow cases with wk_f = 31.25 md-ft, L_f = 800 ft, and k_g = 0.01 md.

Fig. 4. 78 portrays the cumulative gas recovery of the multiphase case (considering cleanup effects) with L_f = 800 ft and the corresponding single-phase cases (ignoring cleanup effects) with different fracture lengths if the wk_f = 500 md-ft and μ_w = 50 cp. The cumulative gas recovery between the multiphase and single-phase cases do not match at early times. For the single-phase cases, a high gas rate is typically achieved following the stimulation, however, when the viscous fluid is present in the proppant pack and/or invaded zone, a slowly increasing gas production rate for several weeks or months typically occurs. The effective fracture half-length ($(L_f)_{effective}$) is approximately 650 ft for the case presented in Fig. 4.78. However, if the

wk_f = 31.25 md-ft and μ_w = 50 cp, **Fig. 4.79** shows that the effective fracture half-length is 180 ft. **Fig. 4.80** through **Fig. 4.83** present the cumulative gas recovery versus production time for the cases where the μ_w's = 200 and 1,000 cp. The effective fracture half-lengths are 600 and 400 ft for the cases where the μ_w's = 200 and 1,000 cp, respectively if the wk_f = 500 md-ft. However, if the wk_f = 31.25 md-ft, the effective fracture half-lengths are 100 and 40 ft for the cases where the μ_w's = 200 and 1,000 cp, respectively.

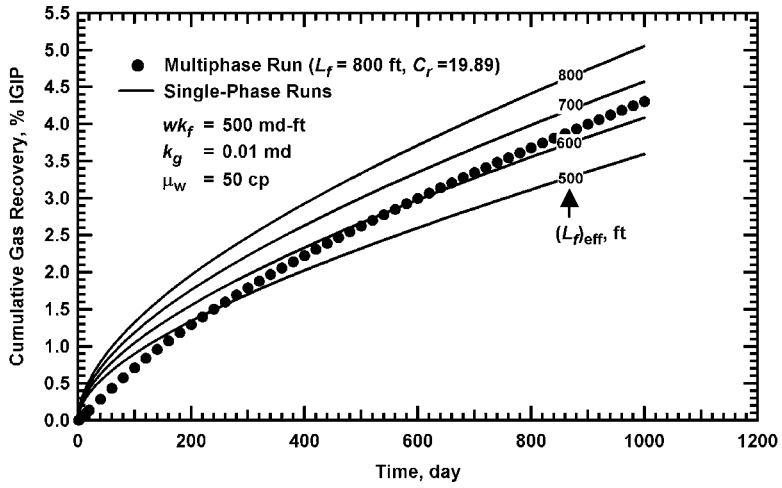

Fig. 4.78—Cumulative gas recovery versus production time for a multiphase and non-Darcy flow case with wk_f = 500 md-ft, L_f = 800 ft, k_g = 0.01 md, and μ_w = 50 cp and corresponding single-phase cases with different fracture lengths.

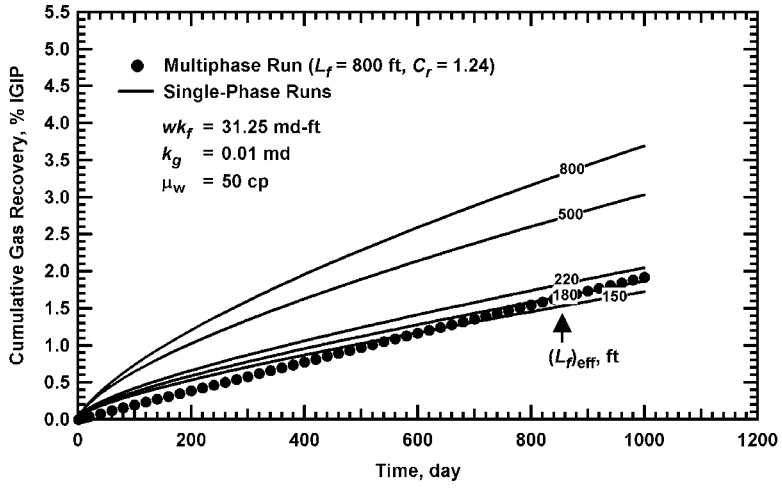

Fig. 4.79—Cumulative gas production versus production time for a multiphase and non-Darcy flow case with wk_f = 31.25 md-ft, L_f = 800 ft, k_g = 0.01 md, and μ_w = 50 cp and corresponding single-phase cases with different fracture lengths.

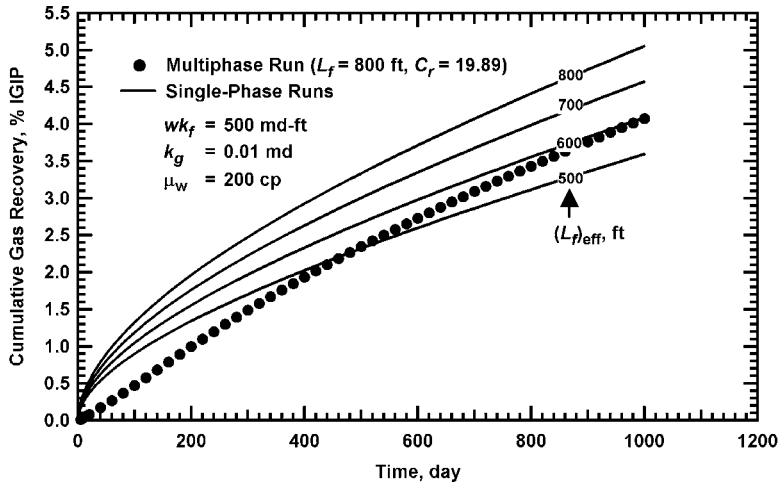

Fig. 4.80—Cumulative gas recovery versus production time for a multiphase and non-Darcy flow case with wk_f = 500 md-ft, L_f = 800 ft, k_g = 0.01 md, and μ_w = 200 cp and corresponding single-phase cases with different fracture lengths.

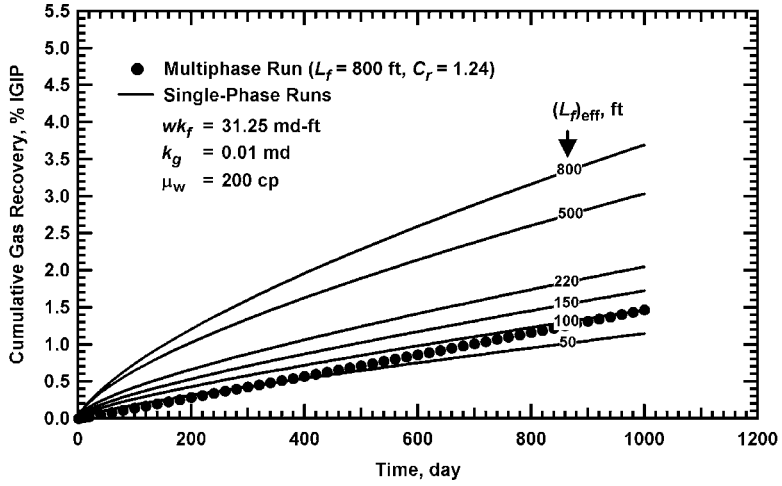

Fig. 4.81—Cumulative gas recovery versus production time for a multiphase and non-Darcy flow case with wk_f = 31.25 md-ft, L_f = 800 ft, k_g = 0.01 md, and μ_w = 200 cp and corresponding single-phase cases with different fracture lengths.

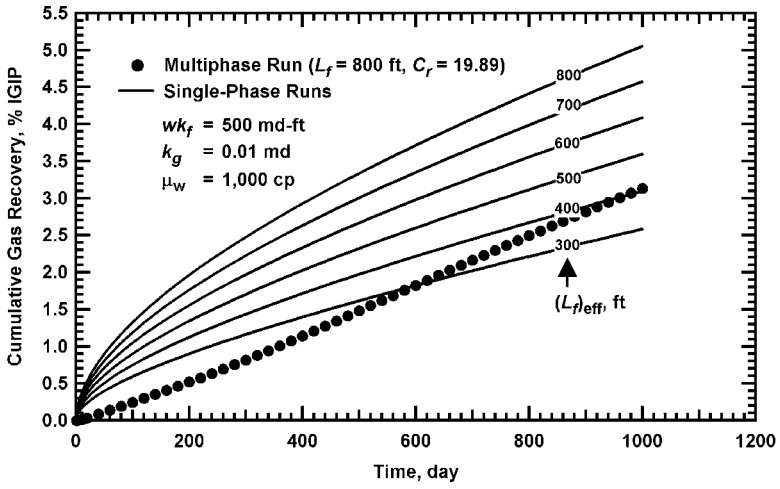

Fig. 4.82—Cumulative gas recovery versus production time for a multiphase and non-Darcy flow case with wk_f = 500 md-ft, L_f = 800 ft, k_g = 0.01 md, and μ_w = 1,000 cp and corresponding single-phase cases with different fracture lengths.

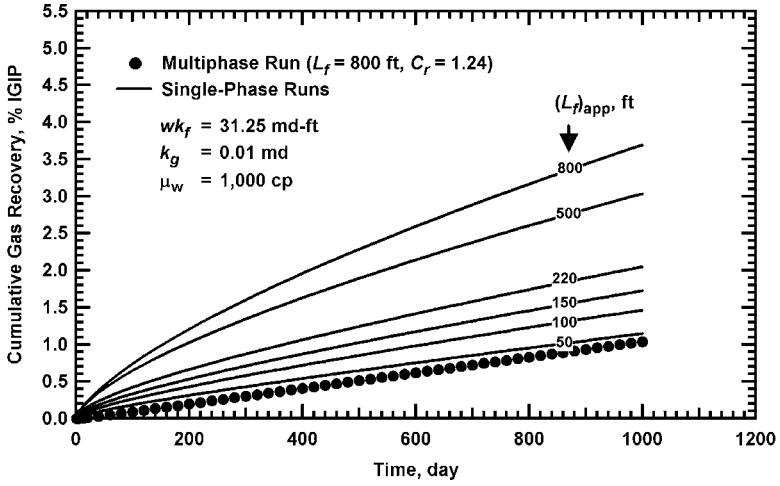

Fig. 4.83—Cumulative gas recovery versus production time for a multiphase and non-Darcy flow case with wk_f = 31.25 md-ft, L_f = 800 ft, k_g = 0.01 md, and μ_w = 1,000 cp and corresponding single-phase cases with different fracture lengths.

Fig. 4.84 through **Fig. 4.89** show the ratio of the multiphase to single-phase gas entry profile for the cases given in Figs. 4.78 to 4.83. The points where the curves intersect (i.e., the ratio of the multiphase to single-phase gas entry profile is unity) is generally close to the effective single-phase fracture length presented in Figs. 4.78 to 4.83. The apparent fracture half-lengths (i.e., where the curves intersect) are 600 ft for the case with the wk_f of 500 md-ft and 220 ft for the case with the wk_f of 31.25 md-ft if the μ_w = 50 cp. For the cases where the μ_w = 200 cp, the apparent fracture half-lengths are 230 ft for the case with the wk_f of 500

md-ft and 210 ft for the case with the wk_f of 31.25 md-ft. Similarly, for the cases where the μ_w = 1,000 cp, the apparent fracture half-lengths are 340 ft for the case with the wk_f of 500 md-ft and 120 ft for the case with the wk_f of 31.25 md-ft.

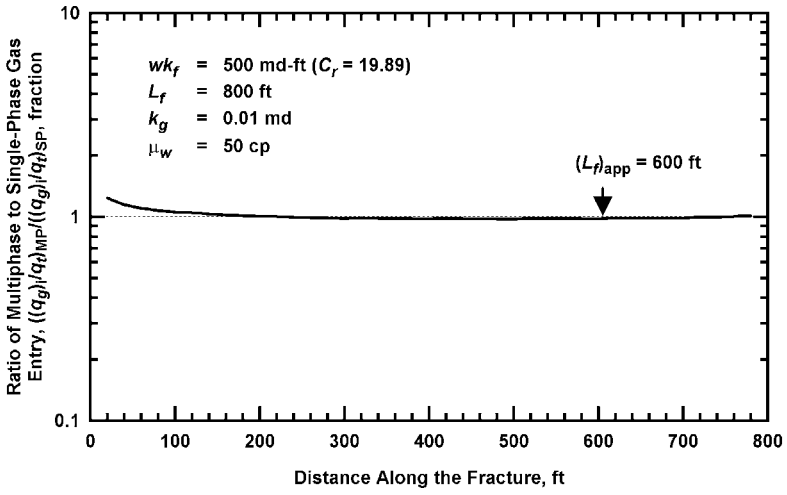

Fig. 4.84—Ratio of multiphase to single-phase gas entry profile for cases with wk_f = 500 md-ft, L_f = 800 ft, k_g = 0.01 md, and μ_w = 50 cp.

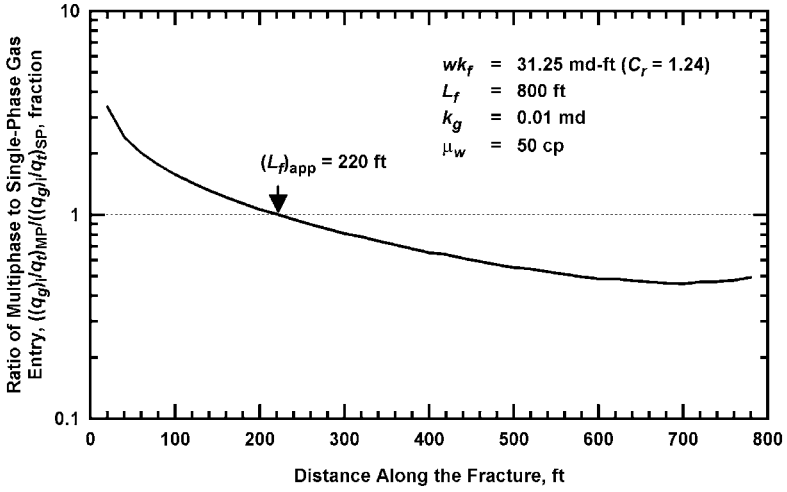

Fig. 4.85—Ratio of multiphase to single-phase gas entry profile for cases with wk_f = 31.25 md-ft, L_f = 800 ft, k_g = 0.01 md, and μ_w = 50 cp.

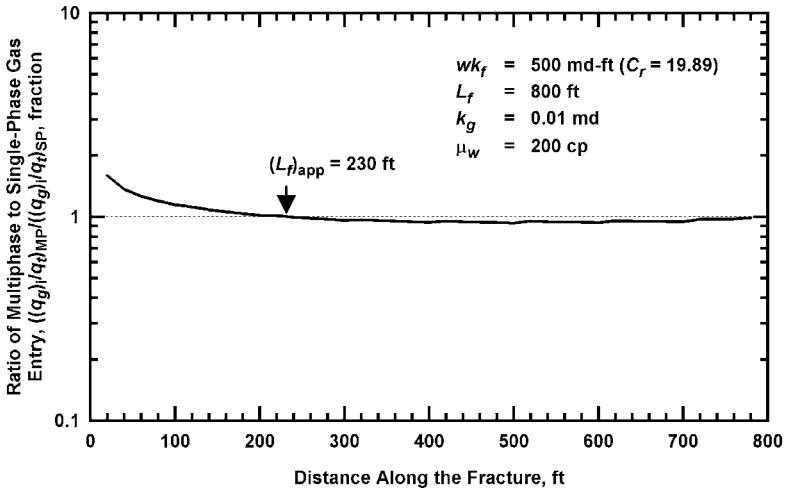

Fig. 4.86—Ratio of multiphase to single-phase gas entry profile for cases with wk_f = 500 md-ft, L_f = 800 ft, k_g = 0.01 md, and μ_w = 200 cp.

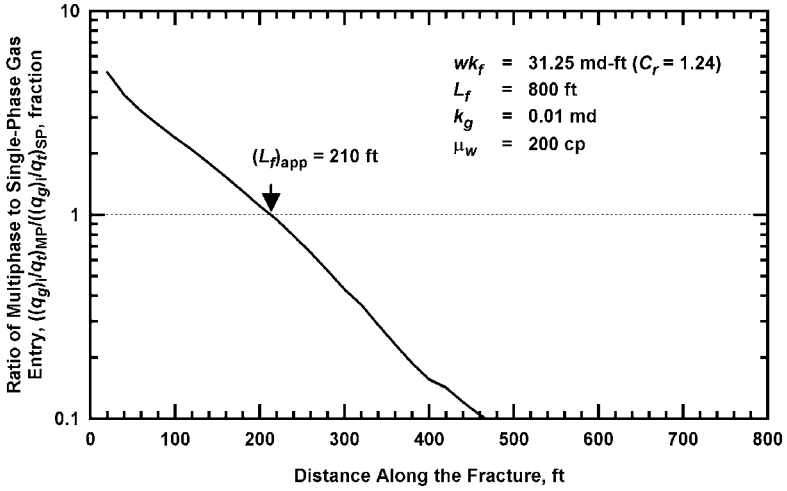

Fig. 4.87—Ratio of multiphase to single-phase gas entry profile for cases with wk_f = 31.25 md-ft, L_f = 800 ft, k_g = 0.01 md, and μ_w = 200 cp.

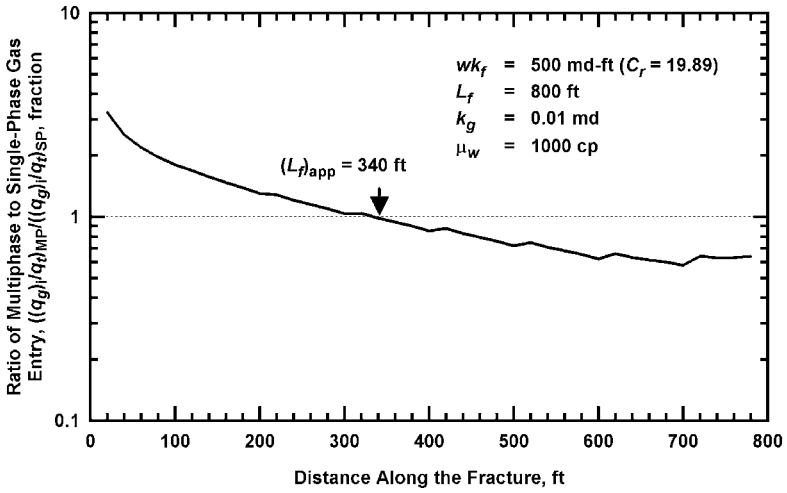

Fig. 4.88—Ratio of multiphase to single-phase gas entry profile for cases with wk_f = 500 md-ft, L_f = 800 ft, k_g = 0.01 md, and μ_w = 1,000 cp.

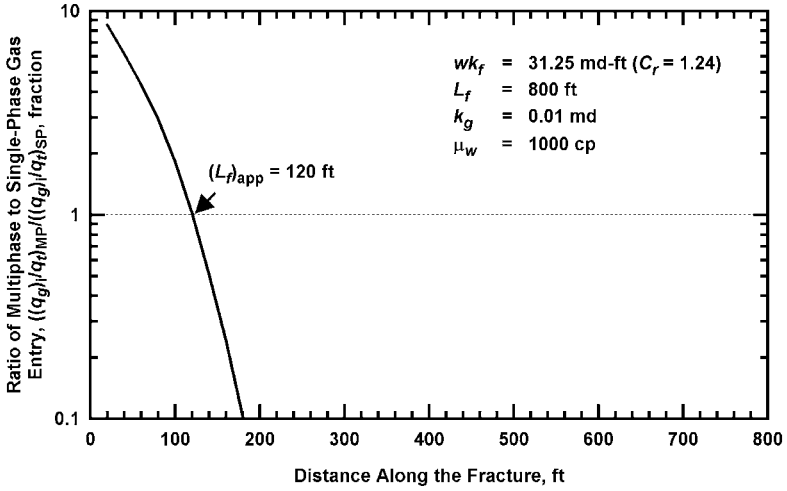

Fig. 4.89—Ratio of multiphase to single-phase gas entry profile for cases with wk_f = 31.25 md-ft, L_f = 800 ft, k_g = 0.01 md, and μ_w = 1,000 cp.

4.2.4 Fracture Closure Effect

In this section, I present the effects of fracture permeability reduction due to closure pressure on the effective fracture length and gas productivity. Closure pressure is the difference between the in-situ stress and the pore pressure in the fracture. Excessive closure stress above the strength of the propping agent causes severe crushing of the proppant and a subsequent reduction of fracture conductivity. In this work, changes in fracture permeability with closure pressure for 20/40 mesh InterProp proppant are given in **Fig. 3.4**. **Fig. 4.90** shows that the impact of closure pressure on the cleanup fracture length is small particularly when the fracture conductivity is high. **Fig. 4.91** and **Fig. 4.92** present the gas flow rates for the multiphase cases with and without closure pressure and the single-phase case (ignoring cleanup effects) when the wk_f's = 500 md-ft and 31.25 md-ft, respectively. For these cases, the viscosity of the fluid injected is assumed to be 1 cp. As shown, the single-phase case reaches a maximum gas flow rate immediately after the well is put on production. When the fracturing fluid is considered and the fracture closure effect is ignored, the well requires a few hours to attain a maximum gas production. The amount of time required to achieve the peak gas production for the multiphase case with the closure pressure included is relatively the same as that for the multiphase case without the closure pressure. However, the gas productivity is reduced if the fracture closure effect is present. Note that the peak gas flow rate for the multiphase case with closure pressure is 7.6 MMscf/D if the wk_f = 500 md-ft (Fig. 4.91). However, the peak gas flow rate for the multiphase case without closure pressure is 2.8 MMscf/D if the wk_f = 31.25 md-ft (Fig. 4.92). Therefore, the gas productivity is affected more by fracture conductivity than by fracture closure effect.

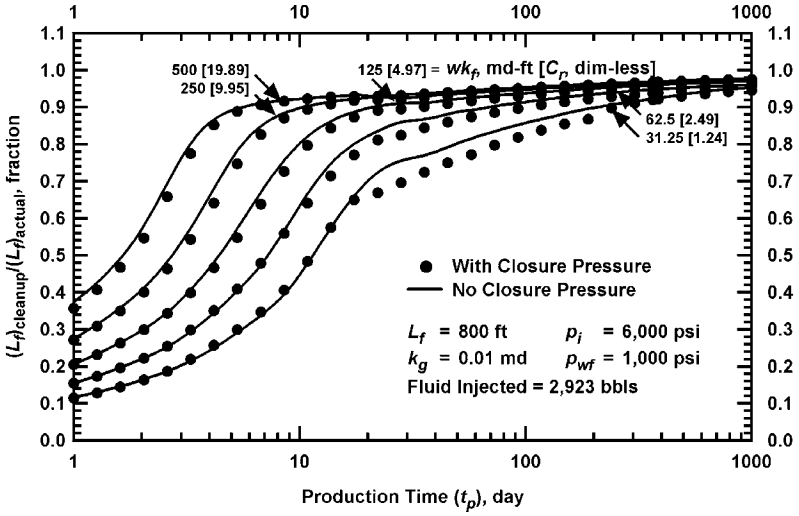

Fig. 4.90—Effect of fracture permeability reduction with closure pressure on cleanup fracture length for multiphase and non-Darcy flow cases with L_f = 800 ft and k_g = 0.01 md.

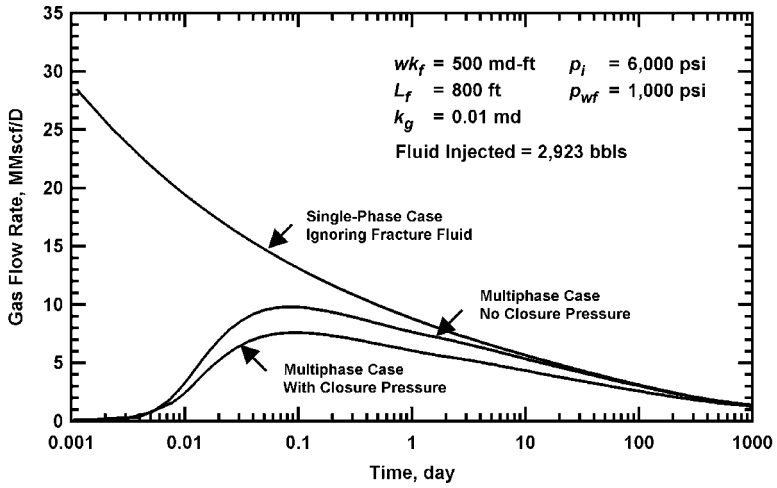

Fig. 4.91—Comparison of single-phase gas flow rate (ignoring cleanup effects) and multiphase gas flow rates with and without closure pressure for cases with wk_f = 500 md-ft, L_f = 800 ft, and k_g = 0.01 md.

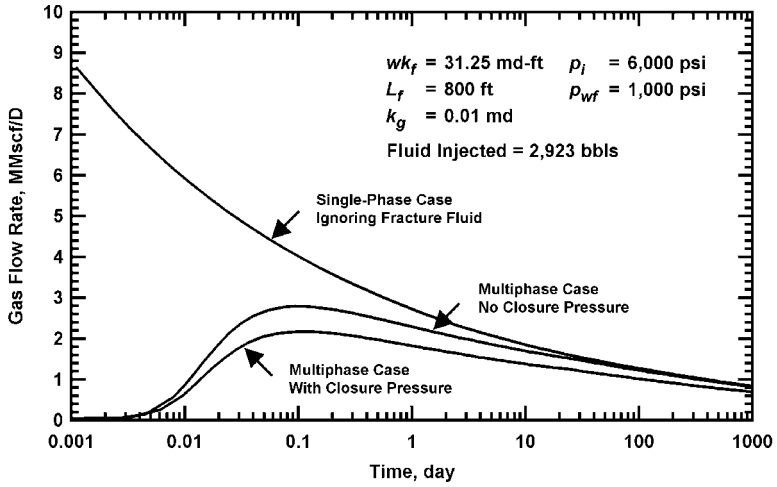

Fig. 4.92—Comparison of single-phase gas flow rate (ignoring cleanup effects) and multiphase gas flow rates with and without closure pressure for cases with wk_f = 31.25 md-ft, L_f = 800 ft, and k_g = 0.01 md.

The fluid recovery for the cases with and without closure pressure for varying fracture conductivities is presented in **Fig. 4.93**. The dashed lines are the fracture fluid recovery when the closure pressure is ignored. The solid lines indicate the fracture fluid recovery when the closure pressure effect is present. The fracture fluid production rates begin to level at about the same time for both the cases. However, the fluid recovery is reduced by 10 to 20% when the closure pressure is included.

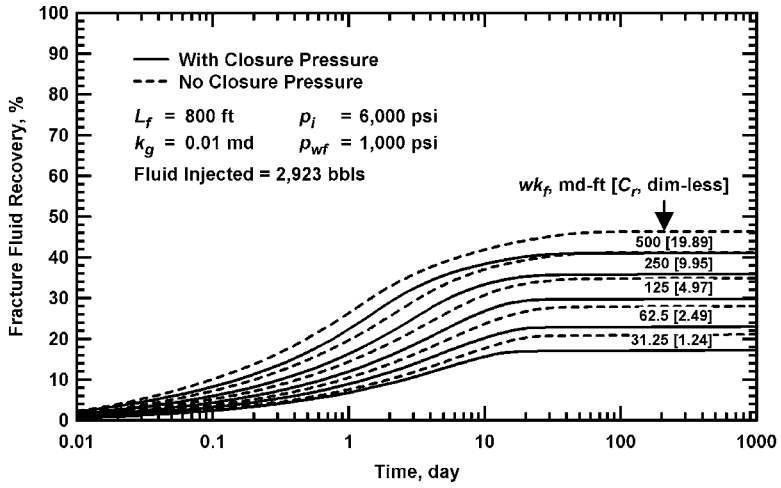

Fig. 4.93—Effect of fracture permeability reduction with closure pressure on fracture fluid recovery for multiphase and non-Darcy flow cases with L_f = 800 ft and k_g = 0.01 md.

The cumulative gas recovery for the cases with and without closure pressure is presented in **Fig. 4.94**. Small arrows at 1,000 days indicate the cumulative gas recovery when the closure pressure is neglected. The IGIP is 45,586 MMscf. For these cases, the cumulative gas recovery is reduced by 11 to 16% due to fracture closure effect.

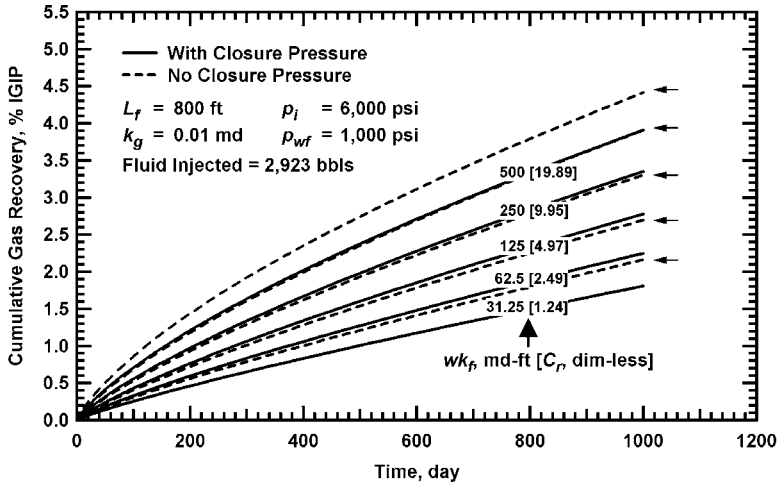

Fig. 4.94—Effect of fracture permeability reduction with closure pressure on cumulative gas recovery for multiphase and non-Darcy flow cases with L_f = 800 ft and k_g = 0.01 md.

Fig. 4. 95 and **Fig. 4.96** compare the cumulative gas recovery of the multiphase cases with and without closure pressure (L_f = 800 ft) and the corresponding single-phase cases (ignoring cleanup effects) with different fracture lengths. The effective fracture half-lengths are approximately 660 ft for the multiphase case without closure pressure and 580 ft for the case with closure pressure if the wk_f = 500 md-ft (C_r = 19.89). In comparison, the effective fracture half-lengths are 220 ft for the multiphase case without closure pressure and 175 ft for the case with closure pressure if the wk_f = 31.25 md-ft (C_r = 1.24). I conclude that the effective fracture lengths decrease when the closure pressure is present. However, the cleanup lengths indicate small difference between the cases with and without closure pressure.

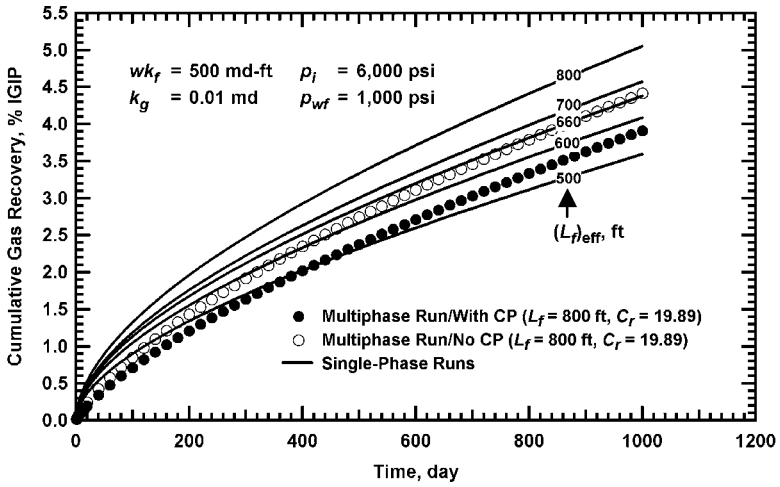

Fig. 4.95—Cumulative gas recovery versus production time for the multiphase cases with and without closure pressure (wk_f = 500 md-ft, L_f = 800 ft, and k_g = 0.01 md) and the corresponding single-phase cases with different fracture lengths.

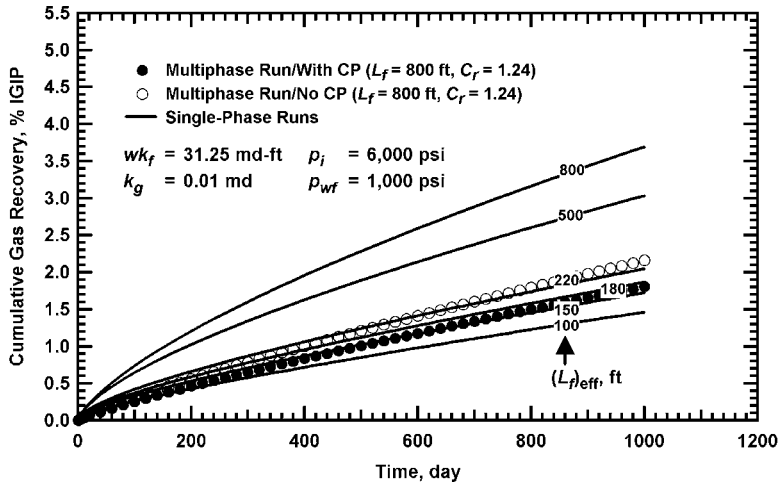

Fig. 4.96—Cumulative gas recovery versus production time for the multiphase cases with and without closure pressure (wk_f = 31.25 md-ft, L_f = 800 ft, and k_g = 0.01 md) and the corresponding single-phase cases with different fracture lengths.

Fig. 4.97 and **Fig. 4.98** show the ratio of multiphase to single-phase gas entry profile for these. The points, where the curves intersect, correlate well with the effective single-phase fracture length presented in Figs. 4.95 and 4.96. The apparent fracture half-lengths (i.e., where the curves intersect) are 600 ft for the case with the wk_f of 500 md-ft and 120 ft for the case with the wk_f of 31.25 md-ft.

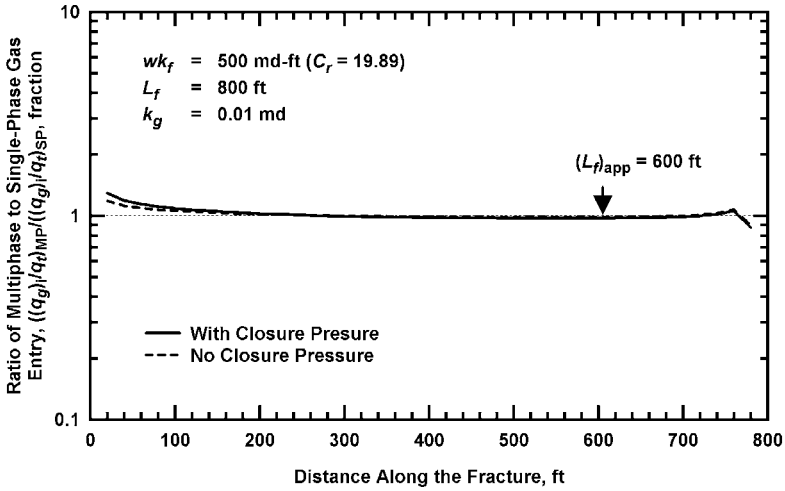

Fig. 4.97—Ratio of multiphase to single-phase gas entry profile for cases with and without closure pressure (wk_f = 500 md-ft, L_f = 800 ft, and k_g = 0.01 md).

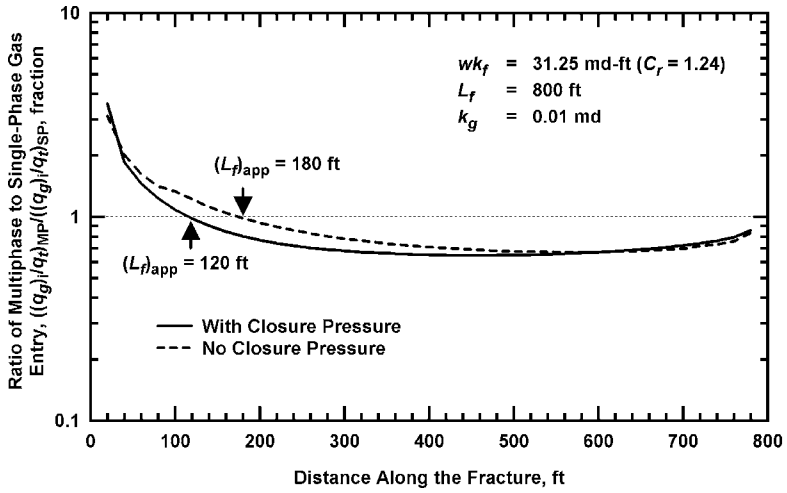

Fig. 4.98—Ratio of multiphase to single-phase gas entry profile for cases with and without closure pressure (wk_f = 31.25 md-ft, L_f = 800 ft, and k_g = 0.01 md).

4.2.5 Reservoir Water Mobility

All runs discussed so far were made using an initial water saturation (S_w) of 40%. At 40% water saturation, the relative water permeability (k_{rw}) is zero and the relative gas permeability (k_{rg}) is 0.438 (Fig. 3.2). Thus, the formation water is immobile at 40% water saturation. To investigate the effect of mobile reservoir water on the effective fracture length and fracture fluid production, I made runs with an initial water saturation of 55%. At this saturation, the k_{rw} = 0.001865 and k_{rg} = 0.239025. In this work the effective gas permeability (k_g) is 0.01 md at S_w = 40%. Thus, at S_w = 55%, the k_g is 0.0055 md (i.e., the absolute formation permeability, k, is constant). **Fig. 4.99** portrays the ratio of the cleanup fracture half-length to the actual fracture half-length versus time for the cases with mobile reservoir water (S_w = 55%) and immobile reservoir water (S_w = 40%). This graph indicates that the reservoir water mobility is relatively unimportant with respect to the cleanup length.

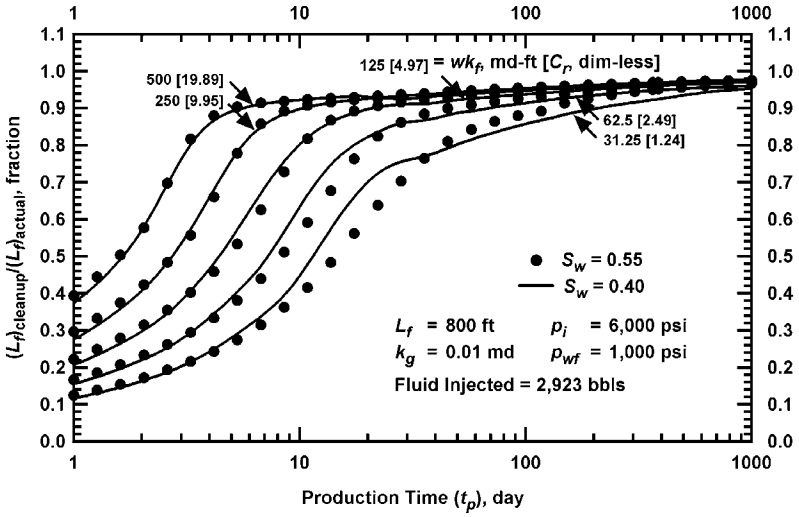

Fig. 4.99—Effect of mobile reservoir water on cleanup fracture length for multiphase and non-Darcy flow cases with L_f = 800 ft and k_g = 0.01 md.

Fig. 4.100 shows the pressure distribution in the reservoir at 365 days for the cases with mobile reservoir water. The reservoir pressure is 6,000 psi (shown by the red color). The bottomhole flowing pressure has not reached the minimum bottomhole pressure (1,000 psi) at 365 days. The light color indicates low reservoir pressures. Comparing Fig. 4.100 (mobile reservoir water) and Fig. 4.22 (immobile reservoir water), the reservoir pressures are much lower around the fracture when the reservoir water is mobile. At 365 days, the average reservoir pressure around the fracture is 4,300 psi if the water saturation is 40% (immobile) and 3,350 psi if the water saturation is 55% (mobile). Fig. 4.100 suggests that the "effective" fracture length is much different depending on fracture conductivity when considering the pressure distribution around the fracture.

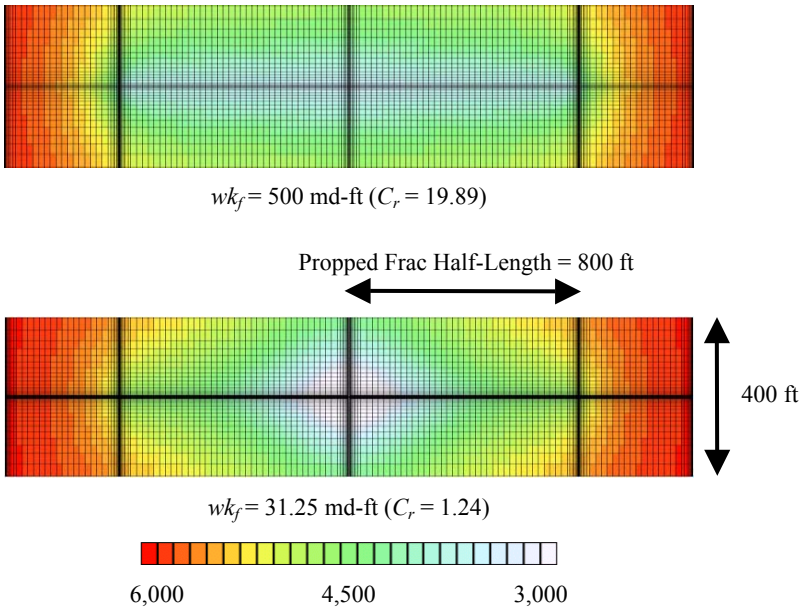

Fig. 4.100—Pressure distribution (psi) in the reservoir at 365 days for multiphase and non-Darcy flow cases with L_f = 800 ft, k_g = 0.01 md, and S_w = 0.55 (S_{wirr} = 0.40).

Fig. 4.101 and **Fig. 4.102** present the water saturation profiles around the fracture at 1 day and 365 days for the cases presented in Fig. 4.100. The entire propped length becomes effective at 365 days for both the high and low conductivity fractures. For these cases, the injected water imbibes much deeper into the formation (~50 ft). At 365 days, the water saturation remains high near the fracture (70 to 80%) and it decreases gradually as it moves away from the fracture.

Fig. 4.103 compares the effective gas permeability around the fracture at 365 days for the high and low conductivity fractures given in Figs. 4.101 and 4.102. Note that the initial gas permeability in the formation (prior to fracturing) is 0.0055 md. Changing nothing else but fracture conductivity, the effective gas permeability around the fracture is greatest near the wellbore if the fracture conductivity is low. The effective gas permeability is reduced more uniformly along the fracture when the fracture conductivity is high.

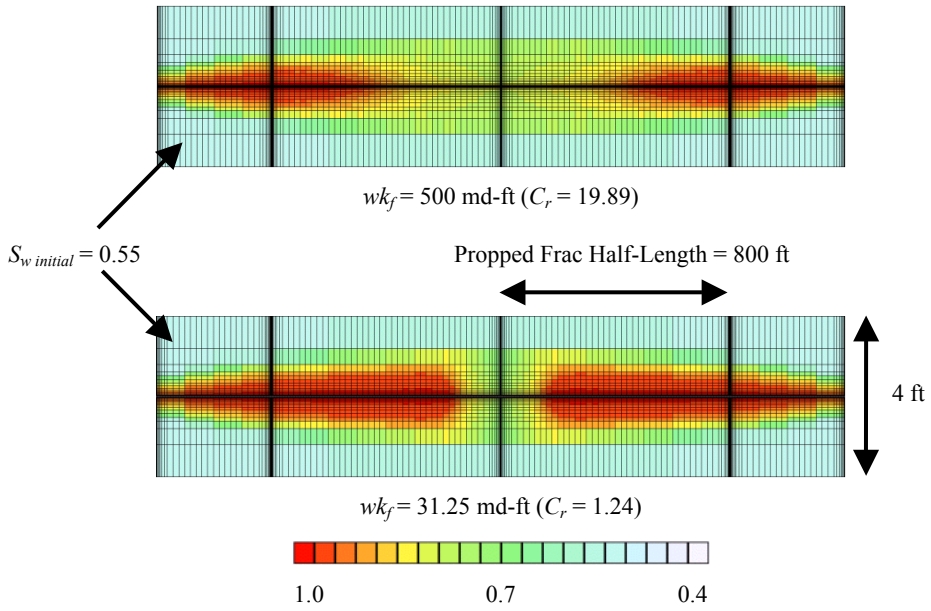

Fig. 4.101—Water saturation (fraction) in the reservoir at 1 day for multiphase and non-Darcy flow cases with L_f = 800 ft, k_g = 0.01 md, and S_w = 0.55 (S_{wirr} = 0.40).

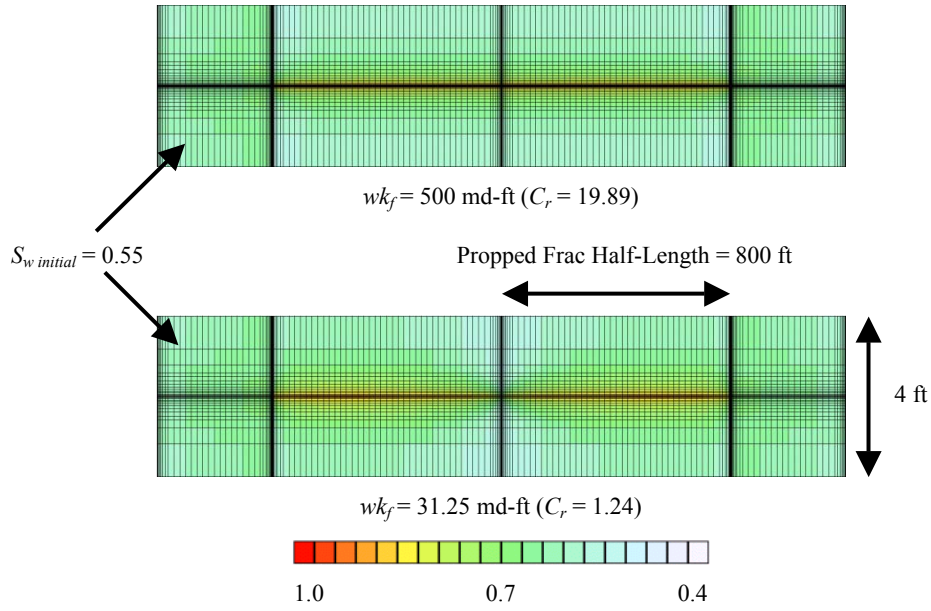

Fig. 4.102—Water saturation (fraction) in the reservoir at 365 days for multiphase and non-Darcy flow cases with L_f = 800 ft, k_g = 0.01 md, and S_w = 0.55 (S_{wirr} = 0.40).

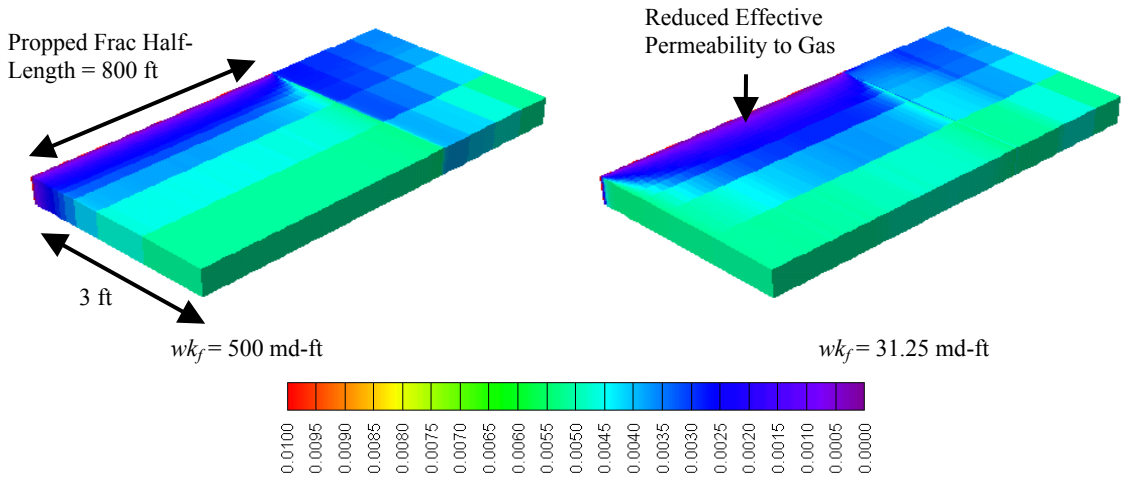

Fig. 4.103—Effective gas permeability map at 365 days for multiphase and non-Darcy flow cases with L_f = 800 ft, k_g = 0.01 md, and S_w = 0.55 (S_{wirr} = 0.40).

Fig. 4.104 portrays the cumulative water production for the cases with S_w = 55% and S_w = 40%, respectively. At 40% water saturation, the water produced is injected water. At 55% water saturation, the water produced is the injected water and formation water. Computer runs were made for the cases with S_w = 55% without the injected water. To determine the amount of injected water recovery for the cases with mobile reservoir water, the water produced from the cases with S_w = 55% without the injected water. (i.e., formation water) was subtracted from the cumulative water produced (i.e., formation and injected water) obtained from Fig. 4.104. The fracture fluid recovery versus production time for the cases with S_w = 55% and S_w = 40% is presented in **Fig. 4.105**. Fig. 4.105 portrays that the fracture fluid recovery increases when the reservoir water is mobile. At 365 days, the fluid recovery is 46% if the S_w = 40% and 73% if the S_w = 55% when the wk_f = 500 md-ft (C_r = 19.89). As a conclusion, the reservoir water mobility helps to increase the fracture fluid recovery.

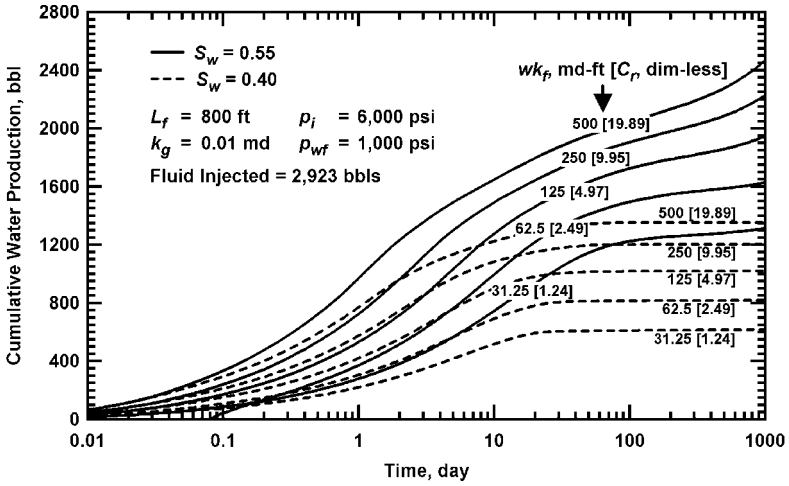

Fig. 4.104—Cumulative water production for multiphase and non-Darcy flow cases with and without mobile reservoir water (L_f = 800 ft and k_g = 0.01 md).

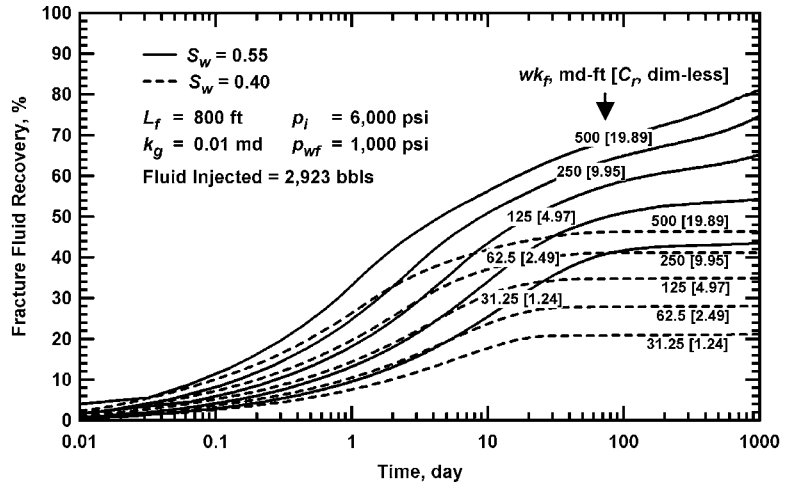

Fig. 4.105—Effect of mobile reservoir water on fracture fluid recovery for multiphase and non-Darcy flow cases with L_f = 800 ft and k_g = 0.01 md.

Fig. 4.106 shows the cumulative gas recovery versus production time for the cases with and without mobile reservoir water. The cumulative gas recovery decreases when the water saturation increases. Even though the fracture fluid recovery is high due to the reservoir water mobility, the cumulative gas recovery is reduced. This is because the effective gas permeability decreases with increasing water saturation. **Fig. 4.107** shows the cumulative gas recovery for the cases with and without injected fluid when the reservoir water is mobile. Small arrows at 1,000 days indicate the cumulative gas recovery for the cases without the injected water. The graph suggests that the effect of fracturing fluid on gas productivity may be small

when the reservoir water is mobile. This is because the fluid recovery is large and the effective gas permeability in the invaded zone has been high enough for these cases.

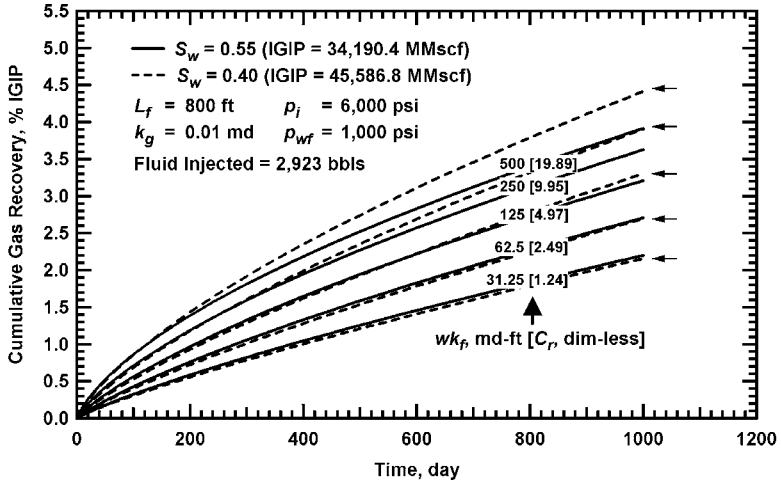

Fig. 4.106—Effect of mobile reservoir water on cumulative gas recovery for multiphase and non-Darcy flow cases with L_f = 800 ft and k_g = 0.01 md.

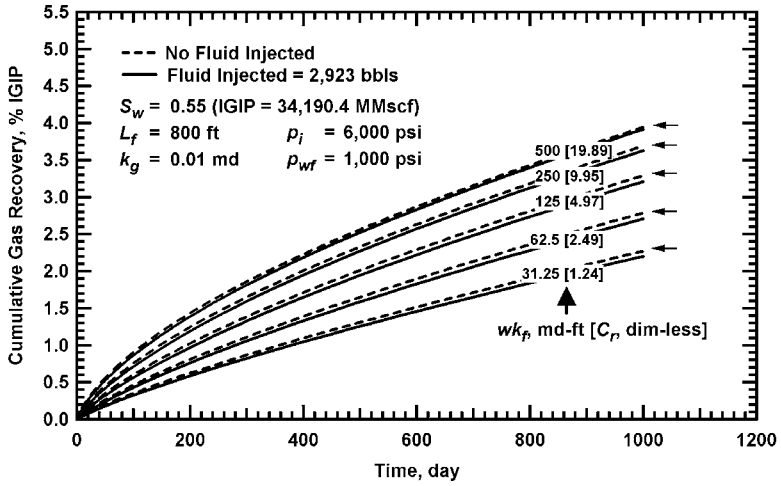

Fig. 4.107—Effect of fracture fluid on cumulative gas recovery for multiphase and non-Darcy flow cases with L_f = 800 ft, k_g = 0.01 md, and S_w = 0.55.

Fig. 4. 108 compares the cumulative gas recovery of the multiphase cases with mobile and immobile reservoir water (L_f = 800 ft) and the corresponding single-phase cases (ignoring cleanup effects) with different fracture lengths if the wk_f = 500 md-ft. The effective fracture half-lengths are approximately 660 ft for the multiphase case with immobile reservoir water and 570 ft for the case with mobile reservoir

water. Accordingly, the effective fracture lengths decrease when the mobile reservoir water is present even though the cleanup lengths indicate small difference between the cases with and without mobile reservoir water. The apparent fracture half-lengths are 220 ft for the multiphase cases with mobile reservoir water and immobile reservoir water if the wk_f = 31.25 md-ft (**Fig. 4.109**).

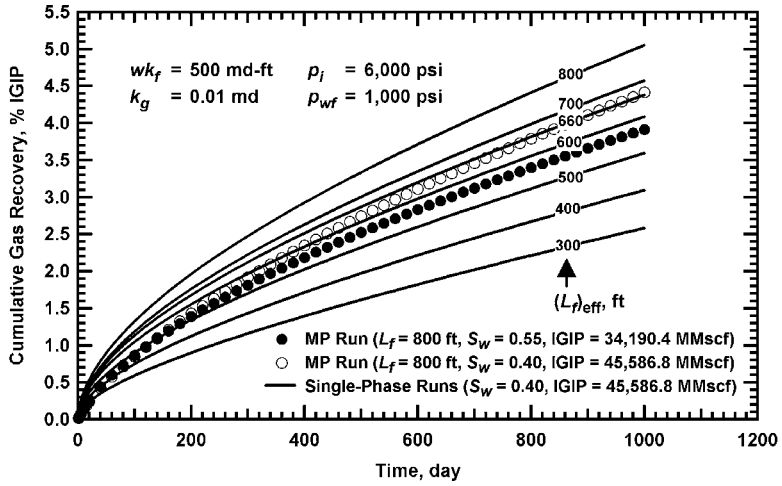

Fig. 4.108—Cumulative gas recovery versus production time for the multiphase cases with and without mobile reservoir water (wk_f = 500 md-ft, L_f = 800 ft, and k_g = 0.01 md) and the corresponding single-phase cases with different fracture lengths.

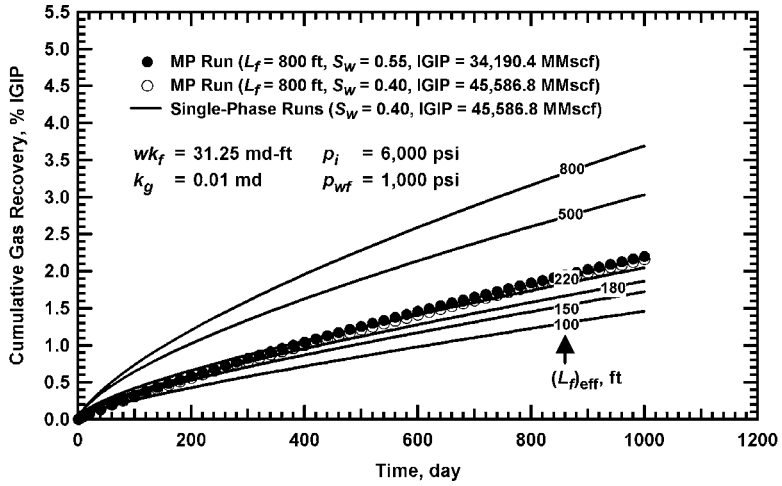

Fig. 4.109—Cumulative gas recovery versus production time for the multiphase cases with and without mobile reservoir water (wk_f = 31.25 md-ft, L_f = 800 ft, and k_g = 0.01 md) and the corresponding single-phase cases with different fracture lengths.

Fig. 4.110 and **Fig. 4.111** show the ratio of the multiphase to single-phase gas entry profile for these cases. The points, where the curves intersect, are generally close to the effective single-phase fracture lengths presented in Figs. 4.108 and 4.109. I conclude that reservoir water mobility has a small effect on the ratio of the multiphase to single-phase gas entry profile. The apparent fracture lengths are 600 ft if the wk_f = 500 md-ft and 180 ft if the wk_f = 31.25 md-ft for both cases with and without mobile reservoir water.

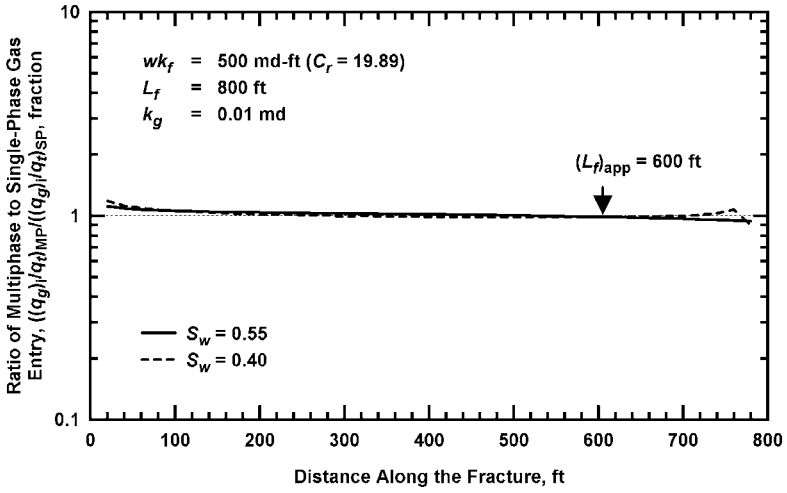

Fig. 4.110—Ratio of multiphase to single-phase gas entry profile for cases with mobile reservoir water (S_w = 55%) and immobile reservoir water (S_w = 40%), wk_f = 500 md-ft, L_f = 800 ft, and k_g = 0.01 md.

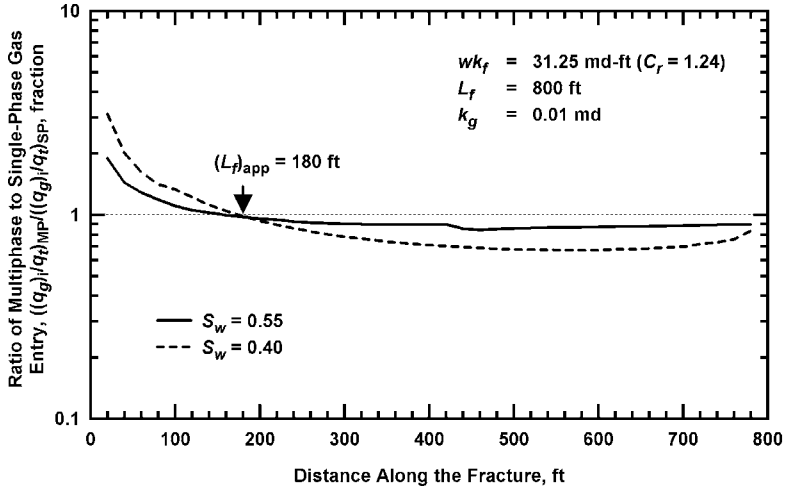

Fig. 4.111—Ratio of multiphase to single-phase gas entry profile for cases with mobile reservoir water (S_w = 55%) and immobile reservoir water (S_w = 40%), wk_f = 31.25 md-ft, L_f = 800 ft, and k_g = 0.01 md.

CHAPTER V
DISCUSSION

In this chapter I discuss the accomplishments achieved in this work and provide explanations of the results derived from this work. Several hundred computer runs were made and a variety of reservoir conditions were investigated during this research project over a two-year period (February 2002 to August 2004).

5.1 Cleanup Fracture Length

My work shows that the proppant pack is generally cleaned up and the cleanup lengths are close to designed lengths in relatively short times. Calculated post-fracture L_f's are typically less than designed because of the distribution of water saturation near the fracture. Although gas enters along entire fracture, the water saturation distribution affects the gas entry rate profile, which determines the effective fracture length. Subtle changes in the gas rate entry profile can result in significant changes in effective fracture length.

The flow resistance in the fracture and the formation after fracture treating is a function of the viscosity of the fracturing fluid and can be large relative to the resistance for single-phase gas flow. The cleanup length may be only a small fraction of the actual length if the viscosity of the fluid to be displaced in the proppant pack and invaded zone around the fracture is a few hundred centipoises.

Fracture conductivity affects the pressure distribution in the reservoir, resulting in different saturation distributions, rate profiles, and effective fracture lengths. The pressure drops in the reservoir are distributed more evenly along the fracture when the fracture conductivity is high. However, when the fracture conductivity is low, the pressure drops are greatest near the wellbore. Therefore, with respect to pressure distribution around the fracture, high conductivity fracture results in more effective well stimulation than low conductivity fracture.

The cleanup of the fracturing fluid starts with the fluid in the proppant pack **(Fig. 5.1)**. When the well is put on production, the fluid in the proppant pack is removed rapidly because of the high fracture conductivity. Once sufficient effective gas permeability is established in the proppant pack, the fracturing fluid in the invaded zone begins to flow into the fracture. The fracturing fluid in the invaded zone will continue to clean up gradually out along the fracture. The conductivity contrast between the fracture and the formation is one of the driving forces affecting the rate of the fluid cleanup in the invaded zone. If the relative flow capacity of the fracture is high (i.e., high fracture conductivity), the fluid in the invaded zone cleans up rapidly and more uniformly along the fracture. If the relative flow capacity of the fracture is low (i.e., low fracture conductivity), the fluid in the invaded zone cleans up slowly and may not readily be displaced from the invaded zone even after a long time. In any cases, even though the entire propped length is accessible for gas flow within a relatively short period of time (18 to 30 days), multiphase effects

still linger because the water saturation in the invaded zone does not completely decrease to the initial water saturation after the treatment.

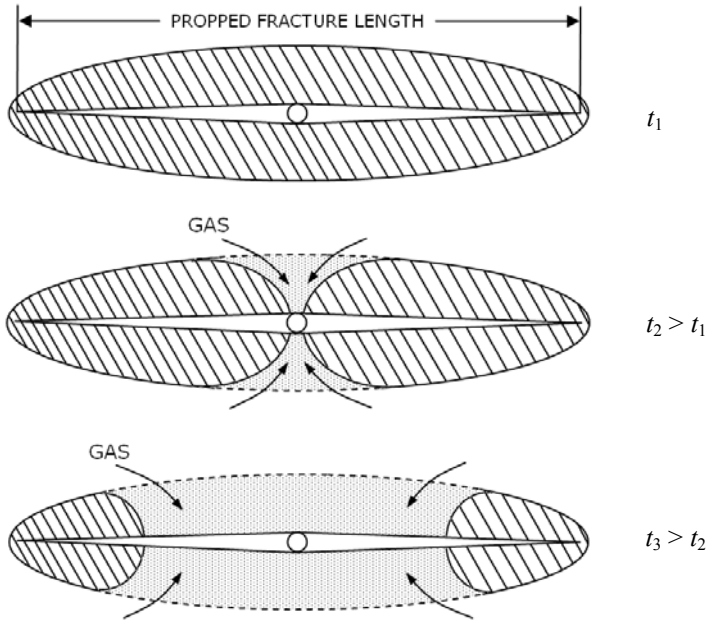

Fig. 5.1—Cleanup of fracture fluid in the invaded zone versus time (this work).

Table 5.1 compares the actual fracture half-length ($(L_f)_{ac}$), the cleanup fracture half-length ($(L_f)_{cleanup}$) at 365 days, and the effective fracture half-length ($(L_f)_{eff}$) for the "high" reservoir pressure cases presented in Chapter IV. Again, the cleanup length is the fracture length determined by direct observation of our simulation results. In this work, the "cleanup" length is the fracture length corresponding to 90% cumulative gas flow rate into the fracture. The effective fracture lengths are the equivalent lengths obtained using the single-phase flow models. The multiphase results for the cases with $(L_f)_{ac}$ = 200 and 500 ft and the cases with k_g = 0.05 and 0.1 md are presented in Appendix A and Appendix B, respectively. Table 5.1 suggests that the effective lengths are affected directly by fracture conductivity, while the cleanup lengths are generally close to the designed lengths at 365 days.

Table 5.1—Comparison of the Actual, Cleanup, and Effective Fracture Lengths
(High-Reservoir Pressure Cases: p_i = 6,000 psi and p_{wf} = 1,000 psi)

Case	wk_f (md-ft)	k_g (md)	$(L_f)_{ac}$ (ft)	$(L_f)_{cleanup}$ (ft) @ 365 days	$(L_f)_{eff}$ (ft)	Fluid Recovery (%) @ 365 days
1	500	0.01	200	195	195	60.3
2	31.25	0.01	200	194	138	49.0
3	500	0.01	500	485	452	53.3
4	31.25	0.01	500	479	210	32.0
5	500	0.01	800	776	660	46.3
6	31.25	0.01	800	738	250	21.0
7	500	0.05	800	776	420	36.6
8	31.25	0.05	800	699	70	13.7
9	500	0.1	800	776	300	34.5
10	31.25	0.1	800	587	35	11.9

At this point, it is appropriate to summarize the results derived from this work:

"High" Pressure/Water-Based Fracture Fluid:

- The cleanup length is 37% of the actual fracture length at 1 day if the wk_f is 500 md-ft (C_r = 19.89) and 12% of the actual fracture length at 1 day if the wk_f is 31.25 md-ft (C_r = 1.24). The entire propped length is accessible for gas flow within 4 to 5 days if the wk_f is 500 md-ft (C_r = 19.89) and 18 to 30 days if the wk_f is 31.25 md-ft (C_r = 1.24).
- The effective fracture half-lengths are 660 ft if the wk_f = 500 md-ft and 220 ft if the wk_f = 31.25 md-ft.
- The fracture fluid recovery versus production time plot indicates that the fracture fluid production rates begin to level off at 30 to 60 days. The fluid recovery is 46% at 365 days for the case with wk_f = 500 md-ft (C_r = 19.89) and 21% for the case with wk_f = 31.25 md-ft (C_r = 1.24).
- Changing nothing else except fracture conductivity (wk_f), the case with wk_f = 500 md-ft results in a cumulative gas recovery that is approximately twice as much as the case with 31.25 md-ft.

***"Low" Pressure/Water-Based Fracture Fluid*:**

- The ratio of the cleanup fracture half-length to the actual fracture half-length generally approaches unity at 365 days for all conductivities.
- The depth of the invasion is approximately 1 ft at the end of the injection. The injected fluid imbibes as far as 3 to 10 ft into the formation at 365 days. The water saturation in the invaded zone does not completely decrease to the initial water saturation.
- The fracture fluid production rates begin to level off at 2 to 5 days. Assuming p_i = 2,325 psi and p_{wf} = 1,000 psi, the fluid recovery at 365 days is 20% for the case with wk_f = 500 md-ft (C_r = 19.89) and 6% for the case with wk_f = 31.25 md-ft (C_r = 1.24). The effective fracture half-lengths are 740 ft if the wk_f = 500 md-ft and 400 ft if the wk_f = 31.25 md-ft.

- The case with wk_f = 500 md-ft results in a cumulative gas recovery that is almost twice as much as that for the case with wk_f = 31.25 md-ft.

***Viscous Fracture Fluid*:**

- The ratio of the cleanup fracture half-length to the actual fracture half-length is close to unity within 2 months if the wk_f = 500 md-ft (assuming μ_w = 50 cp). However, if the wk_f = 31.25 md-ft, this ratio is close to unity within 1 year to 2 years.
- Assuming μ_w = 50 cp, the effective fracture half-lengths are 650 ft if the wk_f = 31.25 md-ft and 180 ft if the wk_f = 31.25 md-ft.
- The injected water for these cases does not imbibe further into the formation. It is either produced or remains essentially stationary in the invaded zone.
- Assuming μ_w = 50 cp, the fluid recovery at 365 days is 38% if the wk_f = 500 md-ft (C_r = 19.89) and 18% if the wk_f = 31.25 md-ft (C_r = 1.24). In general, the fracture is still cleaning up at 365 days when the viscosity of the fluid is greater than 50 cp.

***Fracture Closure Effect*:**

- The effect of fracture closure on the cleanup length is small, particularly when the fracture conductivity is high.
- The effective fracture half-length for the multiphase case with closure pressure is approximately 580 ft if the wk_f = 500 md-ft (C_r = 19.89) and 180 if the wk_f = 31.25 md-ft (C_r = 1.24).
- The fluid recovery is reduced by 10 to 20% because of the fracture closure effect after the well has reached the stabilization period.
- The fracture closure effect results in a cumulative gas recovery that is 11 to 16% lower than that without fracture closure effect.

***Reservoir Water Mobility*:**

- The fracture fluid production rates do not level off within 1 year to 3 years. Assuming S_w = 55% and S_{wirr} = 40%, the fluid recovery is 73% for the case with wk_f = 500 md-ft (C_r = 19.89) and is 41% for the case with wk_f = 31.25 md-ft (C_r = 1.24).
- For these cases (S_w = 55%, $(L_f)_{\text{actual}}$ = 800 ft), the effective fracture half-lengths (i.e., under single-phase flow conditions/reservoir water is immobile) are approximately 570 ft if the wk_f = 500 md-ft (C_r = 19.89) and 220 ft if the wk_f = 500 md-ft (C_r = 19.89).
- The injected water imbibes as far as 50 ft into the formation for these cases. At 365 days, the water saturation is highest near the fracture (70 to 80%) and it decreases gradually as it moves away from the fracture face.
- Even though the fracture fluid recovery is high due to the reservoir water mobility, the cumulative gas recovery is reduced because the effective gas permeability decreases with increasing water saturation.

5.2 Limitations of This Work

It is useful to highlight some of the limitations in our modeling:

- I did not consider damage to the proppant pack due to incomplete fracture fluid (polymer) degradation. In reality, there is a variation in the sand concentration inside the fracture causing the conductivity to be high in some parts of the fracture and low in other parts of the fracture.
- I did not take into account excessive height growth which may account for shorter propped fracture lengths.
- The variation in the temperature inside the fracture that may cause variation in the fluid viscosity was not considered.
- I did not consider problems associated with the improper use of the crosslinker and breaker systems. Ref. 26 shows that if the gel is overcrosslinked or undercrosslinked, the fluid viscosity decreases, and the created fracture dimensions and proppant transport characteristics are affected. If too much breaker is added, the fluid viscosity decreases, once again adversely affecting both the created fracture dimensions and proppant transport. If too little breaker is added, the fluid may never break or may never clean up.

CHAPTER VI
CONCLUSIONS AND RECOMMENDATIONS

6.1 Conclusions

This study provides better explanation of mechanisms that affect fracturing fluid cleanup, effective fracture length, and well productivity than previous work. On the basis of the results of this research, I conclude that

1. Fracture conductivity affects the distribution of gas production into the fracture. High fracture conductivity increases the effectiveness of the propped fracture because the gas enters the fracture more evenly. Greater dimensionless fracture conductivity results in higher fracture fluid recovery, longer cleanup fracture lengths, and greater cumulative gas recovery.

2. The ratio of the cleanup fracture half-length to the actual fracture half-length increases with decreasing actual propped length and formation permeability. The proppant pack is generally cleaned up and the cleanup lengths are close to designed lengths in relatively short times even for low-pressure reservoirs hydraulically fractured using water-based fracturing fluids.

3. When the fracture conductivity is high, the pressure drops in the reservoir are distributed more uniformly along the fracture and, the fracture will drain the reservoir more effectively because the pressure drop inside the fracture is reduced to a minimum. When the fracture conductivity is low (e.g., $C_r < 1$), the pressure drop profile in the reservoir will appear to be "radial" even though the actual fracture length is several hundred feet.

4. The cleanup fracture lengths are reduced significantly when a viscous fracture fluid occupies the invaded zone around the fracture. The cleanup length may be only a small fraction of the actual length even after 365 days if the viscosity of the fracture fluid is greater than 50 cp. When the viscous fluid is present in the proppant pack or invaded zone, a slowly increasing production rate for several weeks or months typically occurs, resulting in shorter effective fracture lengths.

5. With respect to the effective fracture length, the fracture face damage, fracture closure effect, and reservoir water mobility are relatively unimportant. Fracture face damage makes the flux distribution along the fracture more uniform. The reservoir water mobility helps to increase the fracture fluid recovery.

6. The cleanup length is reduced by turbulent flow in the fracture. This is because the pressure drop in the fracture increases due to non-Darcy flow resulting in more gas entering the fracture near the wellbore. To reduce the impact of non-Darcy flow in the fracture, achieving higher fracture conductivity values becomes necessary.

7. This study shows that the cleanup fracture length is generally much longer than the effective fracture lengths predicted from post-fracture pressure buildup tests or production data analysis. Accordingly, one should use pressure buildup and production analysis results carefully because these incorrect results could lead to designs that may or may not improve gas productivity.

6.2 Recommendations for Future Work

Based on the results of this study, I suggest the following tasks for future work in the evaluation of well performance behavior in hydraulic-fractured wells:

- Model the interference in fracture fluid production from condensate buildup around the fracture. This requires a compositional modeling of condensate buildups as a wet gas approaches the propped fracture because the pressure drops below the dew point.

- Generate a spreadsheet model using the results of this work to directly analyze fractured well performance. This would involve applying the results generated in this work in designing optimal fracture treatments for typical tight gas reservoirs.

NOMENCLATURE

Field Variables

A	=	Drainage area, acres
β	=	Beta factor, 1/ft
c_f	=	Rock compressibility, 1/psi
c_w	=	Water compressibility, 1/psi
D	=	Formation depth, ft
$\Delta p/\Delta L$	=	Pressure gradient, psi/ft
Δx	=	Grid size in the x-direction, ft
Δy	=	Grid size in the y-direction, ft
γ_g	=	Specific gas gravity, dimensionless
h	=	Reservoir net thickness, ft
k	=	Formation permeability, md
k_d	=	Formation permeability in damage zone, md
k_f	=	Fracture permeability, md
k_g	=	Effective gas permeability, md
k_w	=	Effective water permeability, md
k_r	=	Relative permeability, md
k_{rg}	=	Relative permeability to gas, md
k_{rw}	=	Relative permeability to water, md
L_f	=	Fracture half-length, ft
ϕ	=	Porosity, percent
P_c	=	Capillary pressure, psi
p_i	=	Initial reservoir pressure, psi
p_{wf}	=	Bottomhole flowing pressure, psi
q	=	Gas flow rate, Mscf/D
S_g	=	Gas saturation, fraction [percent]
S_w	=	Water saturation, fraction [percent]
t	=	Time, day
t_p	=	Production time, day
T	=	Temperature, ^oF
μ	=	Viscosity, cp

μ_w = Water viscosity, cp

v = Velocity, ft/sec

w = Fracture width, in

w_d = Damaged-zone width, in [ft]

wk_f = Fracture conductivity, md-ft

Dimensionless Variables

C_r = Dimensionless fracture conductivity, $(wk_f)/(\pi L_f k)$

F_{CD} = Dimensionless fracture conductivity, $(wk_f)/(L_f k)$

Constant

π = 3.1416

Special Subscripts

ac = actual

app = apparent

eff = effective

REFERENCES

1. Chipolla, C.L., Meehan, D.N., and Stevens, P.L.: "Hydraulic Fracture Performance in the Moxa Arch Frontier Formation," paper SPE 25918 presented at the 1993 SPE Rocky Mountain Regional Meeting/Low Permeability Reservoirs Symposium, Denver, Colorado, 26-28 April.
2. Schubarth, S.K., Chabaud, R.A., and Einhorn, R.B.: "Moxa Arch Frontier Formation Development Success Through Increased Fracture Conductivity," paper SPE 28610 presented at the 1994 SPE Annual Technical Conference and Exhibition, New Orleans, Louisiana, 25-28 September.
3. Schubarth, S.K., Chabaud, R.A., and Penny, G.S.: "Moxa Arch Frontier Formation Development Success Through Increased Fracture Conductivity—Part 2," paper SPE 30717 presented at the 1995 SPE Annual Technical Conference and Exhibition, Dallas, Texas, 22-25 October.
4. Tannich, J.D.: "Liquid Removal From Hydraulically Fractured Gas Wells," *JPT* (November 1975) 1309-1317.
5. Soliman, M.Y. and Hunt, J.L.: "Effects of Fracturing Fluid and Its Cleanup on Well Performance," paper SPE 14514 presented at the 1985 SPE Eastern Regional Meeting, Morgantown, West Virginia, 6-8 November.
6. Montgomery, K.T.: "Factors That Affect Fracture Fluid Cleanup and Pressure Buildup Test Results in Tight Gas Reservoirs," MS Thesis, Texas A&M University, College Station, Texas (1990).
7. Montgomery, K.T., Holditch, S.A., and Berthelot, J.M.: "Effects of Fracture Fluid Invasion on Cleanup Behavior and Pressure Buildup Analysis," paper SPE 20643 presented at the 1990 SPE Annual Technical Conference and Exhibition, Houston, Texas, 23-26 September.
8. Berthelot, J.M.: "Effects of Fracturing Fluid Recovery Upon Well Performance and Ultimate Recovery of Hydraulically Fractured Gas Wells," MS Thesis, Texas A&M University, College Station, Texas (1990).
9. Sherman, J.B. and Holditch, S.A.: "Effects of Injected Fracture Fluids and Operating Procedures on Ultimate Gas Recovery," paper SPE 21496 presented at the 1991 SPE Gas Technology Symposium, Houston, 23-25 January.
10. Robinson, B.M.: "Minimizing Damage to a Propped Fracture by Correct Selection of Proppant and Controlled Flowback Procedures," MS Thesis, Texas A&M University, College Station, Texas (1986).
11. Robinson, B.M., Holditch, S.A., and Whitehead, W.S.: "Minimizing Damage to a Propped Fracture by Controlled Flowback Procedures," *JPT* (June 1988) 753-759.
12. van Poollen, H.K.: "Do Fracture Fluids Damage Productivity?," *Oil and Gas Journal* (27 May 1957) 120-124.
13. Holditch, S.A.: "Factors Affecting Water Blocking and Gas Flow From Hydraulically Fractured Gas Well," *JPT* (December 1979) 1515-1524.

14. Fox, L.T.: "The Effects of Damage in and Around a Fracture Upon the Analysis of Pressure Data from Low Permeability Gas Wells," MS Thesis, Texas A&M University, College Station, Texas (1980).
15. Adegbola, S.A. and Boney, C.: "Effects of Fracture Face Damage on Well Productivity," paper SPE 73759 presented at the 2002 SPE International Symposium and Exhibition on Formation Damage Control, Lafayette, Louisiana, 20-21 February.
16. Schubarth, S.K., Yeager, R.R., and Murphy, D.W.: "Advanced Fracturing and Reservoir Description Techniques Improves Economics in Utah, Green River Formation Oil Project," paper SPE 39777 presented at the 1998 SPE Permian Basin Oil and Gas Recovery Conference, Midland, Texas, 23-26 March.
17. Bastian, P.A.: "The Measurement of the Viscosity of Cross-Linked Fracture Fluids Using a FANN Model 50C Rotational Viscometer," MS Thesis, Texas A&M University, College Station, Texas (1983).
18. Craig, D.P.: "The Degradation of Hydroxypropyl Guar Fracturing Fluids by Enzyme, Oxidative, and Catalyzed Oxidative Breakers," MS Thesis, Texas A&M University, College Station, Texas (1991).
19. Fan, Y.: "Measurements of Viscous and Degradation Properties of Fracturing Fluids at In-Situ Conditions of Shear Rate and Temperature Using Fann 50C Viscometer," PhD Dissertation, Texas A&M University, College Station, Texas (1992).
20. Fan, Y. and Holditch, S.A.: "Viscous and Degradation Properties of Crosslinked HPG Gels: Some Laboratory Observations," paper SPE 26941 presented at the 1993 SPE Eastern Regional Conference and Exhibition, Pittsburgh, Pennsylvania, 2-4 November.
21. Hill, N.C.: "The Effects of Hydraulic Fracturing Fluid Loss on the Resulting Fracture Size," MS Thesis, Texas A&M University, College Station, Texas (1984).
22. Kim, C.M. and Lasacano, J.A.: "Fracture Conductivity Damage due to Crosslinked Gel Residue and Closure Stress on Propped 20/40 Mesh Sand," paper SPE 14436 presented at the 1985 SPE Annual Technical Conference and Exhibition, Las Vegas, Nevada, 22-25 September.
23. Olsen, T.N. and Debonis, M.P.: "Real-Time Optimization of Fracturing Fluid Viscosity to Meet Changing Fracture Conditions," paper SPE 17540 presented at the 1988 SPE Rocky Mountain Regional Meeting, Casper, Wyoming, 11-13 May.
24. Brannon, H.D. and Pulsinelli, R.J.: "Evaluation of the Breaker Concentrations Required to Improved the Permeability of Proppant Packs Damaged by Hydraulic Fracturing Fluids," paper SPE 19402 presented at the 1990 SPE Formation Damage Control Symposium, Lafayette, Louisiana, 22-23 February.
25. Davidson, B.M., Saunders, B.F., and Holditch, S.A.: "Field Measurement of Hydraulic Fracture Fluids: Case Study," paper SPE 27694 presented at the 1994 SPE Permian Basin Oil and Gas Recovery Conference, Midland, Texas, 16-18 March.

26. Rahim, Z., Holditch, S.A., and Davidson, B.M.: "Quantitative Analysis of Production Loss Due to Fracture Fluid Degradation," paper SPE 29590 presented at the 1995 SPE Rocky Mountain Regional/Low-Permeability Reservoirs Symposium, Denver, Colorado, 20-21 March.
27. Elbel, J., Gulbis, J., King, M.T., and Maniere, J.: "Increased Breaker Concentration in Fracturing Fluids Results in Improved Gas Well Performance," paper SPE 21716 presented at the 1991 SPE Production Operations Symposium, Oklahoma City, Oklahoma, 7-9 April.
28. Gamble, S.D.: "The Effect of Temperature and Duration of Initial Shear Time on the Viscous Properties of a Crosslinked Fracture Fluid," MS Thesis, Texas A&M University, College Station, Texas (1984).
29. Nichols, J.E.: "An Investigation into the Effects of Changes in Temperature and Shear Rate Upon the Viscous Behavior of a Crosslinked Fracture Fluid," MS Thesis, Texas A&M University, College Station, Texas (1986).
30. Voneiff, G.W., Robinson, B.M., and Holditch, S.A.: "The Effects of Unbroken Fracture Fluid on Gas Well Performance," SPE 26664 (Peer-Approved Manuscript by the SPE), 1996.
31. Cooke, C.E.: "Effect of Fracturing Fluids on Fracture Conductivity," *JPT* (October 1975) 1273-1282.
32. Siddiqui, M.A., Nasr-El-Din, H.A., Al-Anazi, M.S., and Bartko, K.M.: "Formation Damage in Gas Sandstone Formations by High-Temperature Borate Gels Due to Long Term Shut-In Periods," paper SPE 89476 presented at the 2004 SPE/DOE Fourteenth Symposium on Improved Oil Recovery, Tulsa, Oklahoma, 17-21 April.
33. Johansen, A.T.: "The Effects of Fracture Fluid Cleanup Upon the Analysis of Pressure Buildup Tests in Tight Gas Reservoirs," MS Thesis, Texas A&M University, College Station, Texas (1988).
34. Lee, W.J. and Holditch, S.A.: "Fracture Evaluation with Pressure Transient Testing in Low-Permeability Gas Reservoirs," *JPT* (September 1981) 1776-1792.
35. Holditch, S.A., Lee, W.J., and Gist, R.: "An Improved Technique for Estimating Permeability, Fracture Length, and Fracture Conductivity from Pressure Buildup Tests in Low Permeability Gas Wells," paper SPE/DOE 9885 presented at the 1981 SPE/DOE Low Permeability Symposium, Denver, Colorado, 27-29 May.
36. Gist, S.R.: "An Iterative Calculation for Determining Formation and Fracture Properties in Hydraulically Fractured Reservoirs," MS Thesis, Texas A&M University, College Station, Texas (1984).
37. Elbel, J. and Ayoub, J.: "Evaluation of Apparent Fracture Lengths Indicated from Transient Tests," *JCPT* (December 1992) 41-46.
38. Barree, R.D., Cox, S.A., Gilbert, J.V., and Dobson, M.: "Closing the Gap: Fracture Half Length from Design, Buildup, and Production Analysis," paper SPE 84491 presented at the 2003 SPE Annual Technical Conference and Exhibition, Denver, Colorado, 5-8 October.
39. Hresko, J.C.: "A Qualitative Analysis of Non-Darcy Flow Effects in Hydraulically Fractured Gas Wells," MS Thesis, Texas A&M University, College Station, Texas (1985).

40. Holditch, S.A.: "The Effects of Turbulence on the Behavior of Hydraulically Fractured Gas Wells," PhD Dissertation, Texas A&M University, College Station, Texas (1976).
41. Holditch, S.A. and Morse, R.A.: "The Effects of Non-Darcy Flow on the Behavior of Hydraulically Fractured Gas Wells," *JPT* (October 1976) 1169-1179.
42. Alvarez, C.H., Holditch, S.A, and McVay, D.A.: " Effects of Non-Darcy Flow on Pressure Buildup Analysis of Hydraulically Fractured Gas Reservoirs," paper SPE 77468 presented at the 2002 SPE Annual Technical Conference and Exhibition, San Antonio, Texas, 29 September-2 October.
43. Agarwal, R.G., Carter, R.D., and Pollock, C.B.: "Evaluation and Performance Prediction of Low-Permeability Gas Wells Stimulated by Massive Hydraulic Fracturing," *JPT* (March 1979) 362-372.
44. Bastian, P.A., Holditch, S.A., and Sherman, J.B.: "Analysis of a Hydraulic Fractured, Low-Permeability Gas Reservoir Using Numerical Simulation," paper SPE 21511 presented at the 1991 SPE Gas Technology Symposium, Houston, 23-25 January.
45. Cinco-Ley, H. and Samaniego-V, F.: "Effect of Wellbore Storage and Damage on the Transient Pressure Behavior of Vertically Fractured Wells," paper SPE 6752 presented at the 1977 SPE Annual Technical Conference and Exhibition, Denver, Colorado, 9-12 October.
46. Cramer, D.D.: "Evaluating Well Performance and Completion Effectiveness in Hydraulically Fractured Low-Permeability Gas Wells," paper SPE 84214 presented at the 2003 SPE Annual Technical Conference and Exhibition, Denver, Colorado, 5-8 October.
47. Gatens, J.M.: "A Method for Analyzing Production Data to Estimate Reservoir Properties and Stimulation Effectiveness," MS Thesis, Texas A&M University, College Station, Texas (1987).
48. Gil, J.A., Ozkan, E., and Raghavan, R.: "Fractured-Well-Test Design and Analysis in the Presence of Non-Darcy Flow," paper SPE 71573 presented at the 2001 SPE Annual Technical Conference and Exhibition, New Orleans, Louisiana, 30 September-3 October.
49. Krawtz, J.P.: "Determination of Formation Permeability Using Back-Pressure Test Data from Hydraulically-Fractured, Low-Permeability Gas Wells," MS Thesis, Texas A&M University, College Station, Texas (1984).
50. Liao, Y.: "Well Production Performance and Well Test Analysis for Hydraulically Fractured Wells," PhD Dissertation, Texas A&M University, College Station, Texas (1993).
51. Makoju, C.A.: "Fractured Gas Well Analysis: Evaluation of In-Situ Reservoir Properties of Low Permeability Gas Wells Stimulated by Finite Conductivity Hydraulic Fractures," MS Thesis, Texas A&M University, College Station, Texas (1978).
52. Manohar, M.M.: "Determination of the Length and Compass Orientation of Hydraulic Fractures by Pulse Testing," MS Thesis, Texas A&M University, College Station, Texas (1984).
53. Pratikno, H., Rushing, J.A., and Blasingame, T.A.: "Decline Curve Analysis Using Type Curves– Fractured Wells," paper SPE 84287 presented at the 2003 SPE Annual Technical Conference and Exhibition, Denver, Colorado, 5-8 October.

54. Rahim, Z.: "A New Iterative Scheme to Determine Reservoir and Fracture Properties Using Early Time Test Data for Hydraulically Fractured Wells," MS Thesis, Texas A&M University, College Station, Texas (1984).
55. Rushing, J.A. and Blasingame, T.A.: "Integrating Short-Term Pressure Buildup Testing and Long-Term Production Data Analysis to Evaluate Hydraulically-Fractured Gas Well Performance," paper SPE 84475 presented at the 2003 SPE Annual Technical Conference and Exhibition, Denver, Colorado, 5-8 October.
56. Santhanam, K.S.: "Determination of Fracture and Reservoir Properties Using an Automatic History Matching Technique for Wells with Finite-Conductivity Vertical Fractures," MS Thesis, Texas A&M University, College Station, Texas (1985).
57. Soliman, M.Y., Venditto, J.J., and Slusher, G.L.: "Evaluating Fractured Well Performance Using Type Curves," paper SPE 12598 presented at the 1984 SPE Permian Basin Oil & Gas Recovery Conference, Midland, Texas, 8-9 March.
58. Boriskie, R.J.: "An Investigation of Productivity Increases from Hydraulic Fracturing Treatments," MS Thesis, Texas A&M University, College Station, Texas (1963).
59. Davies, J.P.: "Stress Dependent Permeability in the Travis Peak Formation, East Texas," PhD Dissertation, Texas A&M University, College Station, Texas (1996).
60. Flowers, J.R., Hupp, M.T., and Ryan, J.D.: "The Results of Increased Fracture Conductivity on Well Performance in a Mature East Texas Gas Field," paper SPE 84307 presented at the 2003 SPE Annual Technical Conference and Exhibition, Denver, Colorado, 5-8 October.
61. Holgate, K.E.: "Evaluation of Massive Hydraulic Fracturing Experiments in the Devonian Shales in Lincoln County, West Virginia," MS Thesis, Texas A&M University, College Station, Texas (1987).
62. Lancaster, D.L.: "The Use of Pre- and Post-Stimulation Well Test Analysis in the Evaluation of Stimulation Effectiveness in the Devonian Shales of the Appalachian Basin," MS Thesis, Texas A&M University, College Station, Texas (1988).
63. Nearing, T.R.: "Effects of Stimulation/Completion Practices on Eastern Devonian Shale Well Productivity," MS Thesis, Texas A&M University, College Station, Texas (1988).
64. Pietsch, C.E.: "The Analysis of Liquid Loading Problems in Hydraulically Fractured Gas Wells," MS Thesis, Texas A&M University, College Station, Texas (1986).
65. Pursell, D.A.: "Laboratory Investigation of Inertial Flow in High Strength Fracture Proppants," MS Thesis, Texas A&M University, College Station, Texas (1987).
66. Robinson, B.M., Holditch, S.A., and Peterson, R.E.: "The Gas Research Institute's Second Staged Field Experiment: A Study of Hydraulic Fracturing," paper SPE 21495 presented at the 1991 SPE Gas Technology Symposium, Houston, Texas, 23-25 January.
67. Robinson, B.M., Holditch, S.A., Whitehead, W.S., and Peterson, R.E.: "Hydraulic Fracturing Research in East Texas Through the Gas Research Institute's Third Staged Field Experiment," paper SPE 22878 presented at the 1991 SPE Annual Technical Conference and Exhibition, Dallas, Texas, 6-9 October.

68. Rueda, J.I.: " Optimization of Fracture Treatment Designs," MS Thesis, Texas A&M University, College Station, Texas (1992).
69. Santiago Molina, C.A.: "Characterization and Reservoir Evaluation of a Hydraulically Fractured, Shaly Gas Reservoir," MS Thesis, Texas A&M University, College Station, Texas (1991).
70. Santivongskul, M.: " Well Test Analysis for Wells with Finite Conductivity Vertical Fractures: Application to the Upper Clearfork Formation," MS Thesis, Texas A&M University, College Station, Texas (1992).
71. Satayapunt, J.: "Parametric Study to Evaluate Benefits of Fracture Fluid Quality Control and In-Situ Stress Research," MS Thesis, Texas A&M University, College Station, Texas (1991).
72. Shaw, J.S.: "Reservoir and Stimulation Analysis of a Devonian Shale Gas Field," MS Thesis, Texas A&M University, College Station, Texas (1986).
73. Voneiff, G.W.: "The Benefits of Applying Recent Advances in Tight Gas Sands Technology: Fracturing Fluid Quality Control, In-Situ Stress Profiling and Three Dimensional Fracture Design Models," MS Thesis, Texas A&M University, College Station, Texas (1992).
74. Warner, J.B.: "Numerical Simulation of Hydraulic Fracturing," MS Thesis, Texas A&M University, College Station, Texas (1987).
75. Whittington, W.F.: "The Application of a Type Curve Reservoir Simulator in Low Permeability Gas Reservoirs," MS Thesis, Texas A&M University, College Station, Texas (1980).
76. Lolon, E.P, McVay, D.A., and Schubarth, S.K.: "Effect of Fracture Conductivity on Effective Fracture Length," paper SPE 84311 presented at the 2003 SPE Annual Technical Conference and Exhibition, Denver, Colorado, 5-8 October.
77. Forchheimer, P.: "Wasserbewegung durch Boden," *ZVDI* (1901) 45, 1781.
78. Geertsma, J.: "Estimating the Coefficient of Inertial Resistance in Fluid Flow Through Porous Media," *SPEJ* (October 1974) 445-450.
79. Frederick, D.C. and Graves, R.M.: "New Correlations to Predict Non-Darcy Flow Coefficients at Immobile and Mobile Water Saturation," paper SPE 28451 presented at the 1994 SPE Annual Technical Conference and Exhibition, New Orleans, Louisiana, 25-28 September.

APPENDIX A
MULTIPHASE RESULTS FOR SHORTER FRACTURES

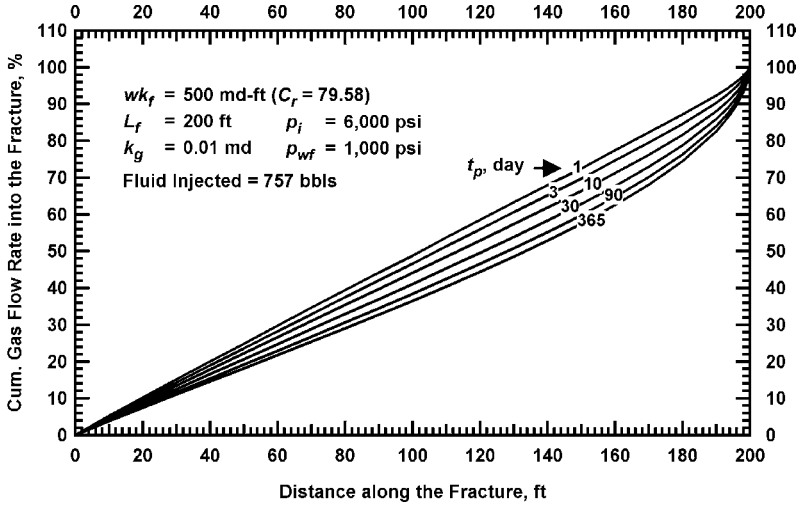

Fig. A.1—Cumulative gas flow rate into the fracture versus distance along the fracture for a multiphase case with wk_f = 500 md-ft, L_f = 200 ft, and k_g = 0.01 md.

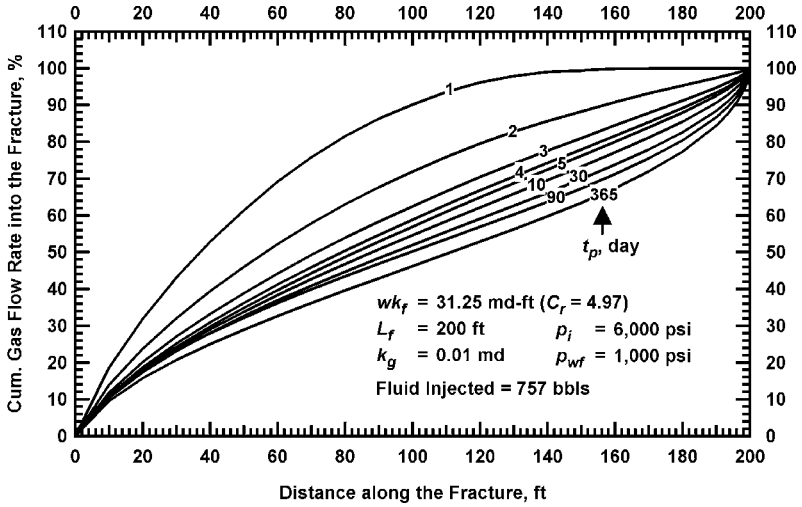

Fig. A.2—Cumulative gas flow rate into the fracture versus distance along the fracture for a multiphase case with wk_f = 31.25 md-ft, L_f = 200 ft, and k_g = 0.01 md.

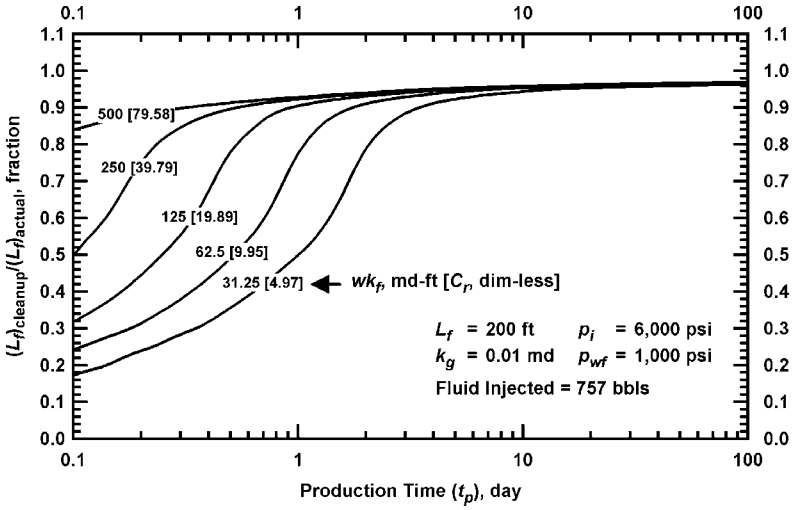

Fig. A.3—Ratio of cleanup fracture half-length to actual fracture half-length for multiphase and non-Darcy flow cases with L_f = 200 ft and k_g = 0.01 md.

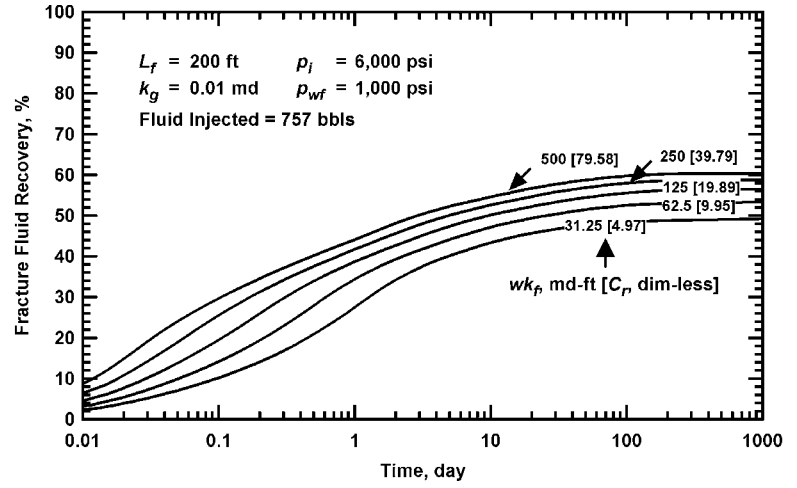

Fig. A.4—Fracture fluid recovery versus production time for multiphase and non-Darcy flow cases with L_f = 200 ft and k_g = 0.01 md.

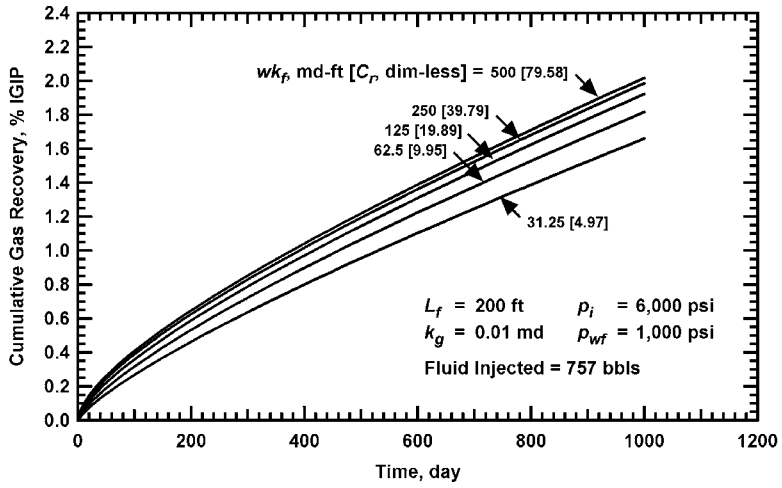

Fig. A.5— Cumulative gas recovery versus production time for multiphase and non-Darcy flow cases with L_f = 200 ft and k_g = 0.01 md.

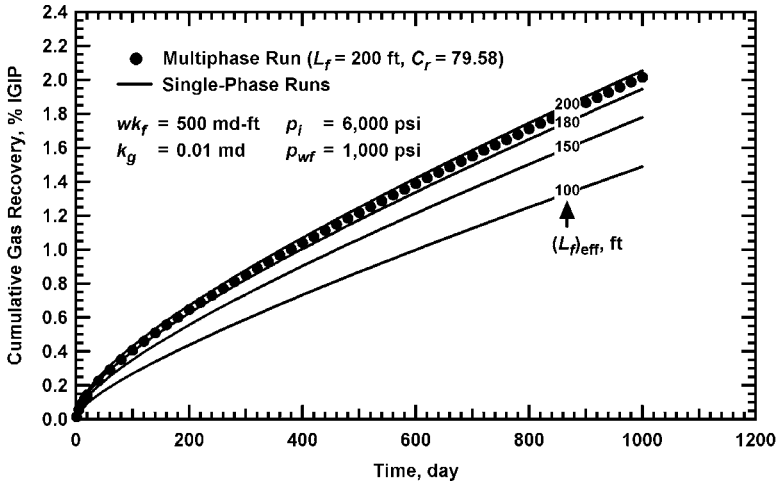

Fig. A.6— Cumulative gas recovery versus production time for a multiphase case with wk_f = 500 md-ft, L_f = 200 ft, and k_g = 0.01 md, and corresponding single-phase cases with different fracture lengths.

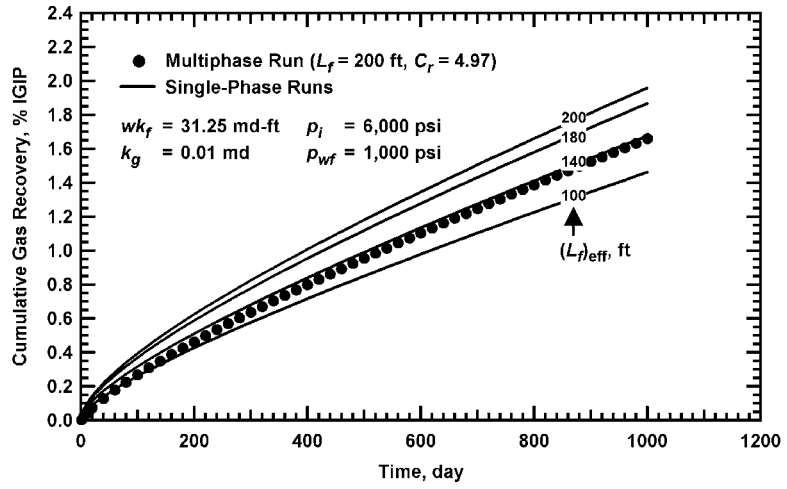

Fig. A.7—Cumulative gas recovery versus production time for a multiphase case with wk_f = 31.25 md-ft, L_f = 200 ft, and k_g = 0.01 md, and corresponding single-phase cases with different fracture lengths.

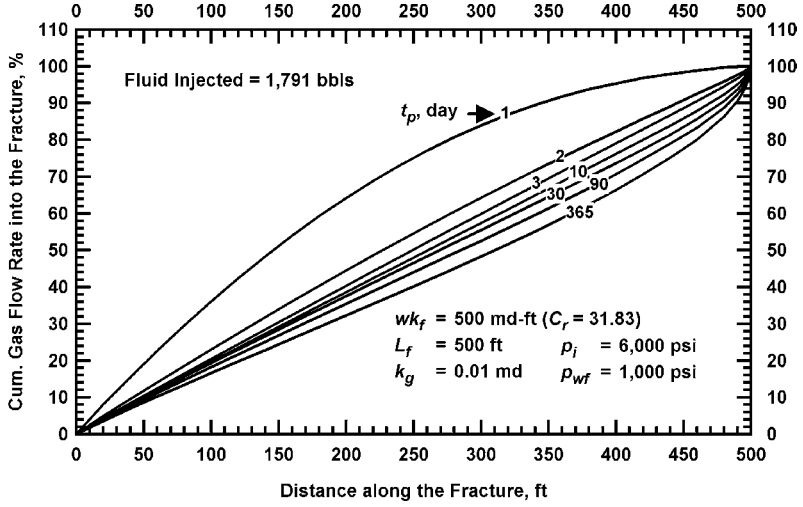

Fig. A.8—Cumulative gas flow rate into the fracture versus distance along the fracture for a multiphase case with wk_f = 500 md-ft, L_f = 500 ft, and k_g = 0.01 md.

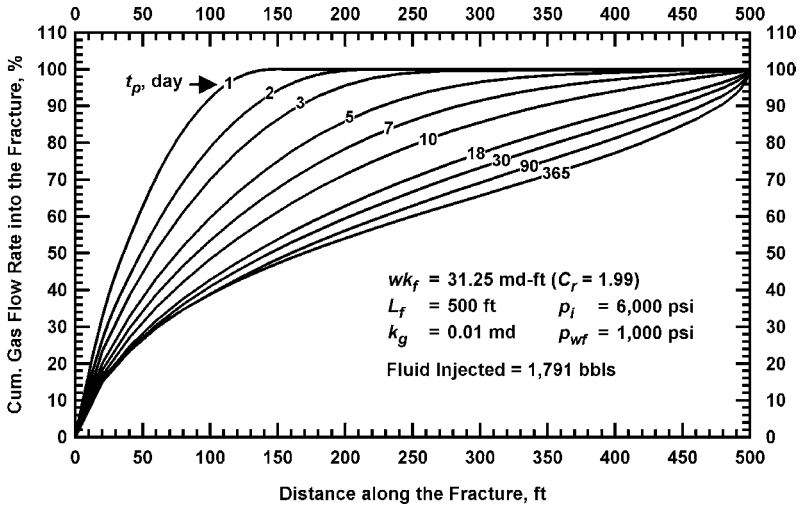

Fig. A.9—Cumulative gas flow rate into the fracture versus distance along the fracture for a multiphase case with wk_f = 31.25 md-ft, L_f = 500 ft, and k_g = 0.01 md.

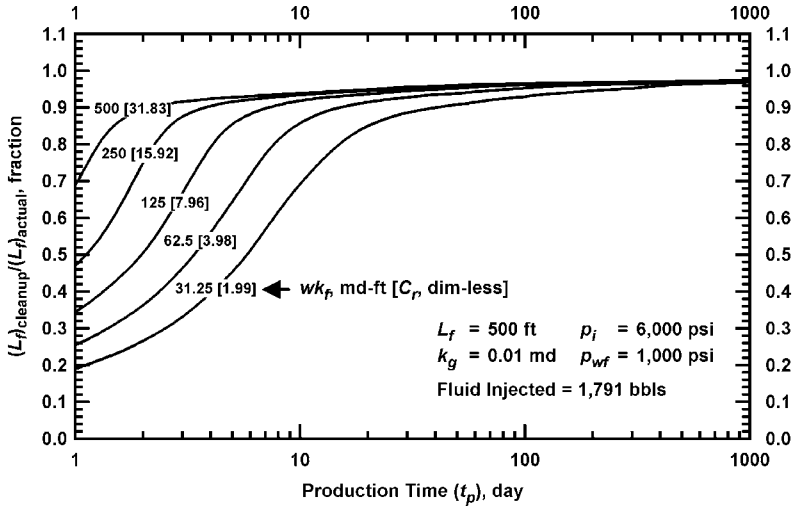

Fig. A.10—Ratio of cleanup fracture half-length to actual fracture half-length for multiphase and non-Darcy flow cases with L_f = 500 ft and k_g = 0.01 md.

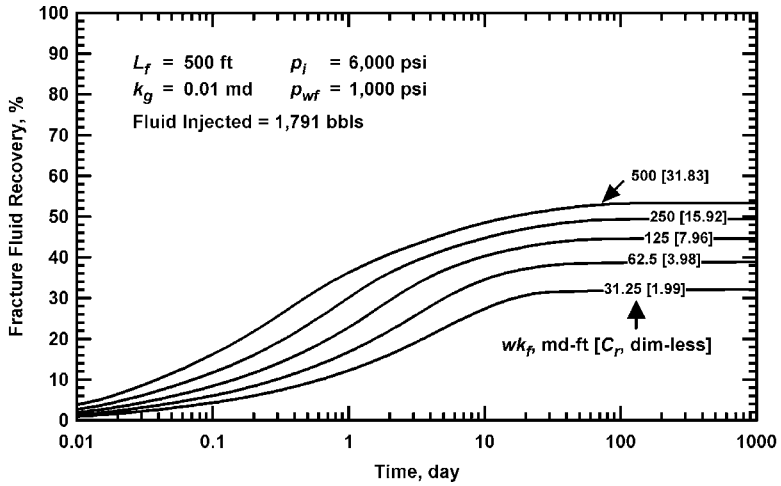

Fig. A.11—Fracture fluid recovery versus production time for multiphase and non-Darcy flow cases with L_f = 500 ft and k_g = 0.01 md.

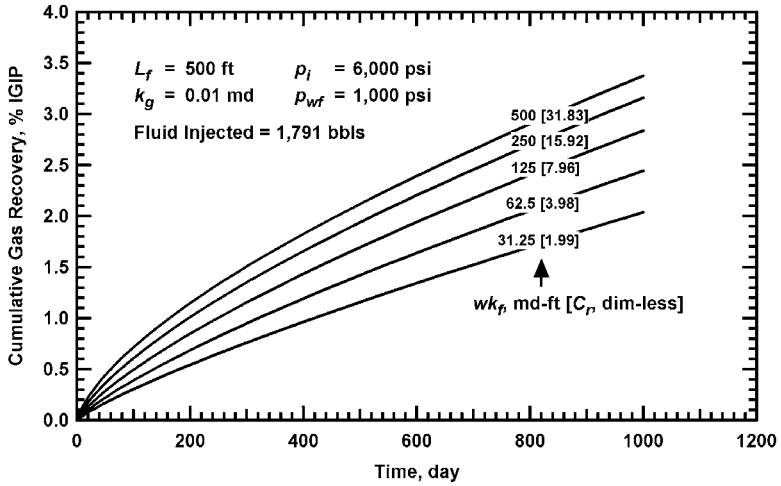

Fig. A.12—Cumulative gas recovery versus production time for multiphase and non-Darcy flow cases with L_f = 500 ft and k_g = 0.01 md.

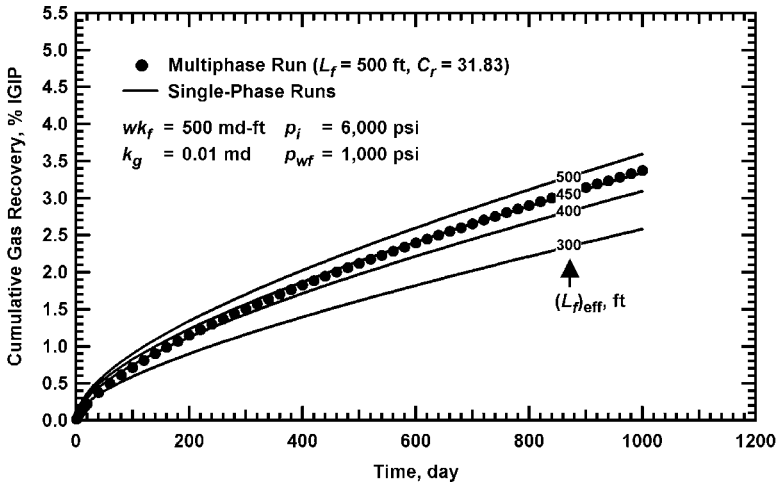

Fig. A.13—Cumulative gas recovery versus production time for a multiphase case with wk_f = 500 md-ft, L_f = 500 ft, and k_g = 0.01 md, and corresponding single-phase cases with different fracture lengths.

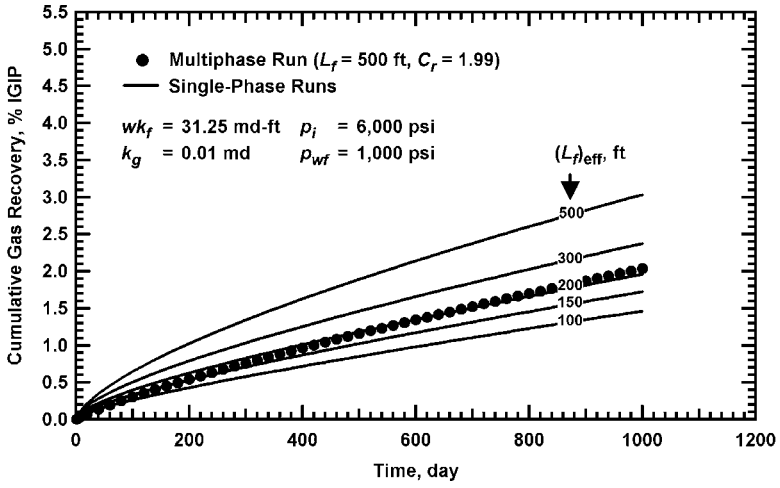

Fig. A.14—Cumulative gas recovery versus production time for a multiphase case with wk_f = 31.25 md-ft, L_f = 500 ft, and k_g = 0.01 md, and corresponding single-phase cases with different fracture lengths.

APPENDIX B
MULTIPHASE RESULTS FOR HIGHER RESERVOIR PERMEABILITIES

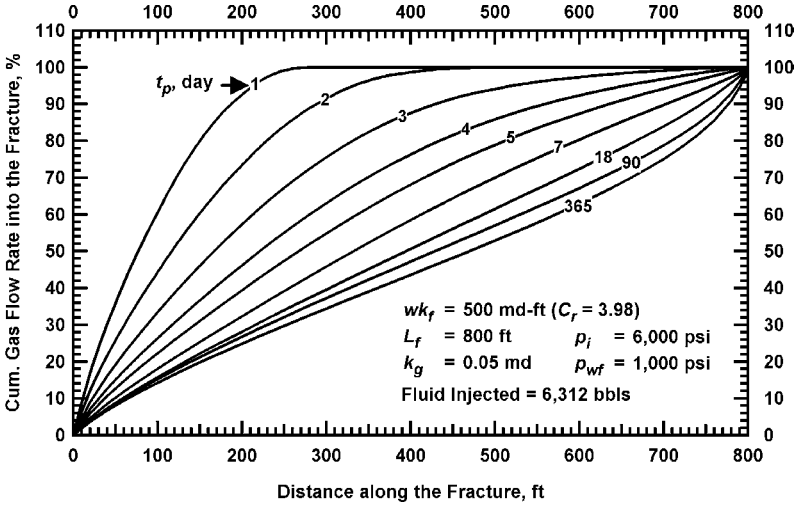

Fig. B.1— Cumulative gas flow rate into the fracture versus distance along the fracture for a multiphase case with wk_f = 500 md-ft, L_f = 800 ft, and k_g = 0.05 md.

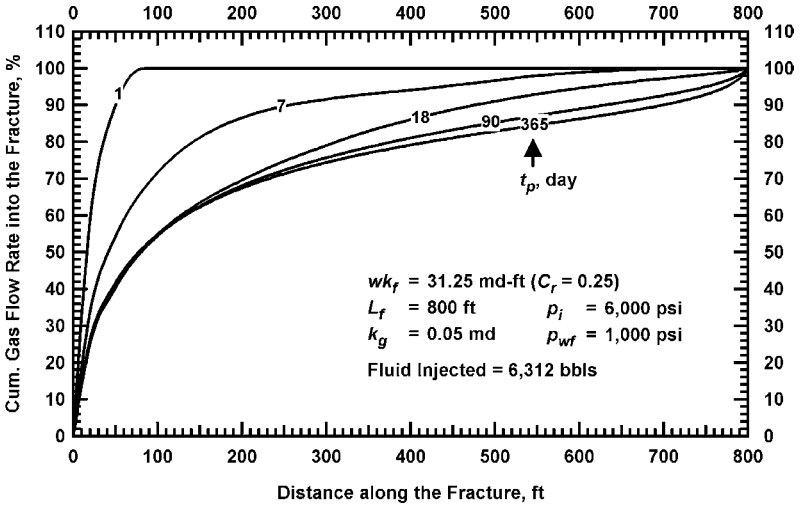

Fig. B.2— Cumulative gas flow rate into the fracture versus distance along the fracture for a multiphase case with wk_f = 31.25 md-ft, L_f = 800 ft, and k_g = 0.05 md.

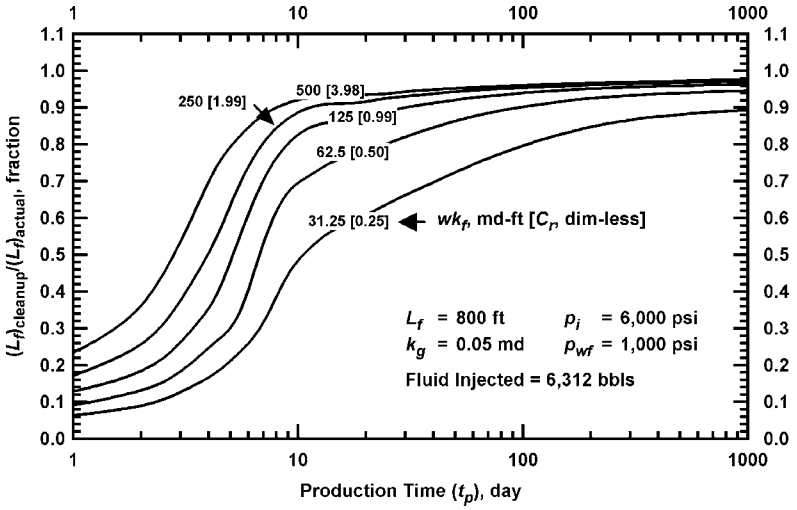

Fig. B.3— Ratio of cleanup fracture half-length to actual fracture half-length for multiphase and non-Darcy flow cases with L_f = 800 ft and k_g = 0.05 md.

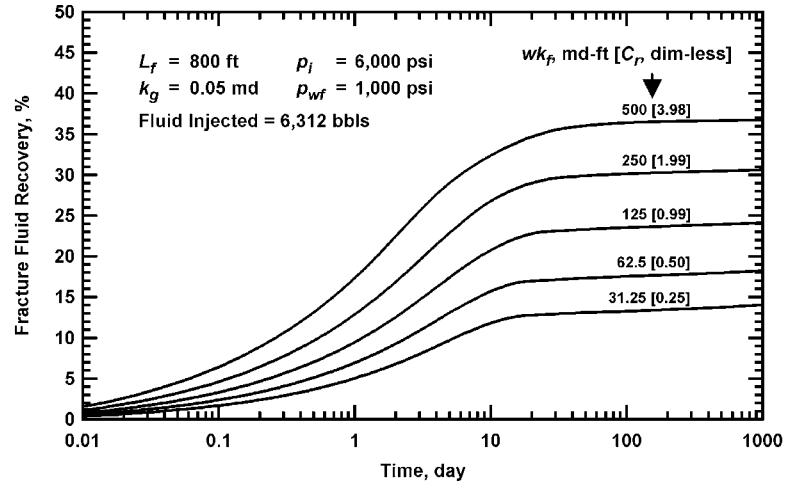

Fig. B.4— Fracture fluid recovery versus production time for multiphase and non-Darcy flow cases with L_f = 800 ft and k_g = 0.05 md.

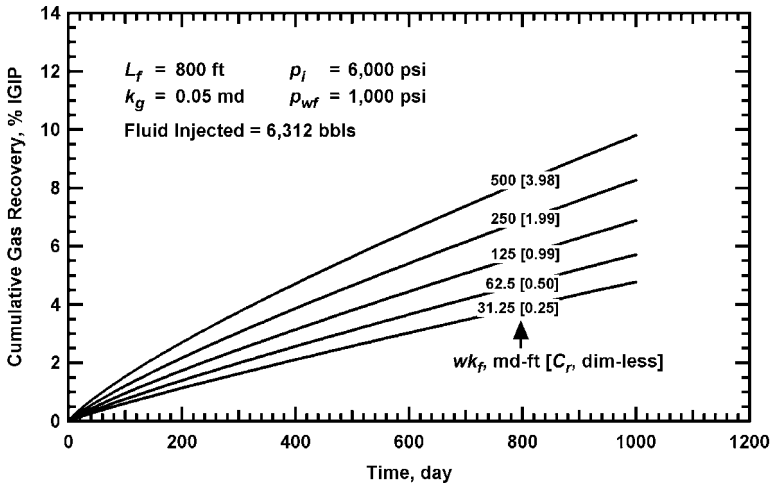

Fig. B.5— Cumulative gas recovery versus production time for multiphase and non-Darcy flow cases with L_f = 800 ft and k_g = 0.05 md.

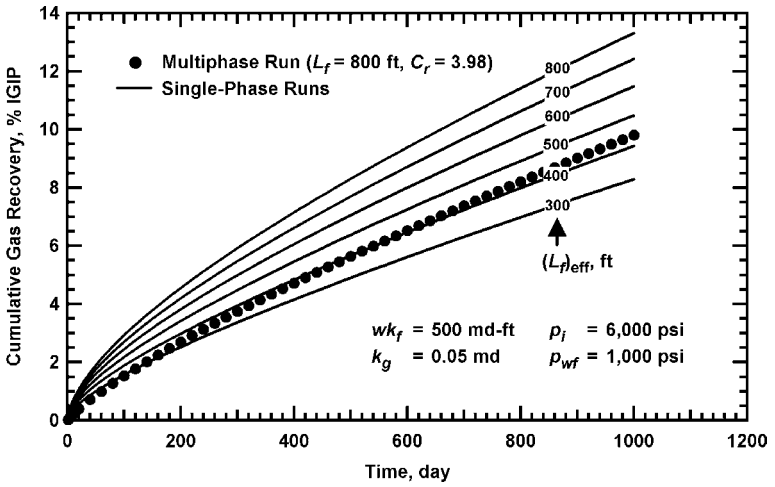

Fig. B.6— Cumulative gas recovery versus production time for a multiphase case with wk_f = 500 md-ft, L_f = 800 ft, and k_g = 0.05 md, and corresponding single-phase cases with different fracture lengths.

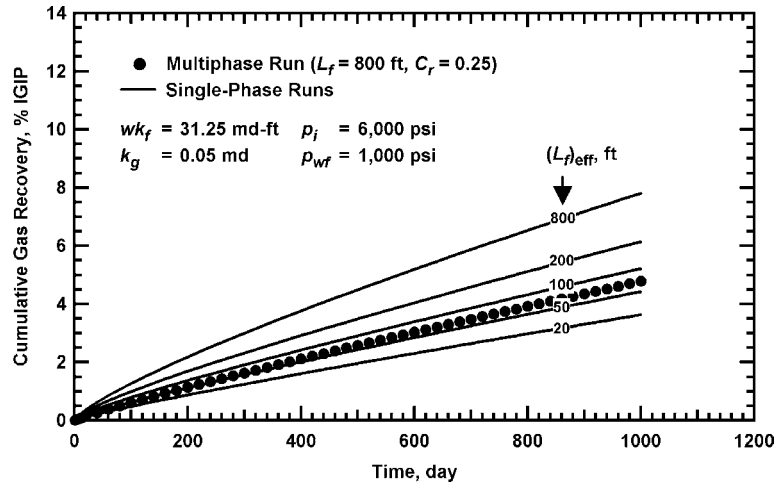

Fig. B.7— Cumulative gas recovery versus production time for a multiphase case with wk_f = 31.25 md-ft, L_f = 800 ft, and k_g = 0.05 md, and corresponding single-phase cases with different fracture lengths.

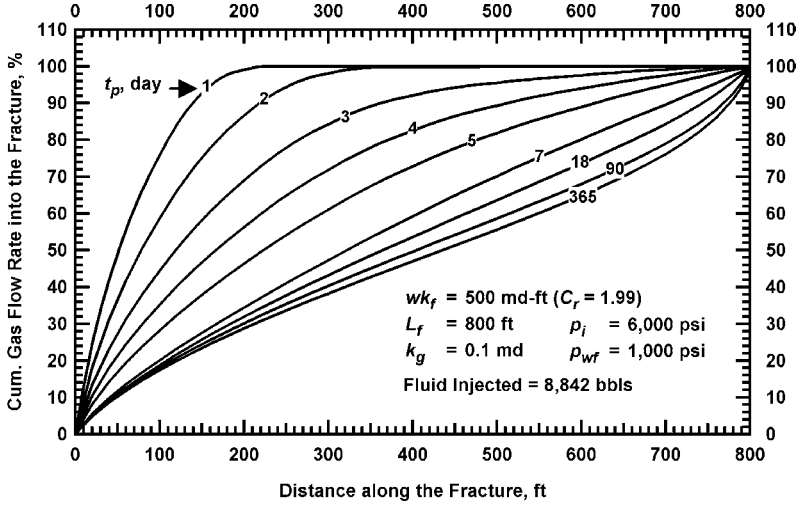

Fig. B.8— Cumulative gas flow rate into the fracture versus distance along the fracture for a multiphase case with wk_f = 500 md-ft, L_f = 800 ft, and k_g = 0.1 md.

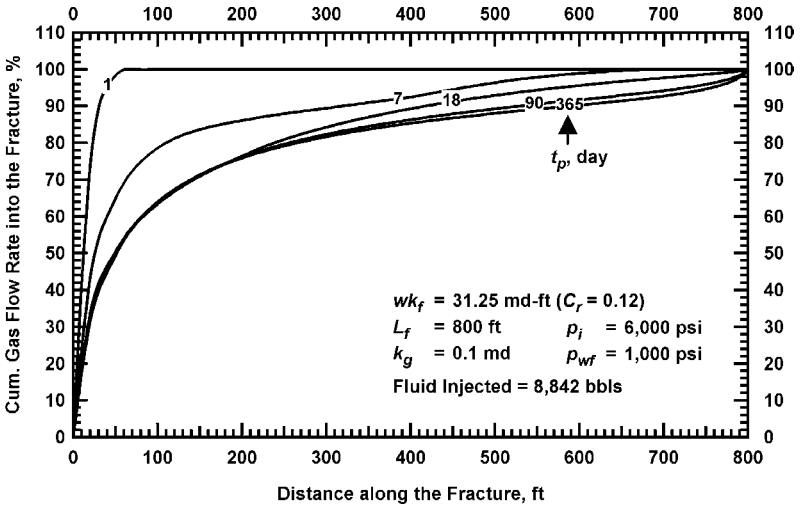

Fig. B.9— Cumulative gas flow rate into the fracture versus distance along the fracture for a multiphase case with wk_f = 31.25 md-ft, L_f = 800 ft, and k_g = 0.1 md.

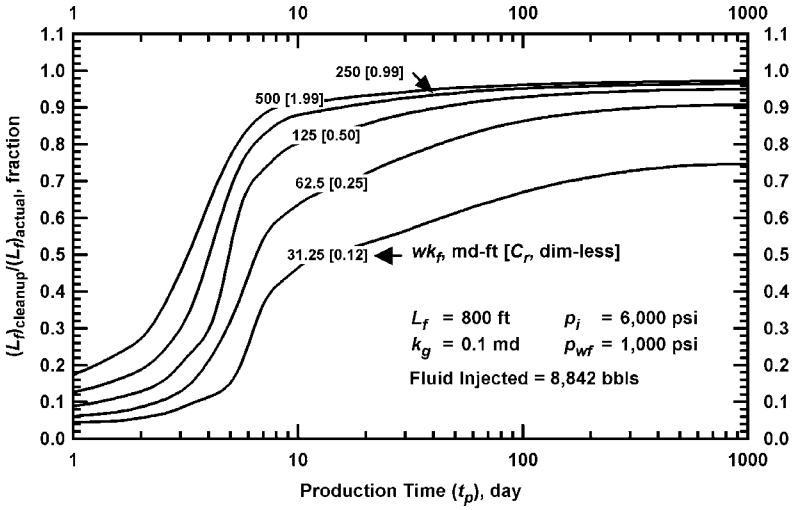

Fig. B.10— Ratio of cleanup fracture half-length to actual fracture half-length for multiphase and non-Darcy flow cases with L_f = 800 ft and k_g = 0.1 md.

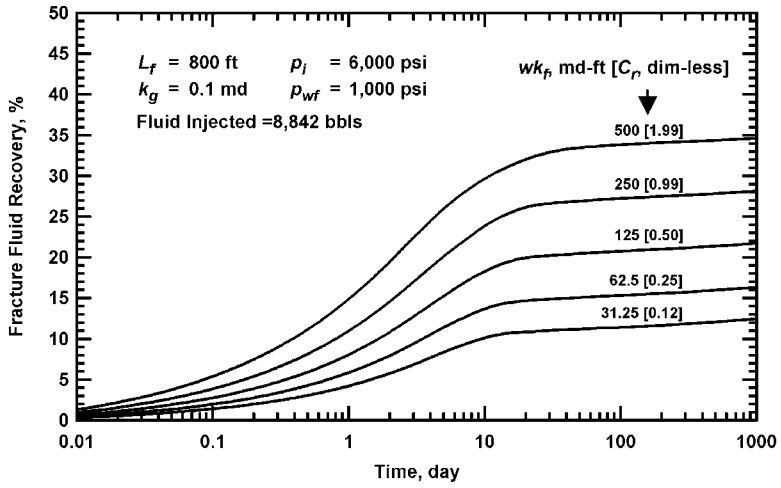

Fig. B.11— Fracture fluid recovery versus production time for multiphase and non-Darcy flow cases with L_f = 800 ft and k_g = 0.1 md.

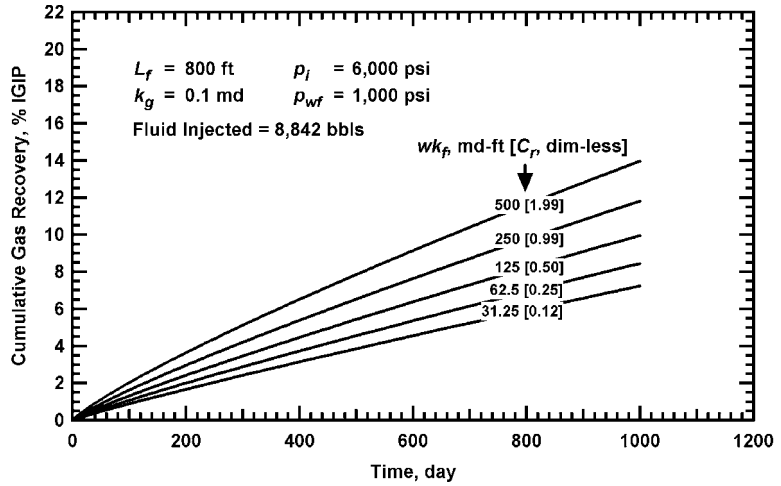

Fig. B.12— Cumulative gas recovery versus production time for multiphase and non-Darcy flow cases with L_f = 800 ft and k_g = 0.1 md.

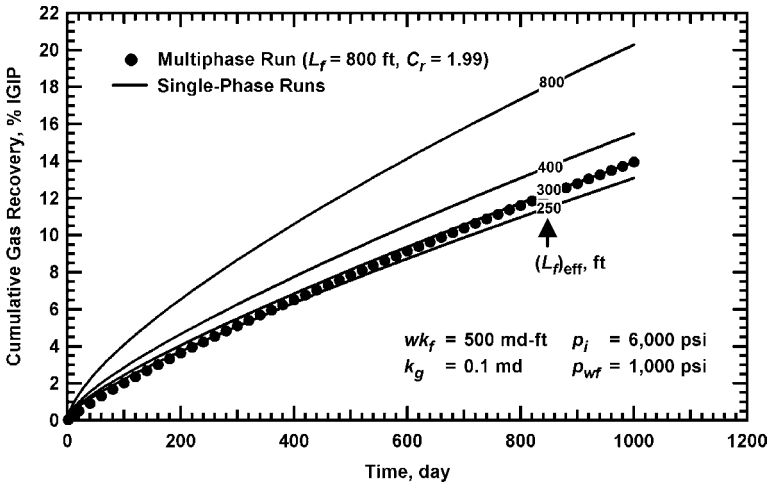

Fig. B.13—Cumulative gas recovery versus production time for a multiphase case with wk_f = 500 md-ft, L_f = 800 ft, and k_g = 0.1 md, and corresponding single-phase cases with different fracture lengths.

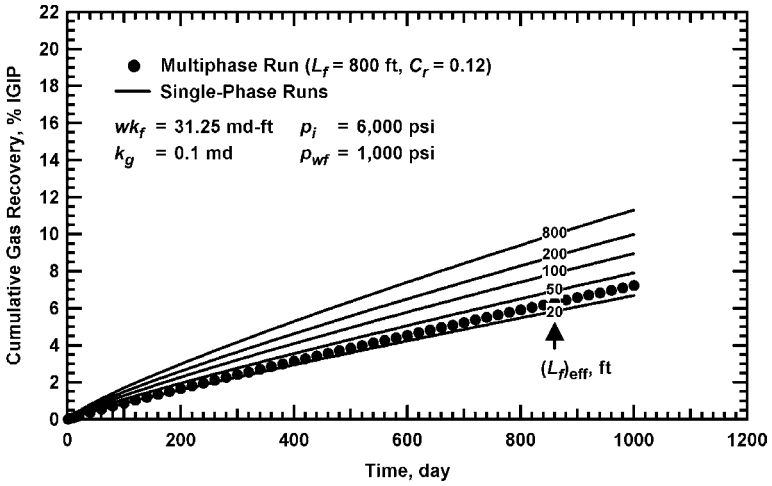

Fig. B.14—Cumulative gas recovery versus production time for a multiphase case with wk_f = 31.25 md-ft, L_f = 800 ft, and k_g = 0.1 md, and corresponding single-phase cases with different fracture lengths.

VITA

Name:	Elyezer P. Lolon
Permanent Address:	Department of Petroleum Engineering Texas A&M University College Station, TX 77840-3116
Education:	Texas A&M University, College Station, Texas *Doctor of Philosophy in Petroleum Engineering* December 2004
	Texas A&M University, College Station, Texas *Master of Science in Petroleum Engineering* December 2001
	Bandung Institute of Technology, Indonesia *Bachelor of Science in Petroleum Engineering* October 1996
Industry Experience:	Petroleum Engineer (1996 to 1999) PT Caltex Pacific Indonesia A subsidiary of ChevronTexaco
Professional Membership:	Society of Petroleum Engineers